

CONTRACTOR REPORT

SAND91-7052
Unlimited Release
UC-721



SAND91-7052
0002
UNCLASSIFIED

04/91
128P STAC

REFERENCE COPY C.2

Analyses of Backfilled Transuranic Wastes Disposal Rooms

G. D. Callahan and K. L. DeVries
RE/SPEC Inc.
PO Box 725
Rapid City, SD 57709

Prepared by Sandia National Laboratories Albuquerque, New Mexico 87185
and Livermore, California 94550 for the United States Department of Energy
under Contract DE-AC04-76DP00789

Printed April 1991

Issued by Sandia National Laboratories, operated for the United States Department of Energy by Sandia Corporation.

NOTICE: This report was prepared as an account of work sponsored by an agency of the United States Government. Neither the United States Government nor any agency thereof, nor any of their employees, nor any of their contractors, subcontractors, or their employees, makes any warranty, express or implied, or assumes any legal liability or responsibility for the accuracy, completeness, or usefulness of any information, apparatus, product, or process disclosed, or represents that its use would not infringe privately owned rights. Reference herein to any specific commercial product, process, or service by trade name, trademark, manufacturer, or otherwise, does not necessarily constitute or imply its endorsement, recommendation, or favoring by the United States Government, any agency thereof or any of their contractors or subcontractors. The views and opinions expressed herein do not necessarily state or reflect those of the United States Government, any agency thereof or any of their contractors.

Printed in the United States of America. This report has been reproduced directly from the best available copy.

Available to DOE and DOE contractors from
Office of Scientific and Technical Information
PO Box 62
Oak Ridge, TN 37831

Prices available from (615) 576-8401, FTS 626-8401

Available to the public from
National Technical Information Service
US Department of Commerce
5285 Port Royal Rd
Springfield, VA 22161

NTIS price codes
Printed copy: A07
Microfiche copy: A01

SAND91-7052
Unlimited Release
Printed April 1991

Distribution
Category UC-721

ANALYSES OF BACKFILLED TRANSURANIC WASTES DISPOSAL ROOMS

G. D. Callahan and K. L. DeVries
RE/SPEC Inc.
P.O. Box 725
Rapid City, SD 57709

ABSTRACT

The Waste Isolation Pilot Plant (WIPP) is a U.S. Department of Energy (DOE) research and development facility established to demonstrate the safe geologic disposal of transuranic (TRU) wastes generated from defense-related activities. Crushed salt and crushed-salt treatments are the candidate materials to be used as backfill around waste and waste packages in the underground disposal rooms. In response to room closure, the backfill is anticipated to compact sufficiently such that an effective seal is formed reducing brine inflow and radionuclide transport. In this report, different backfill and backfill/TRU waste combinations are investigated based on finite element simulations for a 200-year period conducted to examine and compare the sealing efficacy of different backfill scenarios. Specifically, disposal room content scenarios investigated include crushed salt, a crushed salt/bentonite mixture, crushed salt covering TRU waste, crushed salt/bentonite covering TRU waste, crushed salt covering a mixture of crushed salt and shredded metallic waste, and crushed salt covering vitrified waste. The simulations were conducted with the thermomechanical finite element program SPECTROM-32. The report includes a description of constitutive relations used to simulate the backfill and host rock formation including viscoplastic (creep), nonlinear elastic, creep consolidation, and nonlinear elastic and consolidation mixture models. The simulation results show that the backfill attains average void fractions less than 5 percent in all cases except for the case with crushed salt/bentonite covering TRU waste, which is only slightly greater than 5 percent. The time required to attain these void fractions varies considerably between cases.

The content of this report was effective as of April 1991. This report was prepared by RE/SPEC Inc. under Contract 40-2512 with Sandia National Laboratories.

ACKNOWLEDGMENTS

The authors are grateful to Barry M. Butcher and Frederick T. Mendenhall of Sandia National Laboratories for their review and constructive criticism of the report. The authors are appreciative and acknowledge the efforts of Joe L. Ratigan and Joel D. Nieland for their contributions in developing the TRU waste models used in this study.

CONTENTS

1.0 INTRODUCTION	1
1.1 BACKGROUND	1
1.2 SCOPE	2
1.3 REPORT ORGANIZATION	2
2.0 CONSTITUTIVE RELATIONS AND MATERIAL PROPERTIES	3
2.1 INTACT SALT	3
2.1.1 Linear Elastic Model	3
2.1.2 Creep Model	4
2.1.3 Material Properties for Intact Salt	9
2.2 CRUSHED SALT	9
2.2.1 Nonlinear Elastic Model for Crushed Salt	11
2.2.2 Creep Consolidation Model for Crushed Salt	12
2.2.3 Combined Crushed Salt Model	14
2.2.4 Material Properties for Crushed Salt	14
2.3 CRUSHED SALT MIXTURES	15
2.3.1 Crushed Salt/Bentonite Mixture Model	15
2.3.2 Crushed Salt/TRU Waste Mixture Model	15
2.3.2.1 Creep Consolidation Response of TRU Waste and Crushed Salt Mixtures	16
2.3.2.2 Nonlinear Elastic Response of TRU Waste and Crushed Salt Mixtures	18
2.3.3 Material Properties for Crushed Salt Mixtures	22
2.3.3.1 Crushed Salt/Bentonite Mixture	22
2.3.3.2 Crushed Salt/TRU Waste Mixture	24
2.4 TRU WASTE	28
2.4.1 Nonlinear Elastic	29
2.4.2 Vitrified Waste	31
2.4.3 Material Properties for TRU Waste	31

CONTENTS
(Continued)

2.4.3.1	Models for Composite Waste Canisters	33
2.4.3.2	Results	37
2.4.3.3	Composite TRU Waste Properties	37
2.4.3.4	Vitrified Waste Properties	40
3.0	FINITE ELEMENT IDEALIZATION OF DISPOSAL ROOM	41
4.0	RESULTS OF DISPOSAL ROOM ANALYSES	45
4.1	ROOM FILLED WITH CRUSHED SALT	45
4.2	ROOM FILLED WITH CRUSHED SALT/BENTONITE	49
4.3	ROOM FILLED WITH TRU WASTE AND CRUSHED SALT	50
4.4	ROOM FILLED WITH TRU WASTE AND CRUSHED SALT/BENTONITE	54
4.5	ROOM FILLED WITH VITRIFIED WASTE AND CRUSHED SALT	54
4.6	ROOM FILLED WITH CRUSHED SALT AND SHREDDED METAL MIXED WITH CRUSHED SALT	56
5.0	SUMMARY AND CONCLUSIONS	61
6.0	NOMENCLATURE	65
7.0	REFERENCES	71
APPENDIX A.	SIMULATED TRU WASTE STRESS — POROSITY DATA	75
APPENDIX B.	COMPARISON OF SPECTROM-32 AND SANCHO RESULTS	83
APPENDIX C.	AVERAGE VOID FRACTION AND MEAN STRESS RESULTS	99

TABLES

2-1	Material Parameter Values for Intact Salt	10
2-2	Nonlinear Elastic Material Parameters for Crushed Salt	14
2-3	Creep Consolidation Material Parameters for Crushed Salt	15
2-4	Nonlinear Elastic Material Parameters for Crushed Salt/Bentonite	23
2-5	Creep Consolidation Model Parameter Values for Crushed Salt/Bentonite	23
2-6	Metallic Waste Components Properties	28
2-7	Individual Waste Type Characteristics	33
2-8	Composite Waste Characteristics	37
2-9	TRU Waste Drum Characteristics	39
2-10	Elastic Constants for Vitrified Waste	40
5-1	Average Void Fraction Comparisons for the Analyses	64

FIGURES

2-1	Volumetric Strain As a Function of Fractional Density for an Applied Pressure of 15 MPa	25
2-2	Volumetric Strain As a Function of Fractional Density for an Applied Pressure of 0.05 MPa	26
2-3	Change in Volumetric Strain Rate With Time for an Applied Pressure of 0.05 MPa	27
2-4	Compaction Data (Appendix A) and Fits for Individual Waste Types	32
2-5	Composite Series Model	34
2-6	Composite Parallel Model	35
2-7	Generated Data and Fits for Composite Models	38
3-1	Finite Element Mesh of Disposal Room	42
4-1	Room Closure History of a Disposal Room Filled With Crushed Salt	47
4-2	Void Reduction in the Disposal Room Filled With Crushed Salt as a Function of Time	47
4-3	Room Closure History of a Disposal Room Filled With Crushed Salt/Bentonite	51
4-4	Void Reduction in the Disposal Room Filled With Crushed Salt/Bentonite as a Function of Time	51
4-5	Room Closure History of a Disposal Room Filled With TRU Waste and Crushed Salt	53
4-6	Void Reduction in the Disposal Room Filled With TRU Waste and Crushed Salt as a Function of Time	53
4-7	Room Closure History of a Disposal Room Filled With TRU Waste and Crushed Salt/Bentonite	55
4-8	Void Reduction in the Disposal Room Filled With TRU Waste and Crushed Salt/Bentonite as a Function of Time	55
4-9	Room Closure History of a Disposal Room Filled With Vitrified Waste and Crushed Salt	57

FIGURES
(Continued)

4-10	Void Reduction in the Disposal Room Filled With Vitrified Waste and Crushed Salt as a Function of Time	57
4-11	Room Closure History of a Disposal Room Filled With Crushed Salt and a Shredded Metal/Crushed Salt Mixture	59
4-12	Void Reduction in the Disposal Room Filled With Crushed Salt and a Shredded Metal/Crushed Salt Mixture as a Function of Time	59
5-1	Comparisons of Vertical Closure Histories for Different Room Emplacement Scenarios	62
5-2	Comparisons of Horizontal Closure Histories for Different Room Emplacement Scenarios	63

1.0 INTRODUCTION

1.1 BACKGROUND

The U.S. Department of Energy is planning to dispose of transuranic wastes (TRU) at the Waste Isolation Pilot Plant (WIPP) near Carlsbad, New Mexico. The current mission of the WIPP is to provide a research and development facility to demonstrate the safe management, storage, and disposal of TRU wastes generated by U.S. Government defense programs. Sandia National Laboratories is conducting procedural and technical activities to assess compliance of the WIPP with regulatory requirements. Performance of seal, barrier, and backfill materials is being studied as part of these activities.

A key candidate component of the room backfill system is crushed salt. Crushed salt is an attractive candidate because it is readily available from the mining operations, it is compatible with the host rock, and it is expected to consolidate into a low-permeability mass comparable to the intact salt as a result of the creep closure of the surrounding rock mass. Crushed salt has been shown to consolidate relatively quickly when subjected to a hydrostatic stress [Holcomb and Hannum, 1982; Pfeifle and Senseny, 1985; Stroup and Senseny, 1987, and Holcomb and Zeuch, 1988]. Therefore, the backfill is expected to lower the effective permeability in the rooms and reduce the total time required for complete encapsulation of the waste. In addition, the backfill may be engineered so that it actually adsorbs radionuclides and thus, provides an additional barrier around the waste. Crushed salt and varying amounts of bentonite, a montmorillonite-rich clay, have been proposed as candidate backfill materials that improve the properties of pure crushed salt. The addition of bentonite reduces permeability and increases the absorbing ability of the mixture. However, the addition of bentonite may have its drawbacks. Preliminary results from consolidation tests suggest that the rate of consolidation for crushed salt/bentonite backfills is less than that for pure crushed salt [Pfeifle, 1990; Stroup and Senseny, 1987]. This result implies that the time required for complete encapsulation of the waste is longer for the crushed salt/bentonite backfills. Another disadvantage of bentonite is that it swells in the presence of water or brine [Pusch, 1980]. In a storage room where the backfill is confined, a swelling pressure may develop. This swelling pressure may be large and could add significantly to the time required for complete encapsulation of the waste since the natural tendency of the intact rock to deform into the room is decreased.

Because of the importance of backfills at WIPP, knowledge of their constitutive behavior and the ability to perform long-term structural analyses of backfill schemes are required. Clearly, an understanding of the mechanical behavior of crushed salt is important at WIPP. Optimization of the backfill emplacement is necessary to promote room stability, to enable sufficient backfill consolidation to reduce brine

flow which retards the transport of soluble radionuclides, and to maintain sufficient gas permeability to avoid gas pressurization [Butcher, 1990].

1.2 SCOPE

The study presented in this report was conducted to investigate the consolidation of backfill and waste in disposal room configurations at the WIPP. Six cases were investigated that included the following assumed room contents:

1. Completely filled with crushed salt.
2. Completely filled with a 70 percent crushed salt — 30 percent bentonite (by weight) mixture.
3. TRU waste covered with crushed salt.
4. TRU waste covered with a 70 percent crushed salt — 30 percent bentonite (by weight) mixture.
5. An 80 percent crushed salt — 20 percent shredded metallic waste (by volume) mixture covered with crushed salt.
6. Vitrified waste covered by crushed salt.

To solve these six problems, representative constitutive relations were developed and implemented for the crushed salt and TRU waste. Numerical simulations of the backfill, waste, and creeping host bedded salt formation were conducted for 200 years. The finite element program, SPECTROM-32 [Callahan et al., 1990], was used to perform the analyses.

1.3 REPORT ORGANIZATION

This report includes six chapters and three appendixes. Chapter 2 describes the constitutive relations and material parameters used to describe the backfill materials, waste materials, and the host rock formation. Chapter 3 describes the finite element idealization of the disposal room configuration and procedures used to conduct the analyses. The results of the analyses are given in Chapter 4, and Chapter 5 provides the conclusions of the study. References cited in the report are given in Chapter 6. Appendix A includes stress-porosity data from simulated TRU waste compaction experiments. Appendix B contains a comparison of results obtained with the finite element program SANCHO [Weatherby and Brown, 1990 and Weatherby, 1989] to the comparable analyses described here. Appendix C contains average void fraction and mean stress results from the analyses.

2.0 CONSTITUTIVE RELATIONS AND MATERIAL PROPERTIES

This chapter presents the constitutive relationships or models used to represent the various materials associated with the analysis of TRU waste disposal rooms. The models presented are for the natural or intact rock salt, crushed salt, crushed salt mixed with other materials, and TRU waste. Each of these material models are discussed separately in the following subsections. Because temperature variations within the repository are assumed to be small, the thermal strains are neglected in each of the discussions; however, the thermal strain rates may be included as a component of the total strain rate in each of the models as reported previously [Callahan et al., 1990].

2.1 INTACT SALT

The total strain rate for the natural rock salt or intact salt constitutive model is assumed to include two components. The components consist of elastic and creep contributions, and the total strain rate is written as

$$\dot{\epsilon}_{ij} = \dot{\epsilon}_{ij}^e + \dot{\epsilon}_{ij}^c \quad (2-1)$$

The elastic strains (ϵ_{ij}^e) are assumed to be linear elastic and given by Hooke's Law (e.g., Timoshenko and Goodier [1970]). The creep strains (ϵ_{ij}^c) are described by Munson et al. [1989]. Summaries of the linear elastic and creep portions of the model are given here for completeness.

2.1.1 Linear Elastic Model

The elastic strains, ϵ_{ij}^e , are the contribution from the stress field given by Hooke's law

$$\epsilon_{ij}^e = C_{ijkl} \sigma_{kl} \quad (2-2)$$

where C_{ijkl} is the matrix of elastic constants and σ_{kl} is the stress tensor.

For an isotropic body, there are two independent elastic constants and Equation 2-2 can be written as

$$\epsilon_{ij}^e = \frac{1}{E} [(1 + \nu) \sigma_{ij} - \nu \sigma_{kk} \delta_{ij}] \quad (2-3)$$

where the elastic material constants E and ν represent Young's modulus and Poisson's ratio. We may also write Equation 2-3 in terms of the bulk modulus (K) and shear modulus (G) for the material as

$$\epsilon_{ij}^e = \frac{\sigma_m}{3K} \delta_{ij} + \frac{S_{ij}}{2G} \quad (2-4)$$

where

$$\begin{aligned}
\sigma_m &= \frac{\sigma_{kk}}{3}, \text{ mean stress} \\
S_{ij} &= \sigma_{ij} - \sigma_m \delta_{ij}, \text{ deviatoric stress} \\
\delta_{ij} &= \text{Kronecker delta.}
\end{aligned} \tag{2-5}$$

Equation 2-3 may be rearranged to give the elastic constitutive equations for stress in terms of strain

$$\sigma_{ij} = \frac{E}{(1+\nu)(1-2\nu)} \left[(1-2\nu) \epsilon_{ij}^e + \nu \epsilon_{kk}^e \delta_{ij} \right] \tag{2-6}$$

2.1.2 Creep Model

For the inelastic creep strains, the modified Munson-Dawson material model [Munson et al., 1989] is used. The model is written as

$$\dot{\epsilon}_e^c = F \dot{\epsilon}_s \tag{2-7}$$

where $\dot{\epsilon}_e^c$ is the invariant inelastic strain-rate measure, and $\dot{\epsilon}_s$ is the steady-state strain rate. The transient function F consists of three branches — a workhardening branch, an equilibrium branch, and a recovery branch and is written in that order as

$$F = \begin{cases} \exp \left[\Delta \left(1 - \frac{\zeta}{\epsilon_t^f} \right)^2 \right] & \zeta < \epsilon_t^f \\ 1 & \zeta = \epsilon_t^f \\ \exp \left[-\delta \left(1 - \frac{\zeta}{\epsilon_t^f} \right)^2 \right] & \zeta > \epsilon_t^f \end{cases} \tag{2-8}$$

Δ and δ are the workhardening and recovery parameters, respectively, and ϵ_t^f is the transient strain-rate limit. The internal variable ζ is governed by the evolutionary equation

$$\dot{\zeta} = (F - 1) \dot{\epsilon}_s \tag{2-9}$$

and the transient strain-rate limit is given by

$$\epsilon_t^f = K_o e^{cT} \left(\frac{\sigma_e}{\mu} \right)^m \tag{2-10}$$

where K_o , c , m , and μ are material parameters, T is temperature, and σ_e is an invariant stress measure described later.

The workhardening parameter is defined as a function of stress

$$\Delta = \alpha + \beta \log \left(\frac{\sigma_e}{\mu} \right) \quad (2-11)$$

where α and β are material parameters. Because of insufficient laboratory data to allow evaluation, the recovery parameter δ is taken to be a constant.

The steady-state strain rate is the sum of the three individual strain-rate mechanisms acting in parallel

$$\dot{\epsilon}_s = \sum_{i=1}^3 \dot{\epsilon}_{s_i} \quad (2-12)$$

The three contributing mechanisms — dislocation climb, an undefined mechanism, and glide are written respectively as

$$\dot{\epsilon}_{s_1} = A_1 \left(\frac{\sigma_e}{\mu} \right)^{n_1} \exp \left(-\frac{Q_1}{RT} \right) \quad (2-13)$$

$$\dot{\epsilon}_{s_2} = A_2 \left(\frac{\sigma_e}{\mu} \right)^{n_2} \exp \left(-\frac{Q_2}{RT} \right) \quad (2-14)$$

$$\dot{\epsilon}_{s_3} = \left(\hat{B}_1 e^{-Q_1/RT} + B_2 e^{-Q_2/RT} \right) \sinh \left[q \left(\frac{\sigma_e - \sigma_0}{\mu} \right) \right] H(\sigma_e - \sigma_0) \quad (2-15)$$

where

μ = normalizing parameter (MPa)

q = activation volume

$A_1, A_2, \hat{B}_1, B_2, n_1, n_2,$
 $Q_1, Q_2, \sigma_0, K, m, \alpha, \beta, \delta$ = experimental constants (see Table 2-1)

R = 1.987, universal gas constant ($\frac{\text{cal}}{\text{mol-K}}$)

$H(\cdot)$ = Heaviside step function.

To generalize the Munson-Dawson model to three-dimensional states of stress, Fossum et al. [1988] is followed to determine flow potential functions generalized according to Mises and Tresca types of flow potential functions. The inelastic tensorial strain-rate components may be written as

$$\dot{\epsilon}_{ij}^c = \dot{\epsilon}_e^c \frac{\partial \sigma_e^f}{\partial \sigma_{ij}} \quad (2-16)$$

where the invariant inelastic strain-rate measure is

$$\dot{\epsilon}_e^c = \dot{\epsilon}_e^c(T, \sigma_e, \epsilon_e^c) \quad (2-17)$$

The two invariant stress measures in Equations 2-16 and 2-17 are given by

$$\begin{aligned}\sigma_e^f &= \sigma_e^f(\sigma_m, J_2, J_3) \\ \sigma_e &= \sigma_e(\sigma_m, J_2, J_3)\end{aligned}\tag{2-18}$$

where the mean stress (σ_m), the second invariant of the deviator stress (J_2), and the third invariant of the deviator stress (J_3) are given by

$$\begin{aligned}\sigma_m &= \frac{\sigma_{kk}}{3} \\ J_2 &= \frac{1}{2}S_{ij}S_{ji} \\ J_3 &= \frac{1}{3}S_{ij}S_{jk}S_{ki}\end{aligned}\tag{2-19}$$

The Lode angle (ψ), which is a convenient alternative to J_3 , is given by

$$\psi = \frac{1}{3} \sin^{-1} \left[\frac{-3\sqrt{3}J_3}{2J_2^{3/2}} \right], \quad \left(-\frac{\pi}{6} \leq \psi \leq \frac{\pi}{6} \right)\tag{2-20}$$

The partial derivative given in Equation 2-16 may be determined using the chain rule as

$$\frac{\partial \sigma_e^f}{\partial \sigma_{ij}} = \frac{\partial \sigma_e^f}{\partial \sigma_m} \frac{\partial \sigma_m}{\partial \sigma_{ij}} + \frac{\partial \sigma_e^f}{\partial J_2} \frac{\partial J_2}{\partial \sigma_{ij}} + \frac{\partial \sigma_e^f}{\partial \psi} \frac{\partial \psi}{\partial J_3} \frac{\partial J_3}{\partial \sigma_{ij}}\tag{2-21}$$

The derivatives of the invariants in Equation 2-21 are the same regardless of the invariant stress and strain measures selected. These derivatives [Callahan, 1982] are

$$\begin{aligned}\frac{\partial \sigma_m}{\partial \sigma_{ij}} &= \frac{\delta_{ij}}{3} \\ \frac{\partial J_2}{\partial \sigma_{ij}} &= S_{ij} \\ \frac{\partial \psi}{\partial J_3} \frac{\partial J_3}{\partial \sigma_{ij}} &= -\frac{\sqrt{3}}{2J_2^{3/2} \cos 3\psi} t_{ij}\end{aligned}\tag{2-22}$$

where

$$t_{ij} = S_{ip}S_{pj} - \frac{2}{3}J_2\delta_{ij}$$

Therefore, to define completely the inelastic strain-rate measure required by Equation 2-17, the invariant stress and strain-rate measures need to be prescribed. The equivalent inelastic strain-rate measure is given by the Munson-Dawson material model in Equation 2-7. Two types of invariant stress measures are considered.

These are termed the pressure-dependent and frictional forms of the invariant stress measure. The pressure-dependent form is similar to the Mises-Schleicher plastic potential, and the frictional form is similar to the Mohr-Coulomb plastic potential. Mathematically, these stress measures are

$$\sigma_e^f = 3\tau\sigma_m + \sqrt{3J_2} \quad (\text{pressure-dependent}) \quad (2-23)$$

$$\sigma_e^f = 2\sin\tau\sigma_m + \left(\cos\psi - \frac{\sin\psi\sin\tau}{\sqrt{3}}\right) 2\sqrt{J_2} \quad (\text{frictional}) \quad (2-24)$$

The variable τ is a material constant termed the flow dilatancy parameter. The other invariant stress measure (σ_e) that needs to be described is taken to be identical to those given in Equations 2-23 and 2-24, except that the parameter τ is replaced by a different variable (θ), viz

$$\sigma_e = 3\theta\sigma_m + \sqrt{3J_2} \quad (2-25)$$

$$\sigma_e = 2\sin\theta\sigma_m + \left(\cos\psi - \frac{\sin\psi\sin\theta}{\sqrt{3}}\right) 2\sqrt{J_2} \quad (2-26)$$

The variable θ is a material constant termed the frictional parameter. If $\theta = \tau$, then $\sigma_e = \sigma_e^f$; however, this is not required theoretically.

Equation 2-21 requires the partial derivatives of the invariant stress measures with respect to stress. Differentiation of Equations 2-23 and 2-24 provides these quantities for the pressure-dependent and frictional forms for the invariant stress measures. These quantities are as follows:

Pressure-Dependent

$$\frac{\partial\sigma_e^f}{\partial\sigma_m} = 3\tau$$

$$\frac{\partial\sigma_e^f}{\partial J_2} = \frac{\sqrt{3}}{2\sqrt{J_2}} \quad (2-27)$$

$$\frac{\partial\sigma_e^f}{\partial\psi} = 0$$

Frictional

$$\begin{aligned}\frac{\partial \sigma_e^f}{\partial \sigma_m} &= 2 \sin \tau \\ \frac{\partial \sigma_e^f}{\partial J_2} &= \left[\frac{\cos 2\psi}{\cos 3\psi} + \frac{\sin \tau}{\sqrt{3}} (\tan 3\psi \cos \psi - \sin \psi) \right] \frac{1}{\sqrt{J_2}} \\ \frac{\partial \sigma_e^f}{\partial \psi} &= - \left[\sin \psi + \frac{\cos \psi \sin \tau}{\sqrt{3}} \right] 2\sqrt{J_2}\end{aligned}\tag{2-28}$$

By letting τ go to zero in Equations 2-23 and 2-24, we eliminate the mean-stress dependence and obtain Mises- and Tresca-types of invariant stress measures, respectively. θ is also set to zero such that $\sigma_e = \sigma_e^f$. Thus, Equations 2-23 and 2-24 become

$$\sigma_e = \sqrt{3J_2} \quad (\text{Mises})\tag{2-29}$$

$$\sigma_e = 2 \cos \psi \sqrt{J_2} \quad (\text{Tresca})\tag{2-30}$$

and the derivatives in Equations 2-27 and 2-28 become

Mises

$$\begin{aligned}\frac{\partial \sigma_e}{\partial \sigma_m} &= 0 \\ \frac{\partial \sigma_e}{\partial J_2} &= \frac{\sqrt{3}}{2\sqrt{J_2}} \\ \frac{\partial \sigma_e}{\partial \psi} &= 0\end{aligned}\tag{2-31}$$

Tresca

$$\begin{aligned}\frac{\partial \sigma_e}{\partial \sigma_m} &= 0 \\ \frac{\partial \sigma_e}{\partial J_2} &= \left[\frac{\cos 2\psi}{\cos 3\psi} \right] \frac{1}{\sqrt{J_2}} \\ \frac{\partial \sigma_e}{\partial \psi} &= -2 \sin \psi \sqrt{J_2}\end{aligned}\tag{2-32}$$

Substituting Equations 2-31, 2-22, and 2-21 into Equation 2-16 gives the familiar generalization for the Mises flow potential

$$\dot{\epsilon}_{ij}^c = \frac{3\dot{\epsilon}_e^c}{2\sqrt{3}J_2} S_{ij} \quad (2-33)$$

and substituting Equations 2-32, 2-22, and 2-21 into Equation 2-16 gives the generalization for the Tresca flow potential

$$\dot{\epsilon}_{ij}^c = \dot{\epsilon}_e^c \left\{ \left[\frac{\cos 2\psi}{\cos 3\psi} \right] \frac{S_{ij}}{\sqrt{J_2}} + \left[\frac{\sqrt{3} \sin \psi}{J_2 \cos 3\psi} \right] t_{ij} \right\} \quad (2-34)$$

Finally, substitution of Equation 2-7 into Equations 2-33 and 2-34 gives the generalization of the Munson-Dawson model for Mises (octahedral shear) and Tresca (maximum shear) types of flow potentials, respectively. The Tresca flow generalization was used in the analyses reported here.

Equation 2-34 is seen to be indeterminant as the Lode angle approaches $\pm 30^\circ$. In other words, the flow potential forms corners at $\psi = \pm 30^\circ$ and the direction of straining is not unique. To eliminate this problem computationally, Equation 2-34 is evaluated in the limit as $\psi \rightarrow \pm 30^\circ$. Performing this limiting operation, Equation 2-34 becomes

$$\lim_{\psi \rightarrow \pm 30^\circ} (\dot{\epsilon}_{ij}^c) = \dot{\epsilon}_e^c \left\{ \frac{S_{ij}}{\sqrt{3}J_2} \mp \frac{t_{ij}}{2J_2} \right\} \quad (2-35)$$

In SPECTROM-32, Equation 2-35 is used when the Lode angle is within 0.25 degrees of $\pm 30^\circ$.

2.1.3 Material Properties for Intact Salt

The linear elastic parameter values for the constitutive relation given in Equation 2-3 and the parameter values for the Munson-Dawson constitutive equation given in Equation 2-7 are presented in Table 2-1. Density of the intact salt is 2,140 kg/m³. The intact salt material parameters were taken from Munson [1989] for pure halite.

2.2 CRUSHED SALT

The total strain rate for the crushed salt constitutive model is assumed to consist of two components. The components are nonlinear elastic and creep consolidation contributions and the total strain rate is written as

$$\dot{\epsilon}_{ij} = \dot{\epsilon}_{ij}^e + \dot{\epsilon}_{ij}^c \quad (2-36)$$

Table 2-1. Material Parameter Values for Intact Salt^(a)

Parameter	Units	Value
Elastic Parameter Values		
E	MPa	31,000
ν	—	0.25
Munson-Dawson Creep Parameter Values		
A_1	yr ⁻¹ s ⁻¹	2.645E+30 8.386E+22
A_2	yr ⁻¹ s ⁻¹	3.050E+20 9.672E+12
Q_1/R	K	12,581
Q_1	cal/mol	25,000
Q_2/R	K	5,032
Q_2	cal/mol	10,000
n_1	—	5.5
n_2	—	5.0
\hat{B}_1	yr ⁻¹ s ⁻¹	1.919E+14 6.086E+06
B_2	yr ⁻¹ s ⁻¹	9.568E+05 3.034E-02
q	—	5.335E+03
σ_o	MPa	20.57
μ	MPa	12,400
m	—	3
K_o	—	6.275E+5
c	K ⁻¹	9.198E-3
α	—	-17.37
β	—	-7.738
δ	—	0.58

(a) Munson [1989] for pure halite.

The nonlinear elastic, ϵ_{ij}^e , and creep consolidation strains, ϵ_{ij}^c , are described by Callahan [1990] but are included here for completeness. Both the nonlinear elastic and creep consolidation portions of the model describe the material behavior in bulk (volumetric) and in shear (deviatoric). Although other models exist and are under consideration to describe the behavior of crushed salt (e.g., Zeuch [1989]), the nonlinear elastic and creep consolidation models for crushed salt were adapted from those given by Sjaardema and Krieg [1987].

2.2.1 Nonlinear Elastic Model for Crushed Salt

The elastic model described in Section 2.1.1 is applicable to the crushed salt with the following described procedure used to incorporate the nonlinearity in a piecewise manner.

For the nonlinear elastic model, the functional forms for the elastic constants given by Sjaardema and Krieg [1987] are adopted. They propose bulk and shear moduli as exponential functions of the current density, ρ_s . Tensile stresses and extensile strains are assumed to be positive. Functional forms of the elastic constants are written in terms of the total volumetric strain, ϵ_v ($\epsilon_v = \epsilon_{kk} = \epsilon_{11} + \epsilon_{22} + \epsilon_{33}$), using the relation

$$\rho_s = \frac{\rho_0^s}{1 + \epsilon_v} \quad (2-37)$$

where ρ_0^s is the initial or original density of the material. The bulk modulus and shear modulus (K_s and G_s) are given by

$$\begin{aligned} K_s &= K_0 e^{\frac{K_1 \epsilon_v}{1 + \epsilon_v}} \\ G_s &= G_0 e^{\frac{G_1 \epsilon_v}{1 + \epsilon_v}} \end{aligned} \quad (2-38)$$

where K_0 , K_1 , G_0 , and G_1 are material constants.

At any time, the current values of Young's modulus and Poisson's ratio are computed from the current values of bulk and shear modulus using the relations

$$\begin{aligned} E &= \frac{9K_s G_s}{3K_s + G_s} \\ \nu &= \frac{3K_s - 2G_s}{6K_s + 2G_s} \end{aligned} \quad (2-39)$$

Equations 2-39 are used in Equation 2-3 to compute the elastic strains.

To solve the nonlinear elastic problem, the method of load incrementation is used to approximate the tangent modulus. The following set of simultaneous equations has to be solved in the direct stiffness finite element approach

$$[K_t] \{u\} + \{f\} = 0 \quad (2-40)$$

where f is the total load (or unload) vector, u is the displacement, and the tangent stiffness matrix K_t is a function of displacement (strain).

$$K_t = K_t(u) \quad (2-41)$$

The load vector is divided into a number of small increments Δf such that the series of tangent moduli will approximate a given stress-strain curve. K_t is first approximated assuming $\epsilon_v = 0$, or we are assuming that $\Delta u^0 = 0$ and

$$[K_t^0] \{\Delta u^1\} + \{\Delta f^1\} = 0 \quad (2-42)$$

Repetition of this process for each of the load increments may be written as

$$\{\Delta u^n\} = -[K_t^{n-1}]^{-1} \{\Delta f^n\} \quad (2-43)$$

The process is continued for each of the load increments, and the displacement is accumulated, i.e.,

$$\{u\} = \{u\} + \{\Delta \delta^n\} \quad (2-44)$$

Clearly, the functional forms adopted for bulk and shear moduli (Equations 2-38) allow increase without bound. Therefore, maximum values for bulk modulus K_f and shear modulus G_f are introduced based on the fully consolidated or intact values for the material. If either the intact bulk or shear modulus values are reached, the tangent modulus is no longer allowed to change, and the material is assumed to be intact with a constant stiffness.

2.2.2 Creep Consolidation Model for Crushed Salt

To develop the creep consolidation constitutive equation, general considerations are first observed and then specific functional forms are guided by available laboratory data. From the application of thermodynamic concepts, the three-dimensional generalization for creep strain rates is given by Fossum et al. [1988]. Following this approach, two continuum internal variables are assumed, the average inelastic volumetric strain, ϵ_{eq1}^c , and the average equivalent inelastic shear strain, ϵ_{eq2}^c .

$$\dot{\epsilon}_{ij}^c = \dot{\epsilon}_{eq1}^c \frac{\partial \sigma_{eq1}^f}{\partial \sigma_{ij}} + \dot{\epsilon}_{eq2}^c \frac{\partial \sigma_{eq2}^f}{\partial \sigma_{ij}} \quad (2-45)$$

For the first portion (volumetric) of Equation 2-45, the invariant strain-rate measure is

$$\dot{\epsilon}_{eq1}^c = \dot{\epsilon}_v(\sigma_m) \quad (2-46)$$

The volumetric strain rate $\dot{\epsilon}_v^c$ is described empirically by Sjaardema and Krieg [1987] based on hydrostatic laboratory test data on crushed salt as

$$\dot{\epsilon}_v^c = \frac{(1 + \epsilon_v)^2}{\rho_0} B_0 [1 - e^{-B_1 \sigma_m}] e^{\frac{A \rho_0}{1 + \epsilon_v}} \quad (2-47)$$

where

$$\begin{aligned}
\epsilon_v &= \epsilon_{kk}, \text{ total volumetric strain} \\
\epsilon_v^c &= \epsilon_{kk}^c, \text{ volumetric creep strain} \\
\sigma_m &= \frac{\sigma_{kk}}{3}, \text{ mean stress} \\
\rho_0^s &= \text{ initial density} \\
B_0, B_1, A &= \text{ material constants (see Table 2-3)}.
\end{aligned}$$

The invariant stress measure is given by

$$\sigma_{eq1}^f = \sigma_m \quad (2-48)$$

For the second portion (deviatoric) of Equation 2-45, the invariant strain-rate measure is taken to be

$$\dot{\epsilon}_{eq2}^c = \eta \dot{\epsilon}_{eq1}^c = \eta \dot{\epsilon}_v(\sigma_m) \quad (2-49)$$

and the invariant stress is assumed to be a scalar multiple of the octahedral shear stress

$$\sigma_{eq2}^f = \sigma_e = \sqrt{3J_2} \quad (2-50)$$

where J_2 is the second invariant of the stress deviator ($J_2 = \frac{1}{2}S_{ij}S_{ij}$). Substituting into Equation 2-45 and performing the required differentiation gives

$$\dot{\epsilon}_{ij}^c = \dot{\epsilon}_v^c \frac{\delta_{ij}}{3} + \eta \dot{\epsilon}_v^c \frac{3S_{ij}}{2\sigma_e} \quad (2-51)$$

η is selected such that in a uniaxial test, the lateral components of $\dot{\epsilon}_{ij}^c$ equal zero. This requires that $\eta = -\frac{2}{3}$. Simple example problems that illustrate the creep consolidation behavior with and without the deviatoric component are given by Callahan [1990]. After substituting for $\dot{\epsilon}_v^c$ in Equation 2-51, the strain rate components are given by

$$\dot{\epsilon}_{ij}^c = \frac{(1 + \epsilon_v)^2}{\rho_0} B_0 \left[1 - e^{-B_1 \sigma_m} \right] e^{\frac{A \rho_0}{1 + \epsilon_v}} \left\{ \frac{\delta_{ij}}{3} - \frac{S_{ij}}{\sigma_e} \right\} \quad (2-52)$$

Obviously, the creep consolidation equation will allow unlimited consolidation. Therefore, a cap is introduced that eliminates further consolidation when the intact material density ρ_f is reached. Thus, when the condition

$$|\epsilon_v| \geq \left| \frac{\rho_0}{\rho_f} - 1 \right| \quad (2-53)$$

is satisfied, no further creep consolidation occurs. In addition, the creep consolidation is not permitted to generate tensile stresses. The procedure used to eliminate any tensile stresses is the same as described by Callahan et al. [1990]. An option is included that allows a consolidating material's constitutive model to be redefined following complete consolidation. For example, a crushed salt material can be prescribed to behave according to the intact salt constitutive relation given in Equation 2-34 following complete consolidation.

2.2.3 Combined Crushed Salt Model

The final equation for the total strain in the constitutive model for crushed salt (neglecting thermal strains) is obtained by substituting Equations 2-4 and 2-52 into Equation 2-36

$$\dot{\epsilon}_{ij} = \frac{\dot{\sigma}_m}{3K} \delta_{ij} + \frac{\dot{S}_{ij}}{2G} + \frac{(1 + \epsilon_v)^2}{\rho_0} B_0 [1 - e^{-B_1 \sigma_m}] e^{\frac{A \rho_0}{1 + \epsilon_v}} \left\{ \frac{\delta_{ij}}{3} - \frac{S_{ij}}{\sigma_e} \right\} \quad (2-54)$$

The above equation may be collapsed to yield the total volumetric strain-rate ($\dot{\epsilon}_v$) expression for the model. Performing this operation yields

$$\dot{\epsilon}_v = \frac{\dot{\sigma}_m}{K} + \frac{(1 + \epsilon_v)^2}{\rho_0} B_0 [1 - e^{-B_1 \sigma_m}] e^{\frac{A \rho_0}{1 + \epsilon_v}} \quad (2-55)$$

When the combined nonlinear elastic and creep consolidation model is used, the relative change in the Euclidean or L_2 norm of the volumetric strain is monitored over time and the stiffness is updated when the change is greater than a user prescribed tolerance. Further details may be found in Callahan [1990].

2.2.4 Material Properties for Crushed Salt

The nonlinear elastic parameter values describing the nonlinear moduli for crushed salt defined in Equation 2-38 are given in Table 2-2. Table 2-2 also gives the assumed initial and final (intact) densities for the crushed salt used in this study. Engineering of the backfill could change the initial density substantially. Table 2-3 presents the parameter values for the creep consolidation constitutive equation given in Equation 2-52. The crushed salt material parameters are taken from Sjaardema and Krieg [1987].

Table 2-2. Nonlinear Elastic Material Parameters for Crushed Salt

Parameter	Units	Value
K_0	MPa	0.01760 ^(a)
K_1	m ³ /kg	0.00653 ^(a)
G_0	MPa	0.01060 ^(a)
G_1	m ³ /kg	0.00653 ^(a)
K_f	MPa	20,626 ^(b)
G_f	MPa	12,423 ^(b)
ρ_0^s	kg/m ³	1,400 ^(c)
ρ_f	kg/m ³	2,140 ^(a)

(a) Sjaardema and Krieg [1987].

(b) Computed using Equation 2-38 at ρ_f .

(c) Weatherby [1989].

Table 2-3. Creep Consolidation Material Parameters for Crushed Salt

Parameter	Units	Value ^(a)
B_0	$\text{kg}/\text{m}^3 \cdot \text{s}^{-1}$ $\text{kg}/\text{m}^3 \cdot \text{yr}^{-1}$	$1.3 \times 10^{+8}$ $4.10 \times 10^{+15}$
B_1	MPa^{-1}	0.82
A	m^3/kg	-1.73×10^{-2}

(a) Sjaardema and Krieg [1987].

2.3 CRUSHED SALT MIXTURES

For the TRU waste disposal rooms, two crushed salt mixtures are of current interest: (1) crushed salt mixed with bentonite and (2) crushed salt mixed with TRU waste.

2.3.1 Crushed Salt/Bentonite Mixture Model

The functional form of the constitutive model selected to represent crushed salt/bentonite mixtures is identical to the crushed salt model since testing completed to date is inadequate to formulate a new constitutive model for crushed salt/bentonite mixtures. Therefore, Equation 2-52 applies to crushed salt/bentonite using material parameter values specific to the crushed salt/bentonite mixture given in Section 2.3.3.1.

2.3.2 Crushed Salt/TRU Waste Mixture Model

A possible waste treatment consists of simply mixing TRU waste with crushed salt and allowing the crushed salt to encapsulate the waste as the disposal room closes and the crushed salt consolidates. To develop constitutive relations for these types of mixtures, it is assumed that the TRU waste component consists of shredded metal wastes, is linear elastic, and is effectively an inert noninteracting material. Therefore, Equations 2-3 and 2-4 apply to the inert mixture material. Mixture theory is used to combine the crushed salt constitutive relations (nonlinear elasticity and creep consolidation) with the TRU waste.

2.3.2.1 Creep Consolidation Response of TRU Waste and Crushed Salt Mixtures

The creep consolidation model for a consolidating material mixed with another inert material is developed in this section. The creep consolidation relation for crushed salt is developed in Section 2.2.2 with the volumetric creep strain rate for crushed salt consolidation given in Equation 2-47. To distinguish the volumetric strain of the crushed salt from that of the mixture, the following definitions are used in the development:

$$\begin{aligned}\epsilon_{v_s} &= \text{total volumetric strain of crushed salt} \\ \epsilon_v &= \text{total volumetric strain of the mixture.}\end{aligned}$$

The total volume of the mixture (V) is

$$V = V_s + V_m \quad (2-56)$$

where

$$\begin{aligned}V_s &= \text{volume of crushed salt} \\ V_m &= \text{volume of inert material.}\end{aligned}$$

Equation 2-56 may also be written as

$$V = \frac{m_s M}{\rho_s} + \frac{m_m M}{\rho_m} \quad (2-57)$$

where

$$\begin{aligned}m_s &= \text{mass fraction of salt} \\ m_m &= \text{mass fraction of inert material} \\ \rho_s &= \text{current density of the crushed salt} \\ M &= \text{total mass of the mixture.}\end{aligned}$$

Dividing Equation 2-57 by the total mass gives

$$\frac{1}{\rho} = \frac{m_s}{\rho_s} + \frac{m_m}{\rho_m} \quad (2-58)$$

where ρ is the current density of the mixture. If the density of the mixture is known, the density of the crushed salt can be found from Equation 2-58 as

$$\rho_s = \frac{\rho \rho_m m_s}{\rho_m - \rho m_m} \quad (2-59)$$

The initial density of the mixture ρ_0 can be found by substituting the initial crushed salt density into Equation 2-58

$$\rho_0 = \frac{\rho_0^s \rho_m}{m_s \rho_m + m_m \rho_0^s} \quad (2-60)$$

The rate of change of the density of the mixture is given by differentiating Equation 2-58 with respect to time. The volumetric strain of the inert material is assumed to be small such that the density of the inert material is constant. Performing the differentiation yields

$$\dot{\rho} = \frac{m_s \rho^2}{\rho_s^2} \dot{\rho}_s \quad (2-61)$$

If the relationships between the density and volumetric strain, i.e.,

$$\rho = \frac{\rho_0}{1 + \epsilon_v} \quad (2-62)$$

$$\rho_s = \frac{\rho_0^s}{1 + \epsilon_{vs}} \quad (2-63)$$

are substituted into Equation 2-61, the volumetric strain rate for the mixture is determined as

$$\dot{\epsilon}_v = \frac{m_s \rho_0}{\rho_0^s} \dot{\epsilon}_{vs} \quad (2-64)$$

The current density of the crushed salt may be expressed as

$$\rho_s = \frac{M_s}{V_s} = \frac{m_s M}{v_s V} = \frac{m_s \rho}{v_s} \quad (2-65)$$

where M_s is the mass of the salt. Thus, the volume fraction of the crushed salt v_s is

$$v_s = \frac{m_s \rho}{\rho_s} \quad (2-66)$$

The initial volume fraction of crushed salt is obtained by substituting the initial densities into Equation 2-66

$$v_0^s = \frac{m_s \rho_0}{\rho_0^s} \quad (2-67)$$

Substituting Equation 2-67 into Equation 2-64 yields

$$\dot{\epsilon}_v = v_0^s \dot{\epsilon}_{vs} \quad (2-68)$$

Thus, Equation 2-68 describes the volumetric strain rate of crushed salt mixed with an inert material in terms of the volumetric strain rate of the crushed salt. Assuming that the volumetric strain rate is the sum of the elastic and creep portions, Equation 2-68 may be written as

$$\dot{\epsilon}_v^c + \dot{\epsilon}_v^e = v_0^s (\dot{\epsilon}_{vs}^c + \dot{\epsilon}_{vs}^e) \quad (2-69)$$

The elastic strain rates are assumed to be negligible compared to the creep consolidation strain rates. To evaluate the relative magnitudes of the strain rates, conditions applicable to analyses relevant to our situation will be considered. Based on an initial density of 1,400 kg/m³, the initial bulk modulus of crushed salt is about 150 MPa and the final value at full consolidation is that of intact salt, or 20,626 MPa. If the mean stress in the crushed salt is assumed to change from zero to the lithostatic value of nearly 15 MPa compression over a 50-year period, the elastic strain rate can be computed to be about 6.3E-11 s⁻¹ based on the initial bulk modulus and 4.6E-13 s⁻¹ based on the final bulk modulus value. If a pressure of 0.1 MPa compression in the crushed salt is assumed and the initial density is used, a creep consolidation strain rate of about 2.3E-7 s⁻¹ is computed. Thus, the elastic strain rate is about three to six orders of magnitude less than the creep consolidation strain rate. As the crushed salt consolidates, both the elastic and creep consolidation strain rates decrease. However, the effective pressure in the crushed salt also increases with time, which increases the creep consolidation strain rate. In addition, when the inert material is mixed with the crushed salt, the stiffness of the mixture is increased, which reduces the elastic strain rate. Therefore, neglecting the elastic strain rates appears to be a reasonable assumption and the relation for the volumetric creep strain of the mixture becomes

$$\dot{\epsilon}_v^c = v_0^c \dot{\epsilon}_{v_0}^c \quad (2-70)$$

where $\dot{\epsilon}_{v_0}^c$ is given by Equation 2-52.

2.3.2.2 Nonlinear Elastic Response of TRU Waste and Crushed Salt Mixtures

For the nonlinear elastic model, the derivation of the elastic constants for a mixture of two dissimilar materials is required. One material behaves nonlinearly and the other material is linear. Many different methods exist for representing the continuum properties of multiphase materials with different distributions of the phases. Maxwell's model considers randomly sized spheres of one material distributed in another (e.g., Parrott and Stuckes, [1975]). Other examples of property bounds established for multiphase materials may be found in Hashin and Shtrikman [1962], Corson [1974], and Milton [1982]. Corson [1974], referencing another researcher who used energy theorems of classical elasticity theory to establish bounds for effective bulk and shear moduli, states that his resultant bounds were precisely the volume-fraction average of the modulus of each phase (upper bound) and the inverse of the volume-fraction average of the inverse modulus (lower bound). Therefore, although many complex methods exist to establish bounds for the elastic moduli in a mixture, the simple rule of mixtures is relied upon because precise knowledge of the properties and the distribution of the phases in the two-component system is not available.

The rule of mixtures states that a given property for a mixture (Θ) is simply a function of the component properties (θ_i) weighted according to their volume

fractions (v_i). Parallel and series combinations are typical simple forms that may be stated mathematically as

$$\Theta = v_i \theta_i \quad (2-71)$$

$$\frac{1}{\Theta} = \frac{v_i}{\theta_i} \quad (2-72)$$

and $\Sigma v_i = 1$. These two mixture forms provide simple upper and lower bounds. Either Equation 2-71 or 2-72 could be used to formulate the effective moduli for the two-component mixture. Equation 2-71 is used to develop the moduli for the mixture, which gives the upper bound or higher stiffnesses. Thus, the elastic moduli for the mixture are

$$K = v_s K_s + v_m K_m \quad (2-73)$$

$$G = v_s G_s + v_m G_m \quad (2-74)$$

where

v_s = volumetric fraction of crushed salt

v_m = volumetric fraction of inert material

K_m = bulk modulus of the inert material

G_m = shear modulus of the inert material.

The functional form of the nonlinear elastic material model for crushed salt is described in Section 2.2.1 with the bulk (K_s) and shear (G_s) moduli defined by Equations 2-38 as

$$K_s = K_0 e^{K_1 \rho_s} \quad (2-75)$$

$$G_s = G_0 e^{G_1 \rho_s} \quad (2-76)$$

where K_0 , K_1 , G_0 , and G_1 are material constants. The moduli for the inert material are assumed to be constant but the volume fraction and the moduli for the crushed salt will change with consolidation. Since the volume fractions for the compacting material mixture changes, the mass fractions of the components are the desirable input variables since they are constant. Thus, expressions for the mass fractions in terms of the component densities and volume fractions are required. The density of the crushed salt and the inert material may be expressed as

$$\rho_s = \frac{M_s}{V_s} = \frac{m_s M}{v_s V} = \frac{m_s \rho}{v_s} \quad (2-77)$$

$$\rho_m = \frac{M_m}{V_m} = \frac{m_m M}{v_m V} = \frac{m_m \rho}{v_m} \quad (2-78)$$

where

ρ_m = density of the inert material

ρ = density of the mixture

M_s = mass of salt

M_m = mass of inert material.

Solving Equations 2-77 and 2-78 for the volume fractions gives

$$v_s = \frac{m_s \rho}{\rho_s} \quad (2-79)$$

$$v_m = \frac{m_m \rho}{\rho_m} \quad (2-80)$$

The total volume of the mixture (V) at any time is

$$V = V_s + V_m \quad (2-81)$$

Equation 2-81 may also be written as

$$V = \frac{m_s M}{\rho_s} + \frac{m_m M}{\rho_m} \quad (2-82)$$

Dividing Equation 2-82 by the total mass gives

$$\frac{1}{\rho} = \frac{m_s}{\rho_s} + \frac{m_m}{\rho_m} \quad (2-83)$$

After algebraic manipulation, Equation 2-83 may be written

$$\rho = \frac{\rho_s \rho_m}{m_s \rho_m + m_m \rho_s} \quad (2-84)$$

Solving Equation 2-84 for the crushed salt density yields

$$\rho_s = \frac{m_s \rho \rho_m}{\rho_m - m_m \rho} \quad (2-85)$$

Substitution of Equation 2-85 into Equations 2-79 and 2-80 yields expressions for the volume fractions in terms of the mass fractions and densities

$$v_s = \frac{m_s \rho_m}{m_s \rho_m + m_m \rho_s} \quad (2-86)$$

$$v_m = \frac{m_m \rho_s}{m_s \rho_m + m_m \rho_s} \quad (2-87)$$

Similarly, the mass fractions can be expressed as

$$m_s = \frac{v_s \rho_s}{v_s \rho_s + v_m \rho_m} \quad (2-88)$$

$$m_m = \frac{v_m \rho_m}{v_s \rho_s + v_m \rho_m} \quad (2-89)$$

With the volume fractions given by Equations 2-86 and 2-87, the elastic moduli can be determined by substitution into Equations 2-73 and 2-74. The procedure given in Section 2.2.1 can then be followed to solve the nonlinear elastic mixture problem.

Now, expressions are needed for the final values of the bulk and shear moduli, which depend on the final volume fractions of the mixed materials when the void fraction is zero. If the void volume is considered to reside entirely in the crushed salt, the crushed salt volume (V_s) may be expressed as

$$V_s = V_v + V_{i_s} \quad (2-90)$$

where V_v and V_{i_s} are the volumes of the voids and the intact (solid) salt, respectively, and the total volume of the mixture is given in Equation 2-81. The porosity of the crushed salt (ϕ_s) is defined as

$$\phi_s = \frac{V_v}{V_s} = \frac{V_s - V_{i_s}}{V_s} = 1 - \frac{\rho_s}{\rho_{i_s}} \quad (2-91)$$

where ρ_{i_s} is the density of intact salt. The volume fraction of the crushed salt (v_s) is given by

$$v_s = \frac{V_v + V_{i_s}}{V} \quad (2-92)$$

From Equations 2-90, 2-91, and 2-92, we have

$$V_v = \phi_s V_s = \phi_s \{V_v + V_{i_s}\} = \phi_s v_s V \quad (2-93)$$

Using Equation 2-93, the porosity of the mixture (ϕ) is

$$\phi = \frac{V_v}{V} = \phi_s v_s \quad (2-94)$$

Since the sum of the volume fractions equals one, i.e.,

$$\phi + v_{i_s} + v_m = 1 \quad (2-95)$$

the volume fraction of salt is given as

$$v_{i_s} = 1 - \phi - v_m \quad (2-96)$$

Therefore, the final volume of the crushed salt V_s^f , which is the same as the volume of solid salt, is obtained when $V_v = 0$ which implies that $\phi_s = 0$ and $\phi = 0$

$$V_s^f = V_{i_s} = v_{i_s} V \quad (2-97)$$

Thus, the final volume of the mixture is

$$V^f = V_{i_s} + V_m = v_{i_s} V + V_m \quad (2-98)$$

The volume fraction of the mixture remaining after full consolidation (v^f) is obtained by dividing Equation 2-98 by the volume (V) giving

$$v^f = v_{i_s} + v_m = 1 - \phi \quad (2-99)$$

The final volume fractions for salt (v_{is}^f) and the inert material (v_m^f) are then determined as

$$v_{is}^f = \frac{v_{is}}{v^f} \quad (2-100)$$

$$v_m^f = \frac{v_m}{v^f} \quad (2-101)$$

The final density and moduli of the mixture can then be determined from mixture theory as

$$\rho^f = v_{is}^f \rho_{is} + v_m^f \rho_m \quad (2-102)$$

$$K^f = v_{is}^f K_{is} + v_m^f K_m \quad (2-103)$$

$$G^f = v_{is}^f G_{is} + v_m^f G_m \quad (2-104)$$

2.3.3 Material Properties for Crushed Salt Mixtures

2.3.3.1 Crushed Salt/Bentonite Mixture

The functional forms of the crushed salt/bentonite mixture constitutive relations were selected to be the same as those present in Section 2.2 for crushed salt. However, the material parameters were modified based on available information to be more representative of the crushed salt/bentonite mixture. The nonlinear elastic parameter values describing the nonlinear moduli for a 70/30 percent by weight crushed salt/bentonite mixture defined in Equation 2-38 are given in Table 2-4. Table 2-4 also gives the initial and final or intact densities for the crushed salt/bentonite mixture. The final or intact material density was taken to be 2,260 kg/m³. Pfeifle [1990] gives a value of 2,266 kg/m³ for a 70/30 percent by weight crushed salt/bentonite mixture, assuming a solid density for salt of 2,120 kg/m³ and a solid density for bentonite of 2,700 kg/m³. The initial material density was selected such that the initial porosity of the crushed salt/bentonite mixture was the same as that assumed for the crushed salt. Because of the lack of test data for the elastic properties of the crushed salt/bentonite mixtures, the parameter values for the nonlinear elastic moduli were assumed to be the same as crushed salt. However, the K_1 and G_1 parameters were computed based on the final density value such that the ultimate moduli values (K_f and G_f) are reached when the mixture attains the final density.

Table 2-5 presents the parameter values for the creep consolidation constitutive equation given in Equation 2-52. The crushed salt/bentonite material parameters are taken from Pfeifle [1990]. The material parameter values for the creep consolidation model for the crushed salt/bentonite experiments conducted by Pfeifle [1990] at various moisture contents are given in Table 2-5. The property values labeled *Selected* represent the parameter value set chosen to represent the crushed

salt/bentonite backfill. These parameter values were selected because they represent the three tests performed by Pfeifle [1990] reasonably well; however, they do not represent the tests well over a wide range in pressures as discussed in the next paragraphs.

Table 2-4. Nonlinear Elastic Material Parameters for Crushed Salt/Bentonite

Parameter	Units	Value
K_0	MPa	0.01760 ^(a)
K_1	m ³ /kg	0.00945 ^(b)
G_0	MPa	0.01060 ^(a)
G_1	m ³ /kg	0.00945 ^(b)
K_f	MPa	20,626 ^(a)
G_f	MPa	12,423 ^(a)
ρ_0	kg/m ³	1,478.5 ^(c)
ρ_f	kg/m ³	2,260 ^(d)

- (a) Assumed identical to crushed salt (see Table 2-2).
- (b) Computed from Equation 2-38 using ρ_f with K_f and G_f values.
- (c) Computed so that initial porosity was identical to crushed salt.
- (d) Engineering estimate.

Table 2-5. Creep Consolidation Model Parameter Values for Crushed Salt/Bentonite

Test I.D.	Moisture Content (%)	Hydrostatic Pressure (MPa)	Parameter Values ^(a)		
			A (m ³ ·kg ⁻¹ × 10 ⁻³)	B ₀ (kg · m ⁻³ · s ⁻¹ × 10 ²¹)	B ₁ (MPa ⁻¹)
CS1	5.3	3.45 to 14	-33.9	0.972	.693
CS4	5.24	3.45 to 14	-34.5	1.021	.509
CS3	9.97	3.45 to 7	-30.3	0.970	.084
Selected Crushed Salt/Bentonite Values			-34.5	1.000	.600

- (a) CS1, CS4, and CS3 parameter values taken from Pfeifle [1990].

Figure 2-1 plots the log of the volumetric strain rate resulting from the parameter sets given in Table 2-5 for various fractional densities with an assumed applied pressure of 15 MPa. In this series of curves, the selected parameter values for crushed salt/bentonite seem to fairly well represent the parameter values given by Pfeifle [1990]. Since very little pressure build up is observed in the crushed salt until the backfill is nearly compacted, the parameter sets are also illustrated for lower pressures. Figure 2-2 illustrates the same information presented in Figure 2-1 except that the assumed applied pressure is 0.05 MPa. In this series of curves, the curve for the selected parameter values is similar to the lower curve that was generated with the parameter values labeled *CS4* in Table 2-5. Also note that the volumetric strain rates for the crushed salt/bentonite are higher than the crushed salt for low values of fractional density.

Figure 2-3 compares the change in volumetric strain rate with time for crushed salt and crushed salt/bentonite bodies under a constant pressure of 0.05 MPa. The parameter values for the crushed salt model given in Table 2-3 were derived by Sjaardema and Krieg [1987] based on hydrostatic consolidation tests conducted by Holcomb and Shields [1987] on crushed WIPP salt with added water. The test duration for these crushed salt tests was typically 23 days. The parameter values for the crushed salt/bentonite model given in Table 2-5 were derived by Pfeifle [1990] from multistage tests on crushed salt/bentonite mixtures with added water. Pfeifle's test durations ranged from 272 to 305 days, which included a final permeability measurement stage. The duration of Stage One in the tests ranged from 70 to 118 days. The curves in Figure 2-3 were generated using the analytical solution for creep consolidation given in Callahan [1990]. Figure 2-3 shows that the volumetric strain rate for the crushed salt/bentonite is higher than that of the crushed salt during early time with the strain rates for both decreasing with time. After about .01 year, the strain rate for the crushed salt/bentonite becomes less than the crushed salt strain rate.

2.3.3.2 Crushed Salt/TRU Waste Mixture

Material parameter values for crushed salt are given in Section 2.2.4. Therefore, to describe material properties for the crushed salt/TRU waste mixture, only the TRU waste properties need to be defined. Subsequently, mixture properties can be computed from the equations derived in Section 2.3.2.2. The TRU waste mixed with the crushed salt is assumed to consist of shredded metal wastes. The simulated metallic wastes tested by Butcher et al. [1991] included cut up steel, copper, lead, and aluminum scrap, and Butcher et al. [1991] assumed a solid density of 7,360 kg/m³. Additional discussion of probable metallic waste composition is given by Butcher [1989] where the assumed solid density of metallic waste is 7,860 kg/m³. Table 2-6 gives properties and assumed volume fractions of steel, aluminum, copper, lead, and tantalum [Butcher, 1990] used in this study. The composite material properties given in Table 2-6 are assumed to be representative of the shredded metallic waste. For crushed salt, an initial density of 1,400 kg/m³ is assumed. The

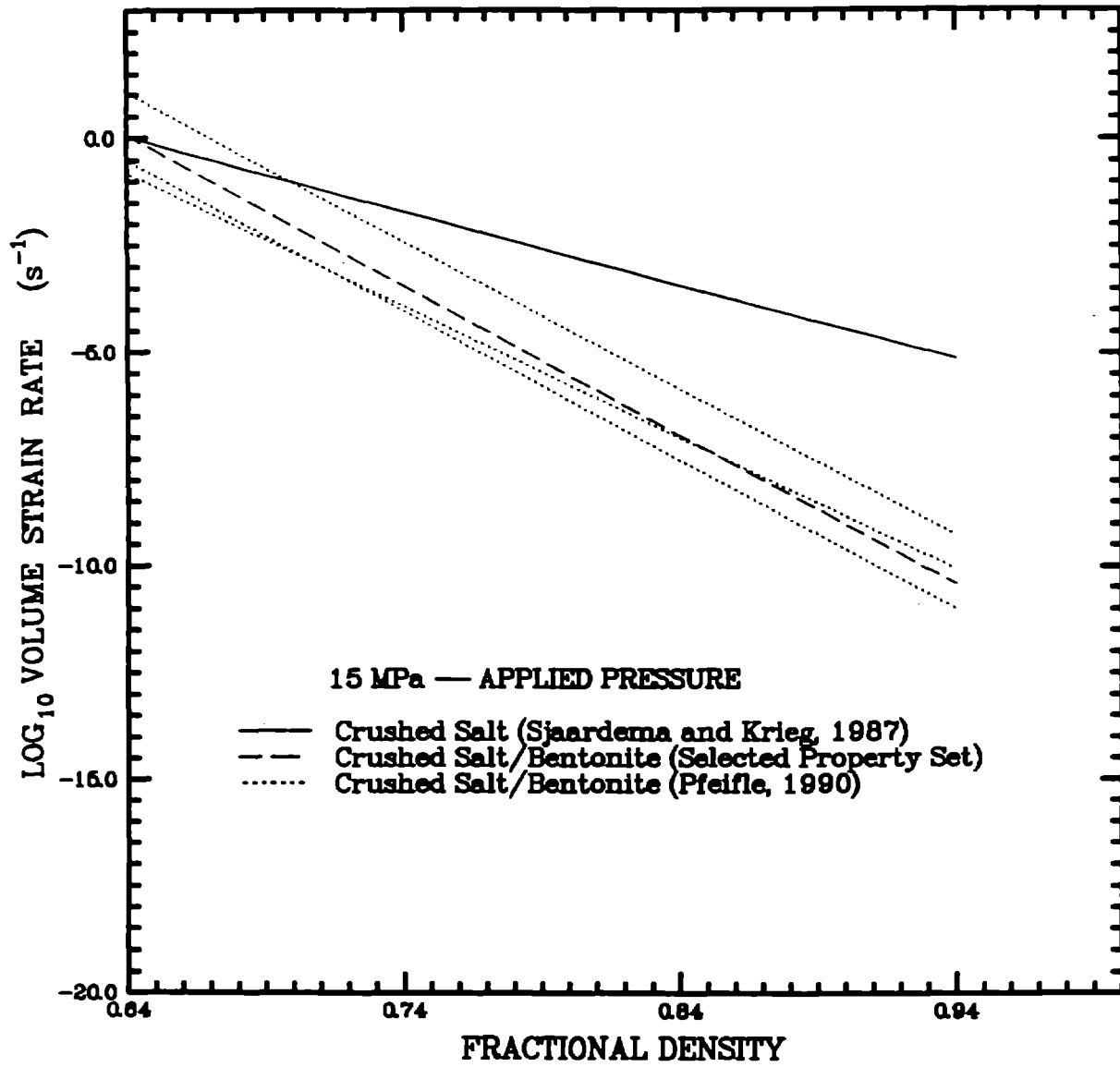


Figure 2-1. Volumetric Strain As a Function of Fractional Density for an Applied Pressure of 15 MPa.

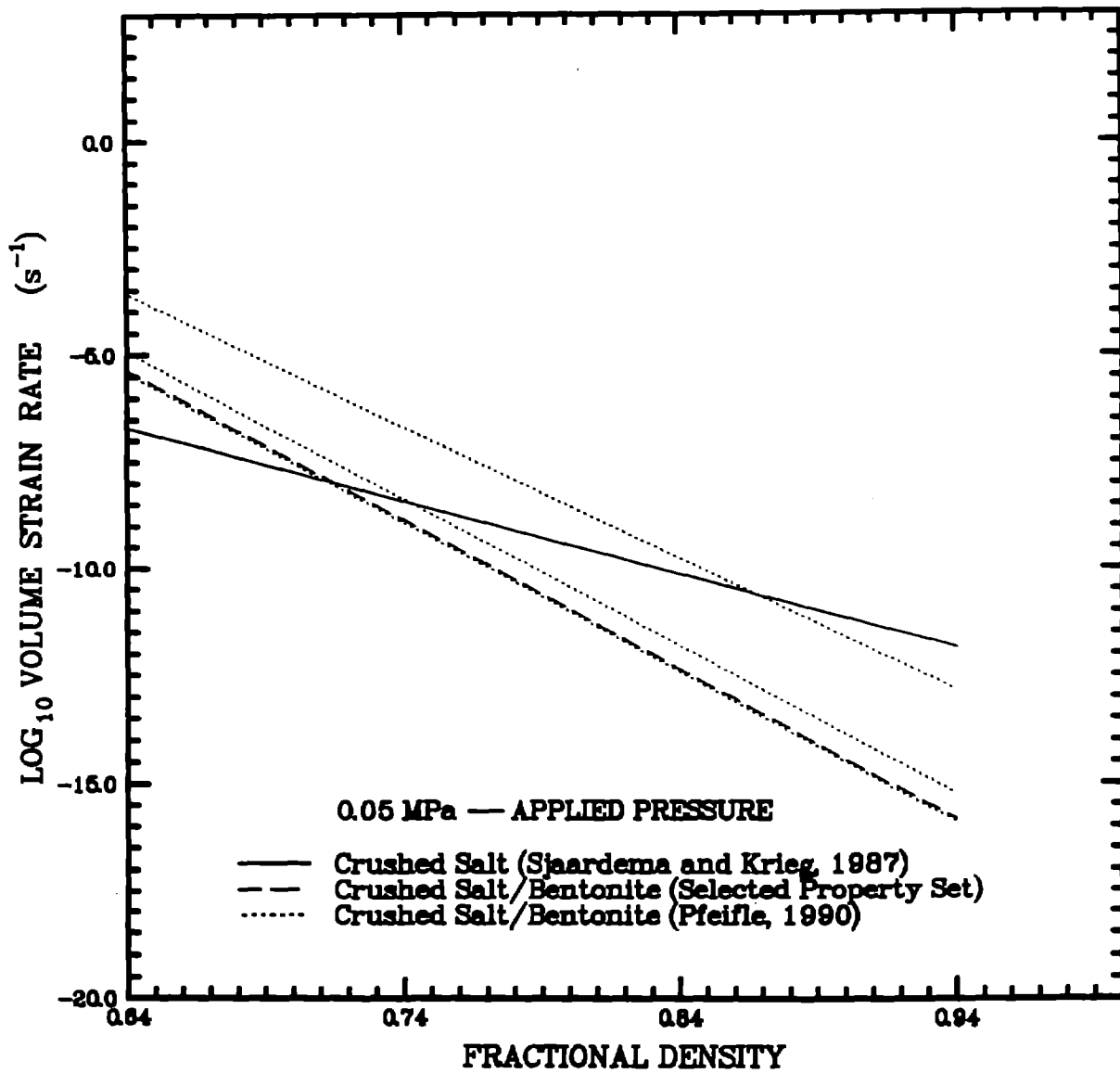


Figure 2-2. Volumetric Strain As a Function of Fractional Density for an Applied Pressure of 0.05 MPa.

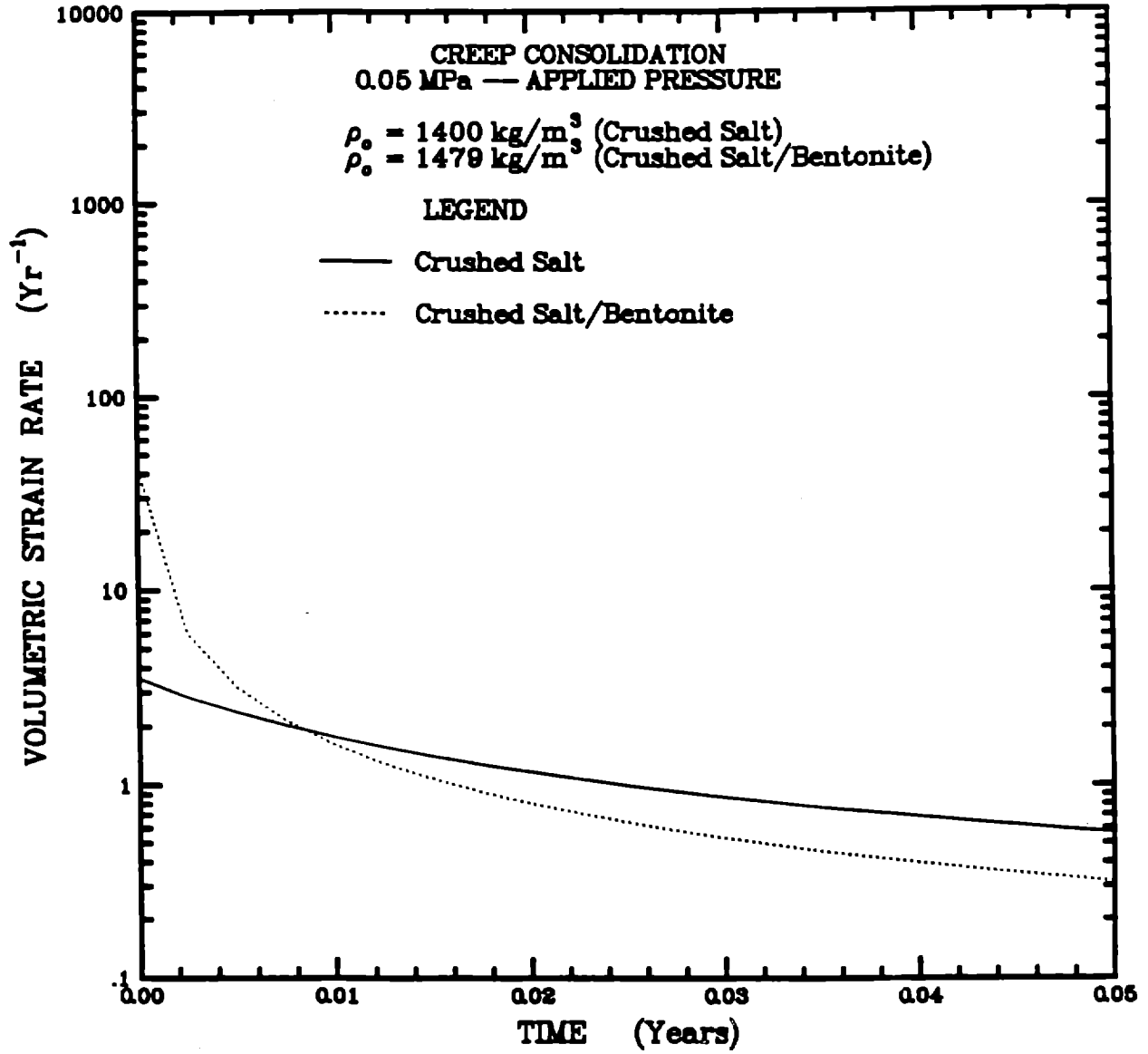


Figure 2-3. Change in Volumetric Strain Rate With Time for an Applied Pressure of 0.05 MPa.

initial crushed salt/shredded metal waste mix is assumed to be 80/20 percent by volume.

Table 2-6. Metallic Waste Components Properties

Component	Volume (%)	Density ($\text{kg} \times \text{m}^{-3}$)	Modulus of Elasticity (GPa)	Poisson's Ratio (—)	Shear Modulus ^(a) (GPa)	Bulk Modulus ^(b) (GPa)
Steel	64	7,860 ^(c)	207 ^(c)	0.27 ^(c)	81	150
Aluminum	14	2,700 ^(d)	69 ^(d)	0.33 ^(c)	26	68
Copper	11	8,960 ^(d)	117 ^(d)	0.34 ^(c)	44	122
Lead	7	11,350 ^(d)	14 ^(d)	0.30 ^(e)	5	12
Tantalum	4	16,600 ^(d)	186 ^(d)	0.27 ^(e)	73	135
Composite ^(f)	100	7,845	163	0.29	64	125

(a) Computed using $\frac{E}{2(1+\nu)}$.

(b) Computed using $\frac{E}{3(1-2\nu)}$.

(c) McClintock and Argon [1966].

(d) Lynch [1974].

(e) Engineering estimate.

(f) Computed using Equation 2-71.

From the given properties, the initial density and mass fractions can be computed using Equations 2-84, 2-88, and 2-89. Substituting the given values yields the initial density of the mixture $\rho_0 = 2,690 \text{ kg/m}^3$, mass fraction of the salt $m_s = 0.417$, and mass fraction of the shredded metallic waste $m_m = 0.584$. From Equations 2-91 and 2-94, initial values for the porosities of the salt and the mixture are found to be $\phi_s = 0.346$ and $\phi = 0.277$. From Equation 2-96, the volume fraction of solid salt is $v_{i_s} = 0.523$. Therefore, from Equations 2-99, 2-100, and 2-101, respectively, $v^f = 0.723$, $v_{i_s}^f = 0.724$, and $v_m^f = 0.277$. From Equations 2-102, 2-103, and 2-104, respectively, the final density is $\rho^f = 3,720 \text{ kg/m}^3$, the final bulk modulus is $K^f = 49,500 \text{ MPa}$, and the final shear modulus is $G^f = 26,600 \text{ MPa}$.

2.4 TRU WASTE

Two TRU waste forms are considered in this section: (1) a mixture of metallic, combustible, and sludge wastes and (2) a vitrified TRU waste. Two material models are required to characterize the behavior of these two TRU waste forms: (1) a

nonlinear elastic model to represent the composite TRU waste mixture and (2) a linear elastic model to represent the vitrified waste.

TRU waste forms are nonstandard and considerably variable in nature and quantity (e.g., see Butcher [1989]). TRU waste drums will be randomly placed within storage rooms at the WIPP site without regard to waste type. Wastes types may also be mixed within individual drums. Because of this random placement and mixture of wastes, it is necessary to assume that the waste drums can be characterized by a composite (or mechanically equivalent) waste drum. Therefore, a nonlinear elastic material model is developed to represent the composite TRU waste. Although TRU waste compaction is known to be irreversible, it is modeled as a nonlinear elastic material recognizing that the model is valid only if the load on the waste is monotonically increasing.

Vitrification is a possible waste treatment. Therefore, a model is developed to represent the glass-like substance resulting from a TRU vitrification process.

2.4.1 Nonlinear Elastic

As a first attempt, the nonlinear elastic model described in Section 2.2.2 was used to describe the behavior of a composite TRU waste. However, the functional form presented for the bulk modulus (Equation 2-38) did not adequately fit the simulated TRU waste compaction data. Therefore, an alternate functional form for the nonlinear elastic model was developed that fits the simulated TRU waste compaction data better. This model is

$$\sigma_a = \frac{1}{\kappa} \ln\left(\frac{\phi}{\phi_0}\right) \quad (2-105)$$

where

σ_a = axial stress, $\sigma_a = 3\sigma_m$

σ_m = mean stress

κ = material parameter

ϕ = porosity

ϕ_0 = initial porosity.

The assumption stated above (i.e., $\sigma_a = 3\sigma_m$) is significant. The need for this assumption stems from the fact that the experiments were conducted on the compaction of simulated waste in rigid steel sleeves [Butcher et al., 1991] and only the axial stress component was measured. To evaluate the parameter values for the TRU waste model, all three stress components need to be known. Two bounding assumptions to infer values for the lateral stress components are (1) the lateral stress components are zero (i.e., $\sigma_a = 3\sigma_m$) and (2) the lateral stress components are equal to the axial stress (i.e., $\sigma_a = \sigma_m/3$). Assumption 1 represents an unconfined test, and Assumption 2 represents a hydrostatic test. Neither assumption is correct

in the sense that it represents the conditions in the experiment; however, the two assumptions bound the true stress conditions. The first assumption was adopted because it provides the less stiff representation of the TRU waste. The less stiff representation is felt to be more conservative because it provides less resistance to room closure and lower back pressure on the surrounding backfill, which increases the time required to obtain lower porosities in the backfill surrounding the TRU waste.

In terms of porosity, Equation 2-105 may be stated as

$$\phi = \phi_0 \exp(\kappa \sigma_a) \quad (2-106)$$

Porosity and density are defined as

$$\phi = 1 - \frac{\rho}{\rho_f} \quad (2-107)$$

$$\rho = \frac{\rho_0}{1 + \epsilon_v} \quad (2-108)$$

where

ρ = current density

ρ_0 = initial density

ρ_f = final density or intact material density

ϵ_v = volumetric strain.

Parameters ϕ_0 and κ are found by fitting Equation 2-106 to axial stress/porosity data (Appendix A) using least squares methods. Equation 2-106 implies an initial porosity of ϕ_0 and a porosity that approaches zero as the compressive stress (compressive stress is taken to be negative) approaches infinity.

From the TRU waste compaction equation, expressions for the moduli need to be derived to complete the nonlinear elastic model. The tangent bulk modulus (K) can be stated as

$$K = \frac{d\sigma_m}{d\epsilon_v} = \frac{d\sigma_m}{d\phi} \frac{d\phi}{d\rho} \frac{d\rho}{d\epsilon_v} \quad (2-109)$$

Performing the differentiation indicated in Equation 2-109 on Equation 2-105 results in

$$K = \frac{\rho^2}{3\kappa\rho_0(\rho_f - \rho)} \quad (2-110)$$

From Equation 2-110, the initial bulk modulus (K_i) is

$$K_i = \frac{\rho_0}{3\kappa(\rho_f - \rho_0)} \quad (2-111)$$

Also note that the bulk modulus is infinite when the final density is reached. Therefore, from a practical standpoint, it is necessary to prescribe a final bulk modulus

value that corresponds to an intact material density that is less than ρ_f when performing analyses. Equation 2-110 may also be expressed in terms of the porosity as

$$K = \frac{(1 - \phi)^2 \rho_f}{3\kappa\phi\rho_0} \quad (2-112)$$

To derive a corresponding functional form for the shear modulus (G), a constant value for Poisson's ratio of $\nu = 0.25$ is assumed. Poisson's ratio expressed in terms of K and G is

$$\nu = \frac{3K - 2G}{6K + 2G} \quad (2-113)$$

Substituting the value for Poisson's ratio into Equation 2-113 and solving for G yields

$$G = \frac{3}{5}K \quad (2-114)$$

Therefore, using Equation 2-110, the expression for the shear modulus is

$$G = \frac{\rho^2}{3\lambda\rho_0(\rho_f - \rho)} \quad (2-115)$$

where $\lambda = \frac{5}{3}\kappa$.

With the nonlinear elastic moduli described by Equations 2-110 and 2-115, the nonlinear elastic model is completed using the procedure described in Section 2.2.1.

2.4.2 Vitrified Waste

Vitrified waste is assumed to be a linear elastic material. Therefore, the constitutive relation given in Section 2.1.1 also applies to the vitrified waste.

2.4.3 Material Properties for TRU Waste

The laboratory data used to determine the constitutive parameters for TRU waste compaction were obtained from Sandia National Laboratories (SNL). Tests were performed on three general types of simulated waste: combustible, metallic, and sludge wastes. The data consist of axial stress (σ_a) versus porosity (ϕ) pairs for each of the waste types and are reproduced in Appendix A. The assumption discussed in Section 2.4.1 (i.e., $\sigma_a = 3\sigma_m$) is applied to interpret and use the axial stress data. The experimental data and their corresponding fits to Equation 2-106 are shown in Figure 2-4. Because of the assumption discussed above, ordinate values in Figure 2-4 need to be divided by three to obtain information relating mean stress to porosity. Equation 2-106 fits the data quite well over most of the stress range; however, as seen in Figure 2-4, the fits are rather poor in the low-stress regime.

Table 2-7 contains parameters describing the individual waste types. The average solid densities for each of the waste types were obtained from Butcher et al.

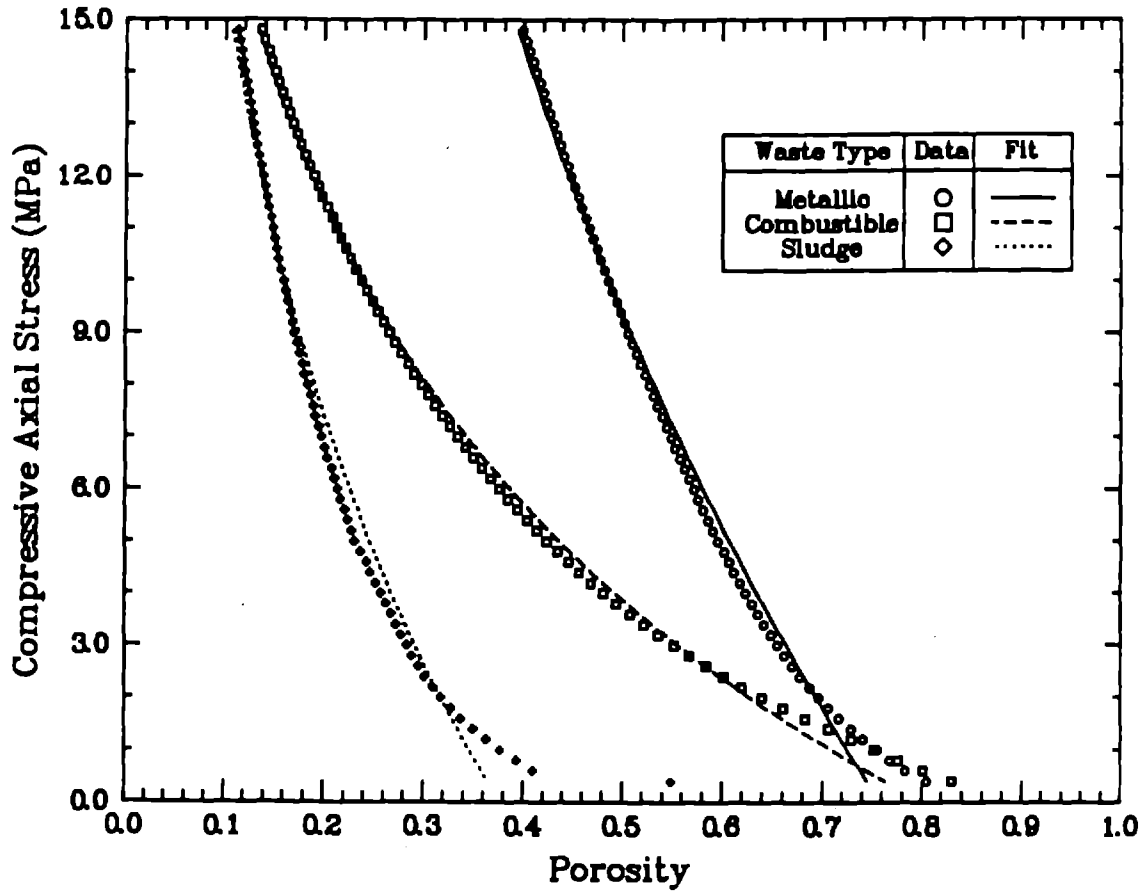


Figure 2-4. Compaction Data (Appendix A) and Fits for Individual Waste Types.

[1991]. The model parameters (ϕ_0 and κ) were determined for each of the waste types by fitting the experimental data to Equation 2-106. Initial densities were calculated from the solid density values and the fitted initial porosity values for each waste type using the following relationship:

$$\rho_0 = \rho_f (1 - \phi_0) \quad (2-116)$$

Table 2-7. Individual Waste Type Characteristics

Waste Type	Solid Density ρ_f (kg/m ³)	Initial Porosity ϕ_0	κ (MPa ⁻¹)	Initial Density ρ_0 (kg/m ³)
Combustible	1,920	0.801	0.121	383
Metallic	4,000	0.758	0.044	967
Sludge	2,370	0.377	0.085	1,480

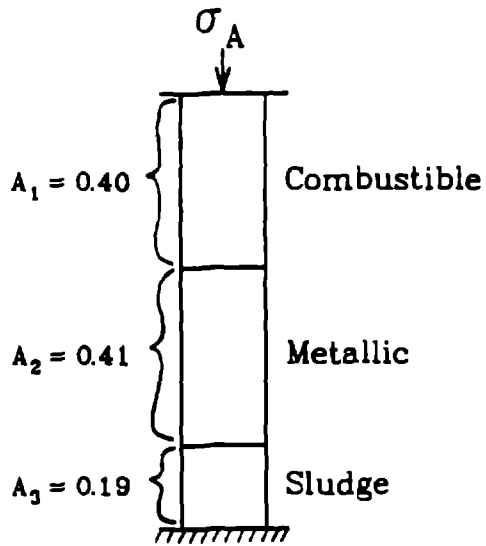
2.4.3.1 Models for Composite Waste Canisters

In this section, the waste drums are characterized by a composite (or mechanically equivalent) waste drum. A composite TRU waste drum as determined by Butcher et al. [1991] initially contains 40 percent combustible waste, 41 percent metallic waste, and 19 percent sludge waste by volume.

Two one-dimensional methods of combining the individual waste characteristics together to form a composite waste model are examined. The first model assumes that the three individual waste types are analogous to three nonlinear springs in series. The second model assumes that the three individual waste types are analogous to three nonlinear springs in parallel. Diagrams of the series and parallel models are shown in Figures 2-5 and 2-6, respectively. The following sections describe how stress/porosity data is generated and fitted to the nonlinear elastic functional form describing the waste.

Series Model

In the series model (Figure 2-5), the initial length of each spring is proportional to the initial volume fraction of the waste type it represents. Axial stress is assumed to be the same in all three materials and is equivalent to the stress in the composite model. Stress/porosity data pairs were generated at stress levels ranging from 0 to -25 MPa. The porosity for each of the individual waste types was found using Equation 2-106 and the parameter values in Table 2-7. The porosity of the

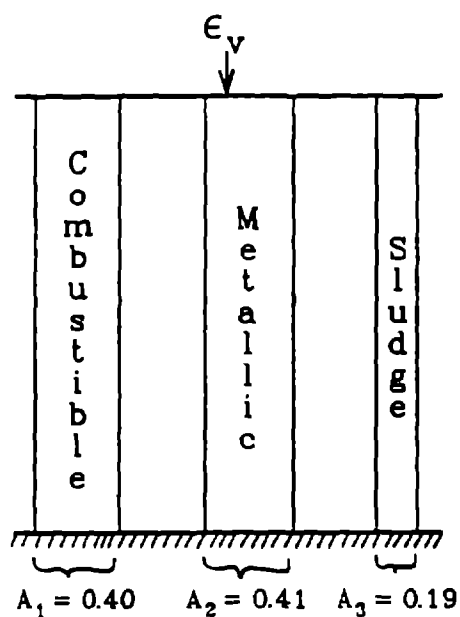


$$\sigma_A = \sigma_1 = \sigma_2 = \sigma_3$$

$$\epsilon_v = \frac{A_1 \epsilon_1 + A_2 \epsilon_2 + A_3 \epsilon_3}{A_1 + A_2 + A_3}$$

Note: Subscripts 1, 2, and 3 refer to the three waste components.

Figure 2-5. Composite Series Model.



$$\sigma_A = \frac{A_1\sigma_1 + A_2\sigma_2 + A_3\sigma_3}{A_1 + A_2 + A_3}$$

$$\epsilon_v = \epsilon_1 = \epsilon_2 = \epsilon_3$$

Note: Subscripts 1, 2, and 3 refer to the three waste components.

Figure 2-6. Composite Parallel Model.

composite series model was determined from

$$\phi = \frac{\text{Void Volume}}{\text{Total Volume}} = \frac{V - V_s}{V} \quad (2-117)$$

where V is the total volume at the current stress and is determined by

$$V = V_0 \sum_{i=1}^3 \frac{A_i \rho_{0i}}{\rho_{s,i} (1 - \phi_i)} \quad (2-118)$$

and V_s is the volume of solid materials and is determined from the individual wastes by

$$V_s = V_0 \sum_{i=1}^3 \frac{A_i \rho_{0i}}{\rho_{s,i}} \quad (2-119)$$

where

V_0 = initial volume of composite waste

A_i = initial volume percentage of waste type i

ρ_{0i} = initial density of waste type i

$\rho_{s,i}$ = solid density of waste type i

ϕ_i = porosity of waste type i , determined from Equation 2-106.

Parallel Model

The parallel model (Figure 2-6) assumes that the cross-sectional area of each spring is proportional to the original volume fraction of the waste type it represents. Each waste type is assumed to strain the same amount. Stress/porosity data pairs were generated at volumetric strain increments of the composite waste. Since the volumetric strain of each of the individual wastes is equivalent to the volumetric strain of the composite waste, the porosity of each component can be found from the following relationship

$$\phi_i = 1 - \frac{\rho_{0i}}{\rho_{s,i} (1 + \epsilon_v)} \quad (2-120)$$

where ϵ_v is the volumetric strain of the composite model. Note that since each of the individual wastes is modeled using Equation 2-106, the composite model can only be strained until one of the individual wastes approaches zero porosity. At this point, stress approaches infinity. In this case, the sludge waste is the first to approach zero porosity.

Once the individual porosities are known, Equations 2-117, 2-118, and 2-119 can be used to determine the porosity of the composite waste. The stress in each individual waste type can be found from Equation 2-106 as

$$\sigma_{a_i} = \frac{\ln(\phi_i) - \ln(\phi_{0i})}{\kappa_i} \quad (2-121)$$

The composite stress can then be determined from the individual stresses as

$$\sigma_a = \frac{\sum_{i=1}^3 A_i \sigma_{a_i}}{\sum_{i=1}^3 A_i} = \sum_{i=1}^3 A_i \sigma_{a_i} \quad (2-122)$$

2.4.3.2 Results

The generated stress/porosity data pairs for both models were fitted to the nonlinear functional form in Equation 2-106. The resulting parameters are shown in Table 2-8. Figure 2-7 shows the generated stress/porosity data pairs and the corresponding least squares fit for each model. The series model fits the nonlinear elastic functional form very well except at very low stresses. The parallel model, however, does not fit the functional form very well. Therefore, the series model was selected to represent the TRU waste. As the compressive stress approaches infinity, the functional form in Equation 2-106 approaches zero porosity; whereas, the parallel model data approaches a porosity of 0.52.

Table 2-8. Composite Waste Characteristics

Model	Solid Density ρ_f (kg/m ³)	Initial Porosity ϕ_0	κ (MPa ⁻¹)	Initial Density ρ_0 (kg/m ³)
Series	2,790	0.650	0.068	978
Parallel	2,790	0.637	0.169	1,010

The solid density of the composite waste is determined from the relationship

$$\rho_f = \frac{m}{V_s} = \frac{V_0 \sum_{i=1}^3 A_i \rho_{0_i}}{V_s} \quad (2-123)$$

where m is the mass of the composite waste and the solid volume, V_s , is found using Equation 2-119. Equation 2-116 can then be used to determine the initial density of the composite waste for each model. The calculated values of initial and solid densities for the two models are shown in Table 2-8.

2.4.3.3 Composite TRU Waste Properties

Series and parallel formulations are derived in the preceding sections to represent the composite TRU waste package. Since the series representation provides the best

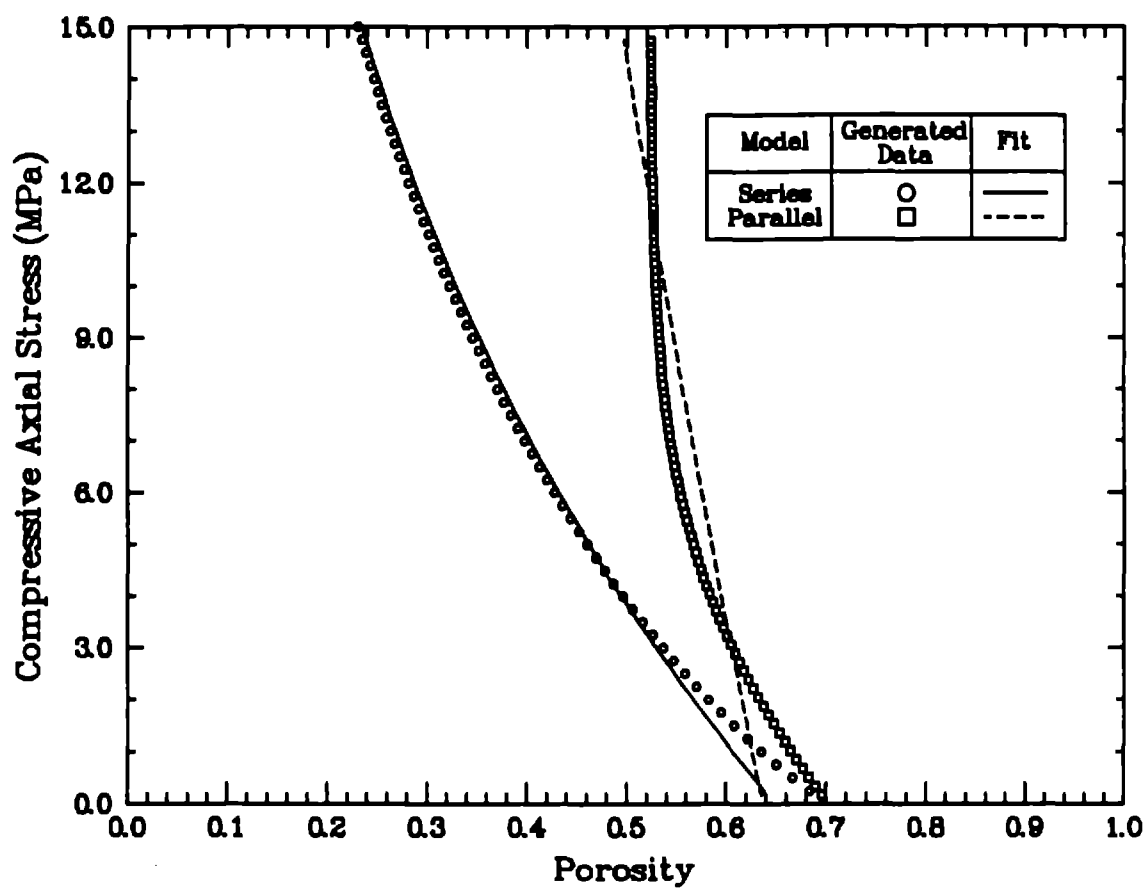


Figure 2-7. Generated Data and Fits for Composite Models.

fit to the simulated TRU waste compaction data, parameter values generated using the series model are chosen to represent the TRU waste. However, the parameter values require modification to represent the selected composite TRU waste. The composite TRU waste drum as determined by Butcher et al. [1991] initially contains 40 percent combustible waste, 41 percent metallic waste, and 19 percent sludge waste by volume. The drum weights and the average solid densities for each of the three waste types is taken from Butcher et al. [1991] and are shown in Table 2-9. The volume of the drum used for encapsulating the wastes is 0.21 m³ (55 gal). The volume of the solids is calculated by dividing the drum weight by the solid density, ρ_f (i.e., the density of fully compacted, consolidated waste). The initial density, ρ_o , is calculated by dividing the drum weight by the drum volume.

Table 2-9. TRU Waste Drum Characteristics

Waste Type	Drum Weight (kg)	Solid Density (kg/m ³)	Solids Volume (m ³)	Initial Density (kg/m ³)
Combustible	77.0	1,920	0.0401	367
Metallic	101.5	4,000	0.0254	483
Sludge	218.0	2,370	0.0920	1,038
Composite ^(a)	114.0	2,593	0.0439	542

(a) Based on Volumetric Distribution of 40 percent Combustible, 41 percent Metallic, and 19 percent Sludge.

Using the percentage volumetric distribution of waste types, the volume of solids in the "typical composite TRU waste package" is 0.044 m³. The weight and initial density of the composite TRU drum are 114 kg and 542 kg/m³, respectively. The solid density of the typical composite TRU waste drum (fully consolidated) can then be calculated to be 2,593 kg/m³. The initial porosity (void fraction), ϕ_o , is calculated from the Equation 2-120, which yields a value of 79 percent.

As shown in Table 2-8, the series model representation corresponds to an initial porosity of 0.65 and an initial density of 978 kg/m³; whereas, the selected representative composite TRU waste has an initial porosity of 0.79 and initial density of 542 kg/m³. Thus, a difference exists between the series model representation of the TRU waste and the described typical composite TRU waste package. The series model results in a poor estimate of initial density and porosity of the typical composite TRU waste package. If the appropriate initial density and porosity values of the typical composite TRU waste package are used, the least squares curve of the series model will not be followed. As a compromise resolution to this problem, the appropriate initial density value was deemed the most important parameter, and the product of κ and initial density was maintained constant. Thus, $\rho_o=542$ kg/m³

and $\kappa=0.122 \text{ MPa}^{-1}$ was used for the selected composite TRU waste. In addition, since the moduli are infinite when the final density is reached, a final density value of $2,599 \text{ kg/m}^3$ was selected so that the actual final density of $2,593 \text{ kg/m}^3$ could be attained without causing numerical difficulties.

In summary, the composite TRU waste has an initial density of 542 kg/m^3 , an initial porosity of 79 percent, and a final density of $2,599 \text{ kg/m}^3$. Equations 2-110 and 2-115 are used to compute the moduli as a function of density. The parameter values used in these equations are $\kappa=0.1224 \text{ MPa}^{-1}$ and $\lambda=0.2040 \text{ MPa}^{-1}$. Substitution of these values into Equations 2-110 and 2-115 gives values for the bulk and shear moduli of $5,442 \text{ MPa}$ and $3,265 \text{ MPa}$, respectively, at a density of $2,593 \text{ kg/m}^3$.

2.4.3.4 Vitrified Waste Properties

The linear elastic parameter values for the constitutive relation given in Equation 2-3 are given in Table 2-10. The vitrified waste material parameters are taken from McClintock and Argon [1966] for glass. Density of glasses range from about $2,200$ to $3,800 \text{ kg/m}^3$.

Table 2-10. Elastic Constants for Vitrified Waste

Parameter	Units	Value
E	MPa	67,560
ν	—	0.25

3.0 FINITE ELEMENT IDEALIZATION OF DISPOSAL ROOM

The finite element program SPECTROM-32 was used in this study to analyze the structural behavior of a hypothetical WIPP room for storing nonheat-producing transuranic (TRU) waste. The configuration modeled consists of an infinite series of disposal rooms 10.06 m wide by 4.0 m high and separated by pillars spaced at 40.54 m on center in the horizontal direction. Because one of the objectives of this study was to obtain results for comparison with the results obtained from similar calculations performed by Weatherby [1989] using SANCHO, geometric simplifications were made for consistency. The geometric simplifications made include:

1. The rooms were assumed to be located in a homogeneous layer of bedded salt thus eliminating the need to model the numerous stratigraphic layers present at the WIPP.
2. The deformation was assumed to be symmetric about a horizontal plane that passes through the center of the rib. Hence, the modeled region consists of the material above the symmetry plane.
3. The vertical extent of the region to be modeled was limited to 27 m above the room centerline. A boundary located this close to an excavation can be expected to influence the results; however, comparisons of the different backfill scenarios should not be compromised.

The finite element mesh used for all of the calculations presented in this report is shown in Figure 3-1. The finite element mesh contains 400 nodes and 399 four-node, quadrilateral elements. The finite element mesh is composed of three distinct regions that were used to represent the materials necessary to analyze the different room scenarios. The room detail given in Figure 3-1 shows the regions used to represent the TRU waste (if present) and the backfill materials. Region One is approximately a 4.69 m wide by 1.45 m high area in the lower left corner of the mesh. This model region represents the space occupied by the TRU waste. Region Two surrounds Region One and extends to the boundary of the room surface. Region Two was used to represent the backfill material that covers the waste. Regions One and Two comprise the disposal room and the remaining region represents the intact salt in the vicinity of the disposal room. The corners of the disposal room were assumed to be round (0.23 m radius) to match those at the WIPP site. The cross-sectional area of the waste and backfill regions are 6.77 m² and 3.28 m², respectively, yielding the total cross-sectional area for one-fourth of the disposal room of approximately 10.05 m². Symmetry conditions require no displacements normal to the boundary along the bottom, left, and right edges of the mesh. These kinematic constraints were prescribed as the boundary conditions for the mesh. The temperature throughout the modeled region was specified as 300 K.

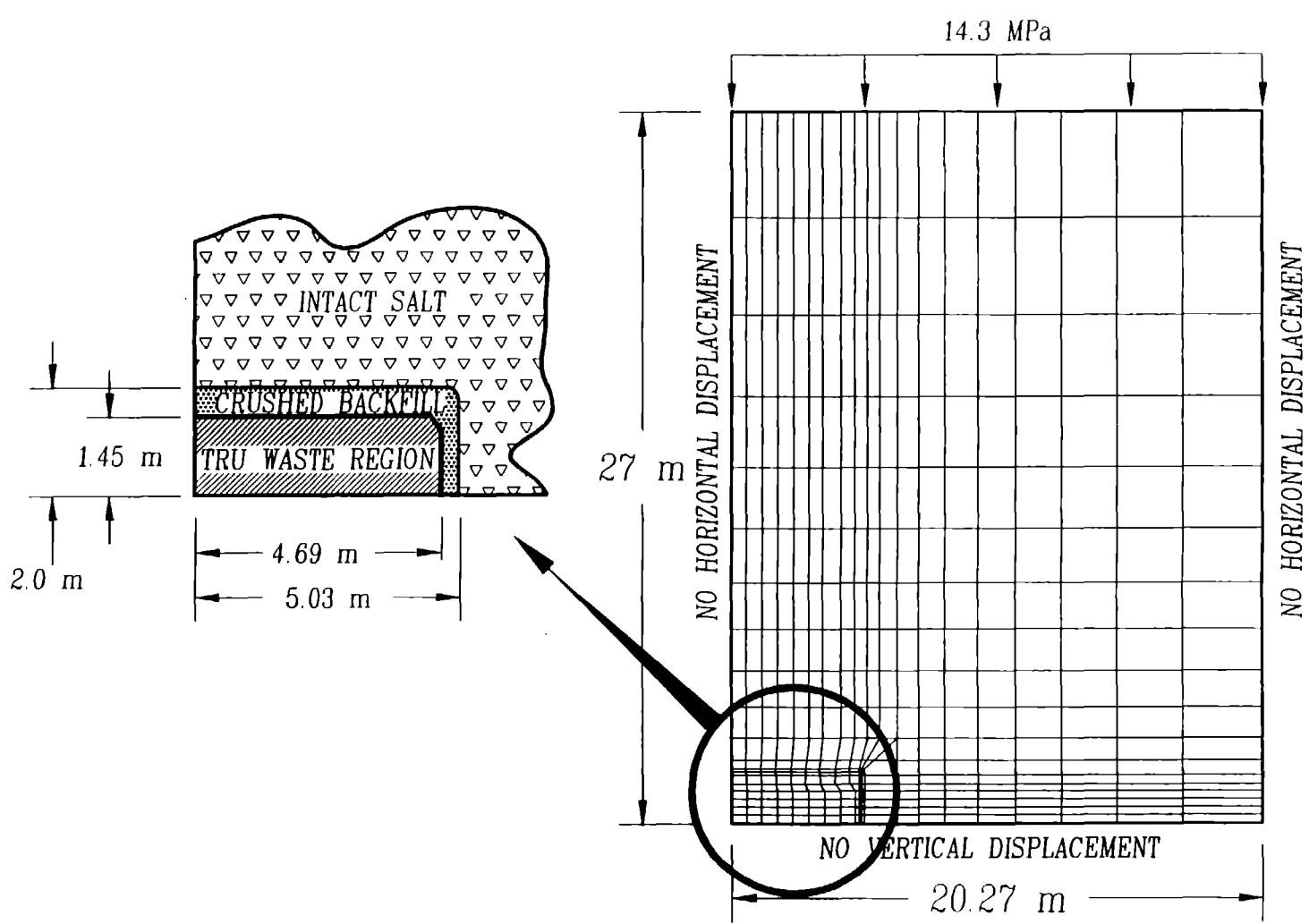


Figure 3-1. Finite Element Mesh of Disposal Room.

The initial stress field before excavation was assumed to be a homogeneous, lithostatic state of stress. The magnitude of the initial stress field was defined by prescribing a superincumbent overburden traction of 14.3 MPa as shown in Figure 3-1. Gravitational forces were neglected with lateral earth pressure coefficients equal to one. Therefore, the initial state of stress everywhere in the defined problem region was $\sigma_x = \sigma_y = \sigma_z = -14.3$ MPa. The initial stress condition for each of the analyses following excavation was established by excavating the disposal room into the host medium under the assumed lithostatic stress condition. Subsequently, the backfill was emplaced under stress-free conditions (i.e., body forces were neglected in the backfill). As a consequence of the assumed symmetry condition about the bottom boundary, the waste in the finite element model is located in the center of the room and is surrounded on all four sides by the backfill material. In the actual configuration, the waste will rest on the floor of the room and be surrounded by the backfill material on three sides.

4.0 RESULTS OF DISPOSAL ROOM ANALYSES

In this chapter, results are presented for six different room emplacement scenarios. Because these results are based on mechanical properties derived from a limited number of experiments and the constitutive models considered are currently in the development stage, results should be tempered with the validity of the specific properties and constitutive relations used to produce them. Numerical simulations of the different room emplacement scenarios were conducted assuming the following room contents.

1. Room completely filled with crushed salt.
2. Room completely filled with a 70 percent crushed salt — 30 percent bentonite (by weight) mixture.
3. TRU waste covered with crushed salt.
4. TRU waste covered with a 70 percent crushed salt — 30 percent bentonite (by weight) mixture.
5. An 80 percent crushed salt — 20 percent shredded metallic waste (by volume) mixture covered with crushed salt.
6. Vitrified waste covered with crushed salt.

The constitutive relations and material properties of the intact salt, backfill materials, and wastes used for these calculations are given in Chapter 2 and the finite element idealization is discussed in Chapter 3. In each of these analyses, the backfill and TRU waste were stress-free in the room at the beginning of the simulation (time = 0), and the creep deformation was simulated for 200 years. Additional details of each analysis and specific results are provided in the remainder of this chapter. Appendix B provides a comparison of selected results obtained from this study and those obtained by Weatherby [1989] and Weatherby and Brown [1990] using SANCHO for the first three aforementioned analyses. Appendix C includes history plots of void fraction and mean stress for each of the analyses.

4.1 ROOM FILLED WITH CRUSHED SALT

The closure of a room filled with crushed salt was analyzed assuming an initial density for the crushed salt to be approximately 65 percent of the intact density of salt. The initial and fully compacted densities specified for the crushed salt were $1,400 \text{ kg/m}^3$ and $2,140 \text{ kg/m}^3$, respectively. This corresponds to an initial void fraction of approximately 35 percent. During the course of the simulation, the volume of the crushed salt backfill was sufficiently reduced such that all of the

voids were removed and the density of the crushed salt reached the intact density of salt. When crushed salt elements attained the intact salt density, the crushed salt elements were changed to a creeping material obeying the Munson-Dawson constitutive model. The Munson-Dawson model parameter values used are the same as those for intact salt given in Chapter 2.

The room closure history of the disposal room backfilled with crushed salt is shown in Figure 4-1. In this figure and throughout this report, the horizontal closure is the change in the width at the midheight of the room expressed as a percentage of the original room width. Similarly, the vertical closure is the change in the height of the room at the center of the roof expressed as a percentage of the original room height. The maximum horizontal and vertical closures obtained for this analysis are 11 percent and 28 percent, respectively.

The void reduction in the disposal room expressed as a percentage of the initial void volume is shown in Figure 4-2 as a function of time. In this figure and throughout this report, the void reduction is the difference between the initial void volume and the current void volume expressed as a percentage of the initial void volume. Thus, the void reduction value will always be zero at the beginning of an analysis and will increase to 100 percent when the material becomes fully consolidated (voids are no longer present). The void reduction values were computed from the following relationship.

$$v = \frac{V_v^o - V_v}{V_v^o} \quad (4-1)$$

where

v = the void reduction in the element or region

V_v = the void volume in the element or region

V_v^o = the initial void volume inside the element or region.

As shown in Figure 4-2, 95 percent of the original void in the room is eliminated after approximately 19 years. The average void fractions presented in Appendix C were calculated using the following relationship:

$$v_f^o \equiv \frac{V_v}{V^o} = \frac{V_v^o + \Delta V}{V^o} \quad (4-2)$$

where

v_f^o = the void fraction in the element or region

V^o = the original volume of the element or region

ΔV = the difference between the current volume and the initial volume inside the element or region.

RSI-163-90-051

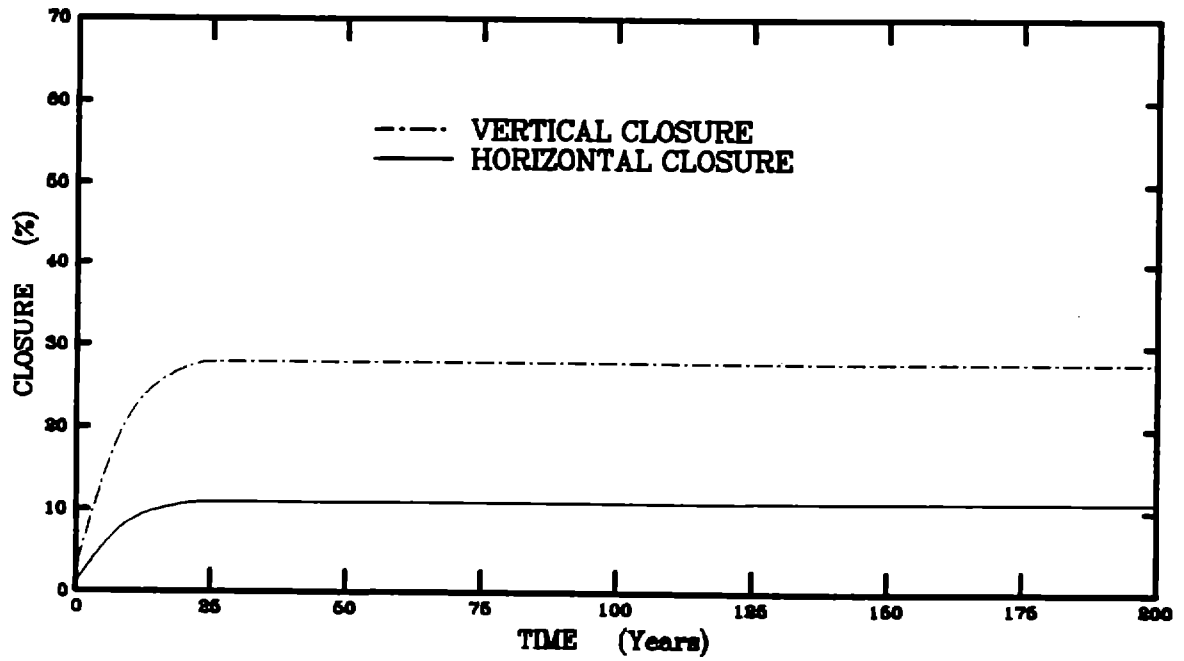


Figure 4-1. Room Closure History of a Disposal Room Filled With Crushed Salt.

RSI-163-90-052

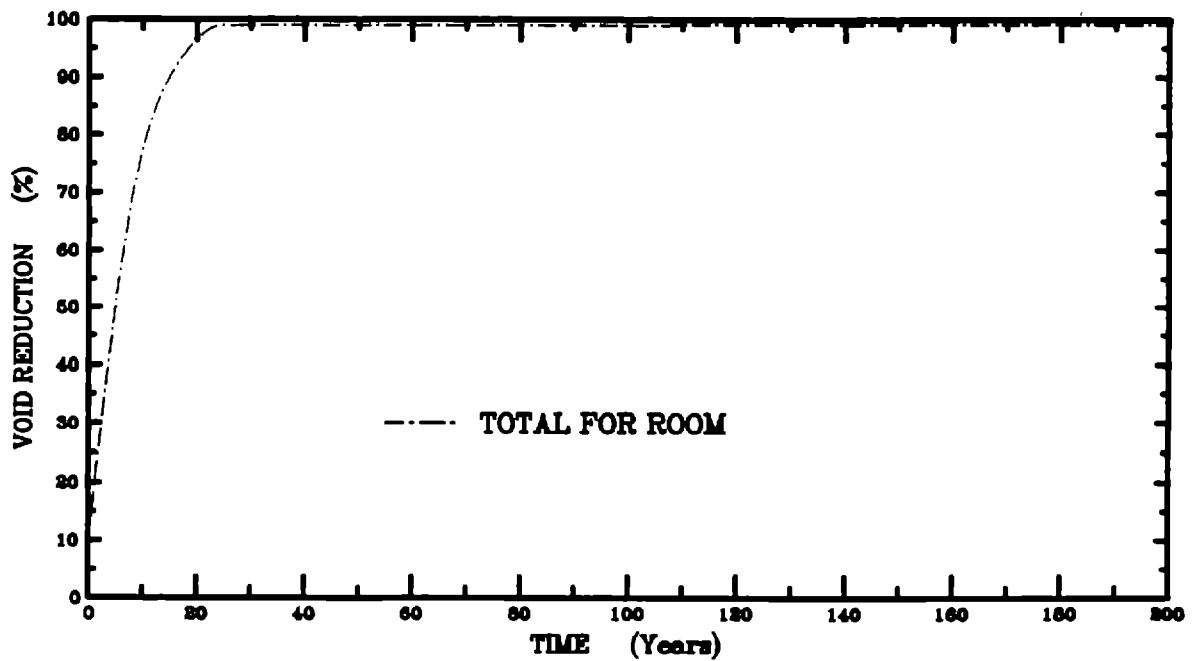


Figure 4-2. Void Reduction in the Disposal Room Filled With Crushed Salt as a Function of Time.

As illustrated in Appendix C, the average void fraction in the room decreases to 5 percent of the total room volume approximately 13 years after emplacement of the backfill. Note, however, that Weatherby [1989] used the current volume for V^o rather than the original volume. Therefore, his computed values are expected to be consistently higher than values computed using Equation 4-2 since the volume is decreasing.

The relationship between void fractions that are computed based on the initial volume and current volume can be easily developed. Equation 4-2 is written for the void fraction v_f in terms of the current volume as

$$v_f = \frac{V_v}{V^o + \Delta V} = \frac{V_v^o + \Delta V}{V^o + \Delta V} \quad (4-3)$$

From Equation 4-2, the volume change may be computed as

$$\Delta V = v_f^o V^o - V_v^o \quad (4-4)$$

The void fraction based on current volume is obtained by substituting Equation 4-4 into Equation 4-3, which gives

$$v_f = \frac{v_f^o V^o}{V^o (1 + v_f^o) - V_v^o} \quad (4-5)$$

Dividing the numerator and denominator in Equation 4-5 by the initial volume, V^o , and noting that the initial porosity is $\phi_0 = \frac{V_v^o}{V^o}$ gives

$$v_f = \frac{v_f^o}{1 + v_f^o - \phi_0} \quad (4-6)$$

When a two component backfill system such as TRU waste (superscript t) and crushed salt (superscript c) is considered, Equation 4-6 can be used to develop the void fraction equations based on the current volume. Assuming that the void fractions based on the initial volume for the TRU waste and crushed salt regions (i.e., $v_f^{t^o}$ and $v_f^{c^o}$) are known from Equation 4-2, the void fractions in the TRU waste and crushed salt based on the current volume are

$$v_f^t = \frac{v_f^{t^o}}{1 + v_f^{t^o} - \phi_0^t} \quad (4-7)$$

$$v_f^c = \frac{v_f^{c^o}}{1 + v_f^{c^o} - \phi_0^c} \quad (4-8)$$

where ϕ_0^t and ϕ_0^c are the initial porosities for the TRU waste and crushed salt regions, respectively.

The total room void fraction (superscript r) can be computed on a volume-weighted basis from the TRU waste and crushed salt void fractions based on their current volumes

$$v_f^r = \frac{v_f^t V^t + v_f^c V^c}{V^t + V^c} \quad (4-9)$$

The current volumes of the TRU waste and the crushed salt are

$$V^t = V^{t^o} + \Delta V^t \quad (4-10)$$

$$V^c = V^{c^o} + \Delta V^c \quad (4-11)$$

where

V^{c^o} = initial volume of the backfill element or region

V^{t^o} = initial volume of the waste element or region

ΔV^c = volume change of the backfill element or region

ΔV^t = volume change of the waste element or region.

From Equation 4-4, Equations 4-10 and 4-11 become

$$V^t = V^{t^o} (1 + v_f^{t^o}) - V_v^{t^o} \quad (4-12)$$

$$V^c = V^{c^o} (1 + v_f^{c^o}) - V_v^{c^o} \quad (4-13)$$

where

$V_v^{c^o}$ = initial void volume of the backfill element or region

$V_v^{t^o}$ = initial void volume of the waste element or region.

Substituting Equations 4-12 and 4-13 into Equation 4-9 gives the void fraction for the room based on the current volume of the room.

4.2 ROOM FILLED WITH CRUSHED SALT/BENTONITE

The closure of a room filled with a crushed salt/bentonite mixture (70 percent crushed salt and 30 percent bentonite by weight) was simulated for 200 years. The initial density and fully compacted or final density of the crushed salt/bentonite mixture used in this calculation was 1,478.5 kg/m³ and 2,260 kg/m³, respectively, which corresponds to an initial void fraction of approximately 35 percent (the same as that used for the crushed salt backfill calculations). In this simulation, the crushed salt/bentonite backfill did not consolidate sufficiently to reduce all of the voids and the fully consolidated density was not reached.

The horizontal and vertical closures of the disposal room backfilled with crushed salt are shown in Figure 4-3. The maximum horizontal and vertical closures obtained are 10 percent and 24 percent, respectively. Comparing these results with the crushed salt results in Figure 4-1 shows that the crushed salt and crushed salt/bentonite closures are nearly the same in both magnitude and rate for the first 5 years. This indicates that the room closure is primarily driven by the initial state of stress in the host rock formation and that there is little host rock — backfill interaction during the first 5 years. Thereafter, the crushed salt/bentonite backfill room closure rates become significantly less than the crushed salt backfill room closure rates until about 23 years when the crushed salt is essentially fully compacted. After 23 years, the crushed salt backfill room closure rate is close to zero and closure is virtually complete; the crushed salt/bentonite backfill room closure rate is nonzero but small and closure continues. Thus, the crushed salt/bentonite room closures accumulate slowly and approach the fully compacted, crushed salt room closures asymptotically. Since the crushed salt and crushed salt/bentonite backfilled rooms were both at the same initial void fractions, the ultimate or final state of closures of each should be the same. The comparison of closure rates between crushed salt and crushed salt/bentonite backfills may be better understood using Figures 2-1 through 2-3. These figures compare the volumetric strain rates for simple constant stress situations. The crushed salt/bentonite consolidation rates are initially greater than those of the crushed salt and eventually become significantly less which causes the crushed salt/bentonite backfill to approach full consolidation at a much slower rate than crushed salt.

The void reduction in the disposal room expressed as a percentage of the total initial void volume is shown in Figure 4-4 as a function of time. As shown in Figure 4-4, approximately 14 percent of the original void volume remains in the room after 200 years. Comparison of the crushed salt (Figure 4-2) and crushed salt/bentonite void reductions again shows the much slower rate at which the crushed salt/bentonite backfill approaches full consolidation. As illustrated in Appendix C, the average void fraction reached 5 percent after approximately 191 years.

4.3 ROOM FILLED WITH TRU WASTE AND CRUSHED SALT

The closure of a room filled with TRU waste surrounded by crushed salt was simulated for a 200-year period. The initial and fully compacted densities used in this calculation for the TRU waste were 542 kg/m³ and 2,593 kg/m³, respectively, corresponding to an initial void fraction of approximately 79 percent. The initial and fully compacted densities specified for the crushed salt were 1,400 kg/m³ and 2,140 kg/m³, respectively, corresponding to an initial void fraction of approximately 35 percent. The crushed salt was changed to a creeping material obeying the Munson-Dawson constitutive model when the volume of the crushed salt was sufficiently reduced such that all of the voids were removed and the density reached the intact density of salt. The Munson-Dawson model parameter values used are the same as

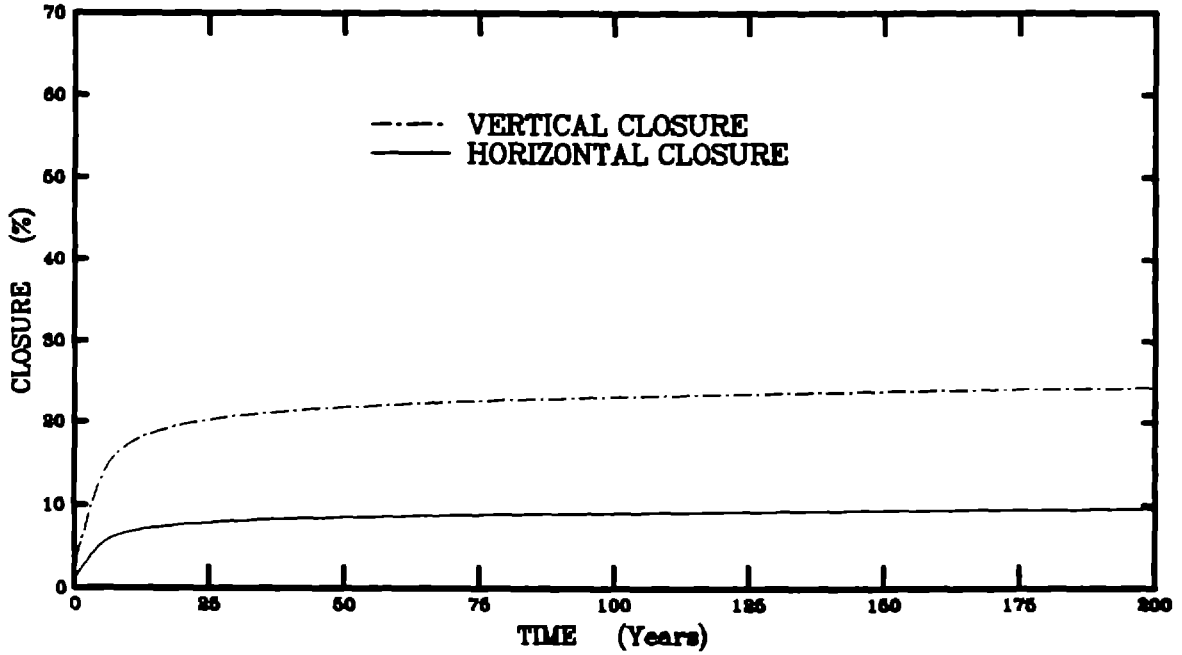


Figure 4-3. Room Closure History of a Disposal Room Filled With Crushed Salt/Bentonite.

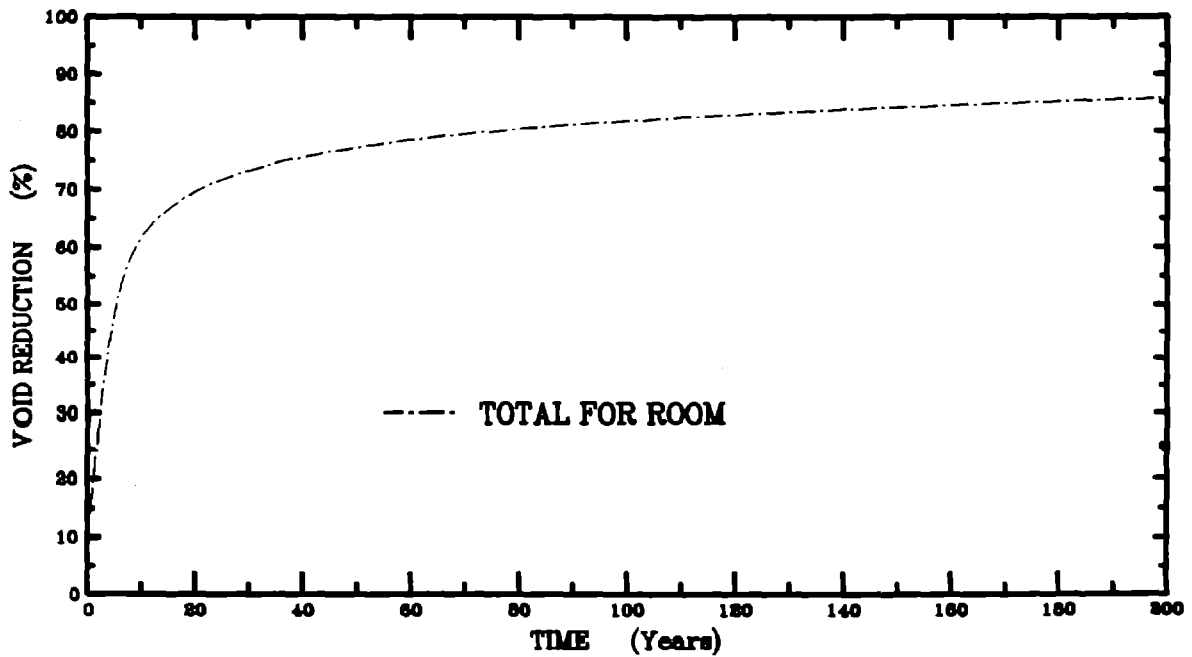


Figure 4-4. Void Reduction in the Disposal Room Filled With Crushed Salt/Bentonite as a Function of Time.

those for intact salt given in Chapter 2. Thus, following complete consolidation, the crushed salt becomes intact salt. Initially, the stiffnesses of the crushed salt and TRU waste are very low compared to the host salt formation and the initial porosity of the TRU waste is very high (79 percent) compared with the crushed salt (35 percent). Therefore, very little resistance to room closure is provided by the backfill and waste. As the crushed salt and TRU waste compact, they become stiffer and provide stabilizing forces for the underground structure and reduce the room closure rate. However, the stiffness of the TRU waste remains quite low until it is compacted to within 80 percent of its fully compacted density. Because the stiffness of the TRU waste is low, little support is provided for the crushed salt backfill, and the rate of consolidation of the crushed salt is slower than when the room is completely filled with crushed salt.

The horizontal and vertical closures of the disposal room backfilled with TRU waste and crushed salt are shown in Figure 4-5. The maximum horizontal and vertical closures obtained are 21 percent and 54 percent, respectively. Comparing these closure results with the closure results obtained for the room completely filled with crushed salt (Figure 4-1) shows that the crushed salt and crushed salt/TRU waste closures are nearly the same in both magnitude and rate for the first 5 years. This supports the earlier supposition that there is little interaction between the host rock formation and the room contents during this initial period. When the TRU waste, which has an initial void ratio of 79 percent, is present in the room, the closure rates remain large until about 50 years. At 50 years, the average void fraction in the TRU waste is about 7 percent, and the TRU waste has become stiffer and provides more resistance to room closure.

The void reduction in the waste region, backfill region, and for the entire disposal room expressed as a percentage of the total initial void volume of the respective regions are shown in Figure 4-6 as a function of time. The percent void reduction for each region was computed using Equation 4-1. Comparison of Figure 4-6 with Figure 4-2 for the crushed salt further supports the observation made above with regard to room closure rates and backfill interaction. During the simulation period, the contents of the backfilled region were changed to intact salt one element at a time upon full consolidation. During the 200 years simulated, all of the crushed salt became fully consolidated except for a small region in the corner of the room. Similarly, all the void in the waste was virtually eliminated; however, the waste required considerably more time to reach a fully compacted state. Approximately 30 years were required to reduce the void volume to 95 percent of the initial void volume for the crushed salt, while 68 years were required for the TRU waste. As shown in Figure 4-6, the combined contents of the room required approximately 60 years to reduce the void volume by 95 percent. As illustrated in Appendix C, the average void fraction reached 5 percent in the backfill region, waste region, and in the room after 15, 60, and 50 years, respectively.

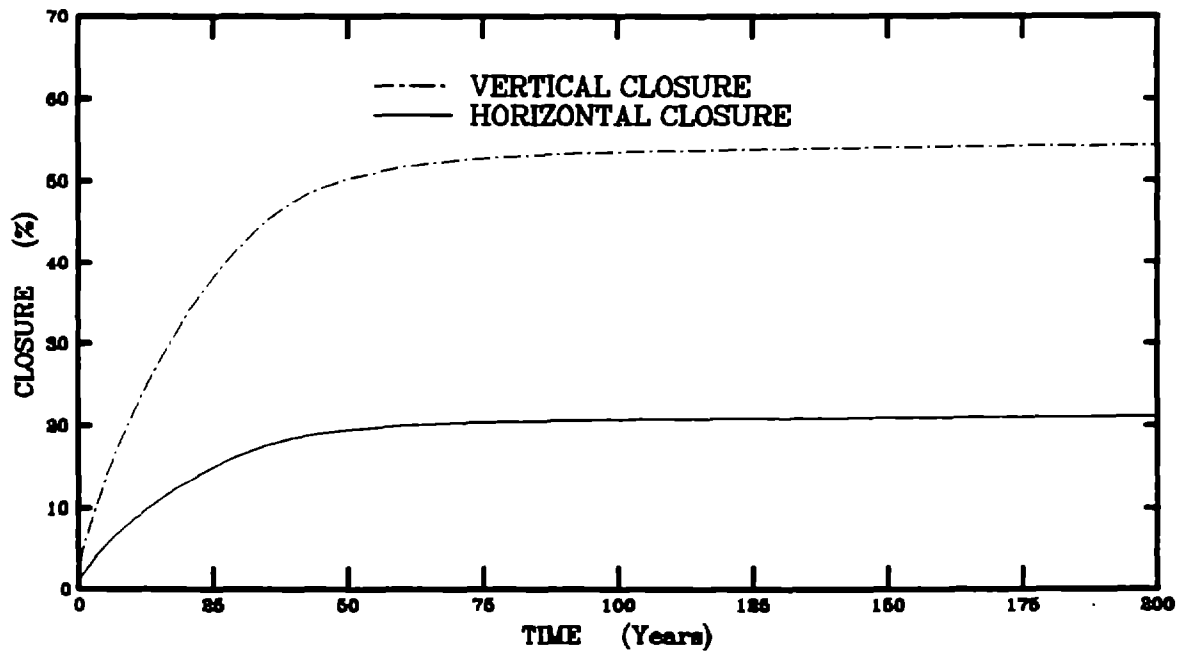


Figure 4-5. Room Closure History of a Disposal Room Filled With TRU Waste and Crushed Salt.

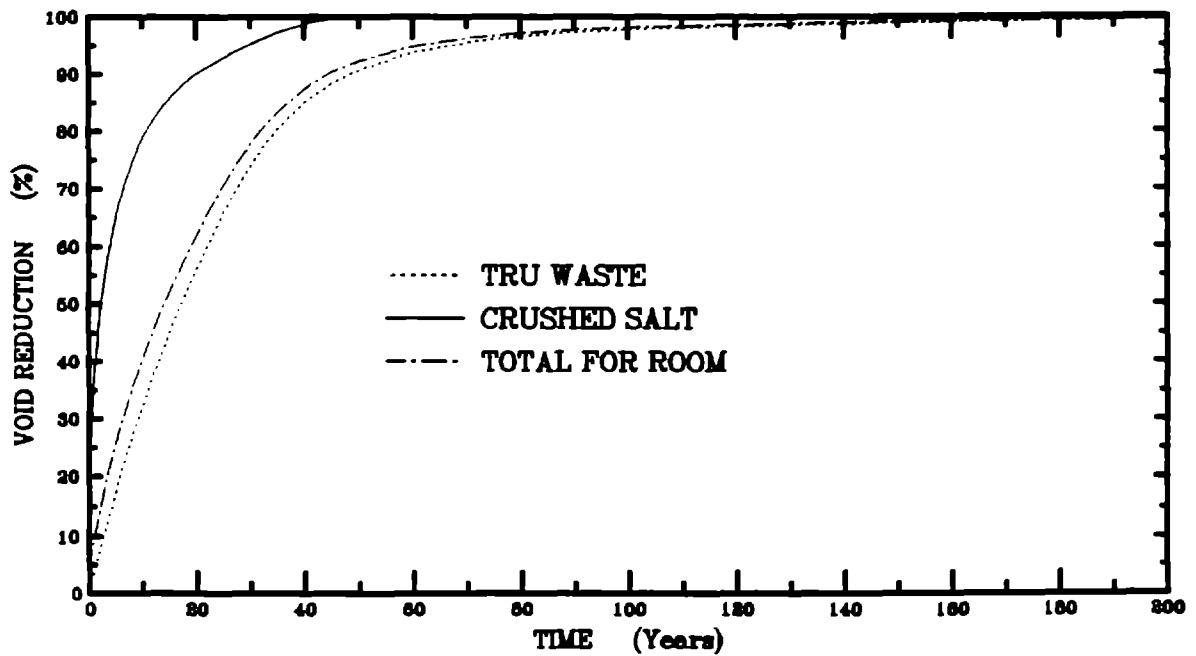


Figure 4-6. Void Reduction in the Disposal Room Filled With TRU Waste and Crushed Salt as a Function of Time.

4.4 ROOM FILLED WITH TRU WASTE AND CRUSHED SALT/BENTONITE

The closure of a room filled with TRU waste surrounded by a crushed salt/bentonite mixture was simulated for a 200-year period. The initial and fully compacted densities for the TRU waste used in this calculation were 542 kg/m^3 and $2,593 \text{ kg/m}^3$, respectively, corresponding to an initial void fraction of approximately 79 percent. The initial and fully compacted densities specified for the crushed salt/bentonite mixture were $1,478.5 \text{ kg/m}^3$ and $2,260 \text{ kg/m}^3$, respectively, corresponding to an initial void fraction of approximately 35 percent. During the simulation, the volume of ten crushed salt/bentonite material elements were sufficiently reduced such that all of the voids were removed and the density reached the intact density of the fully consolidated salt/bentonite mixture. For this analysis, the crushed salt/bentonite was changed to a nonlinear elastic material following complete consolidation. The elastic properties for a mixture of crushed salt and bentonite are given in Chapter 2.

The horizontal and vertical closures of the disposal room backfilled with TRU waste and crushed salt are shown in Figure 4-7. The maximum horizontal and vertical closures obtained are 18 percent and 55 percent, respectively. As discussed previously, the room closure rates and magnitudes during the initial 5-year period are essentially the same as in the other analyses. The void reduction in the waste region, backfill region, and for the entire disposal room expressed as a percentage of the total initial void volume of the respective regions are shown in Figure 4-8 as a function of time. The percent void reduction for each region was computed using Equation 4-1. During the 200 years simulated, little of the crushed salt/bentonite backfill or the TRU waste became fully consolidated. After 200 years, the initial void volume was reduced by 87 percent for the crushed salt/bentonite, 93 percent for the TRU waste. As shown in Figure 4-8, the void volume of the total combined contents of the room was ultimately reduced by 92 percent. As illustrated in Appendix C, the average void fractions in the backfill region, waste region, and in the room after 200 years are 4.4 percent, 5.4 percent, and 5.1 percent, respectively.

4.5 ROOM FILLED WITH VITRIFIED WASTE AND CRUSHED SALT

The closure of a room filled with vitrified waste surrounded by crushed salt was analyzed assuming an initial density for the crushed salt to be 65 percent of the density of intact salt. The initial and fully compacted densities specified for the crushed salt were $1,400 \text{ kg/m}^3$ and $2,140 \text{ kg/m}^3$, respectively. This corresponds to an initial void fraction of approximately 35 percent. The vitrified waste was modeled as a linearly elastic material as described in Chapter 2. In this simulation, the crushed salt backfill consolidated sufficiently to remove all of the voids, and the density of the crushed salt reached the intact density of salt. At this point in the simulation, the crushed salt was changed to a creeping material obeying the

RSI-163-90-057

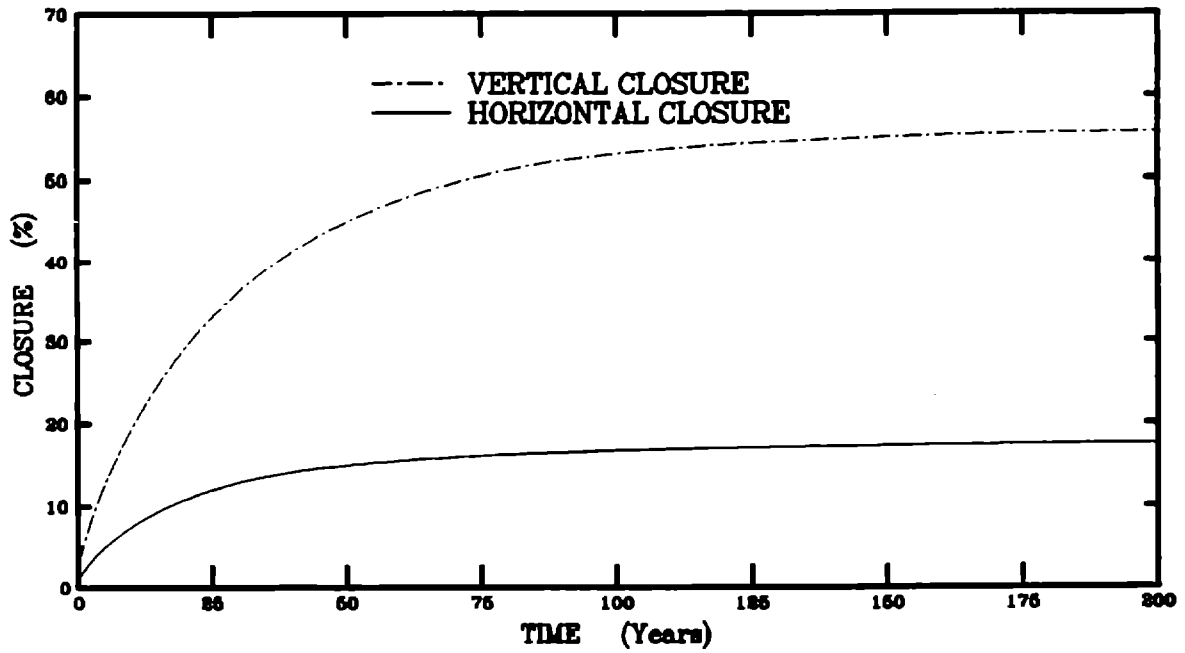


Figure 4-7. Room Closure History of a Disposal Room Filled With TRU Waste and Crushed Salt/Bentonite.

RSI-163-90-058

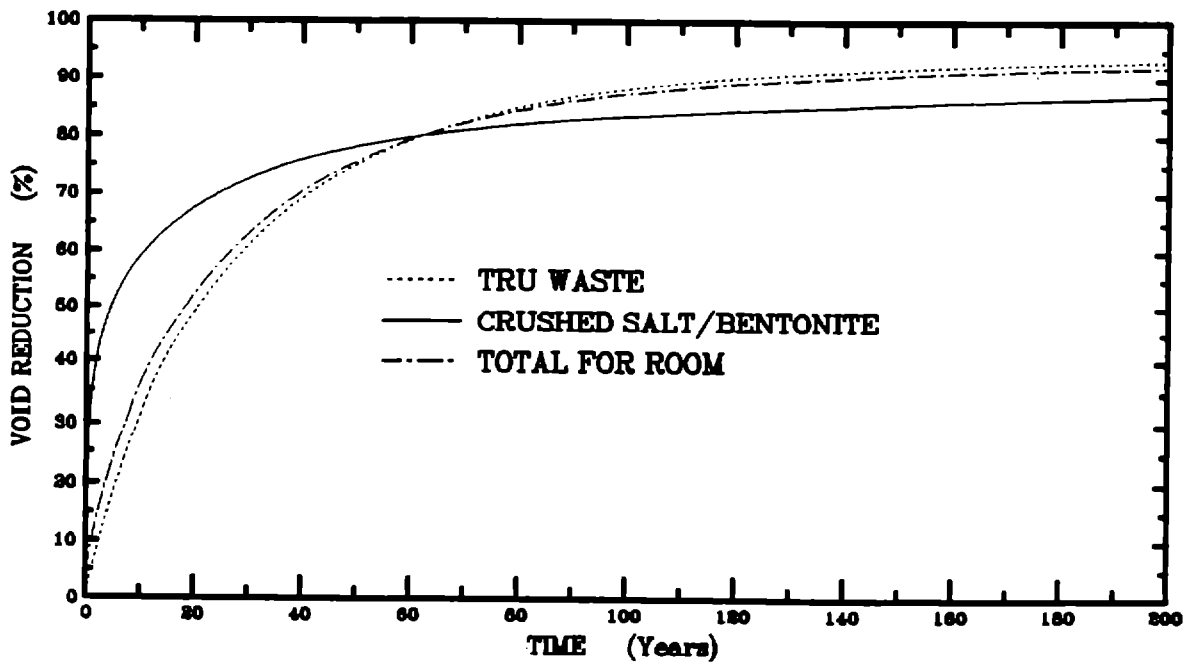


Figure 4-8. Void Reduction in the Disposal Room Filled With TRU Waste and Crushed Salt/Bentonite as a Function of Time.

Munson-Dawson constitutive model. The Munson-Dawson model parameter values used are the same as those given for intact salt in Chapter 2.

The horizontal and vertical closures of the disposal room backfilled with vitrified waste and crushed salt are shown in Figure 4-9. The maximum horizontal and vertical closures obtained are 2.4 percent and 9.4 percent, respectively. These closures are substantially less than the other cases examined which illustrates the effect of a stiff TRU waste component with zero initial porosity. In this case, with the stiff TRU waste component, the waste and backfill interact with the host rock formation earlier in time. Comparing Figure 4-9 with the closure results from the other analyses shows that the vitrified waste and backfill have little effect on the host rock deformation for approximately 1 year; whereas, the other cases show little impact for approximately 5 years. The stiffness of the vitrified waste provides the mechanism for more rapid consolidation of the surrounding crushed salt backfill and subsequent back pressure on the host formation, which slows the rate of deformation and reduces the overall magnitude of room closure. As shown in Figure 4-10, 95 percent of the void in the region filled with crushed salt is eliminated after 13 years. As illustrated in Appendix C, the average void fraction reaches 5 percent in the backfill region within 6 years.

4.6 ROOM FILLED WITH CRUSHED SALT AND SHREDDED METAL MIXED WITH CRUSHED SALT

The closure of a room filled with shredded metallic waste mixed with crushed salt was analyzed assuming the mixture contained 80 percent crushed salt and 20 percent metallic waste by volume. The shredded metal/crushed salt mixture was surrounded on all sides by crushed salt. The initial and fully compacted densities specified for the crushed salt were 1,400 kg/m³ and 2,140 kg/m³, respectively. This corresponds to an initial void fraction of approximately 35 percent. The initial and fully compacted densities specified for the crushed salt/shredded metal mixture were 2,689 kg/m³ and 3,717 kg/m³, respectively. This corresponds to an initial void fraction of approximately 28 percent. During the simulation, the shredded metal/crushed salt mixture and the crushed salt backfill consolidated sufficiently to remove all of the voids. When the crushed salt and shredded metal/crushed salt elements attained their respective intact densities, the elements were changed to a creeping material obeying the Munson-Dawson constitutive model. The Munson-Dawson model parameter values used are the same as those given for intact salt in Chapter 2.

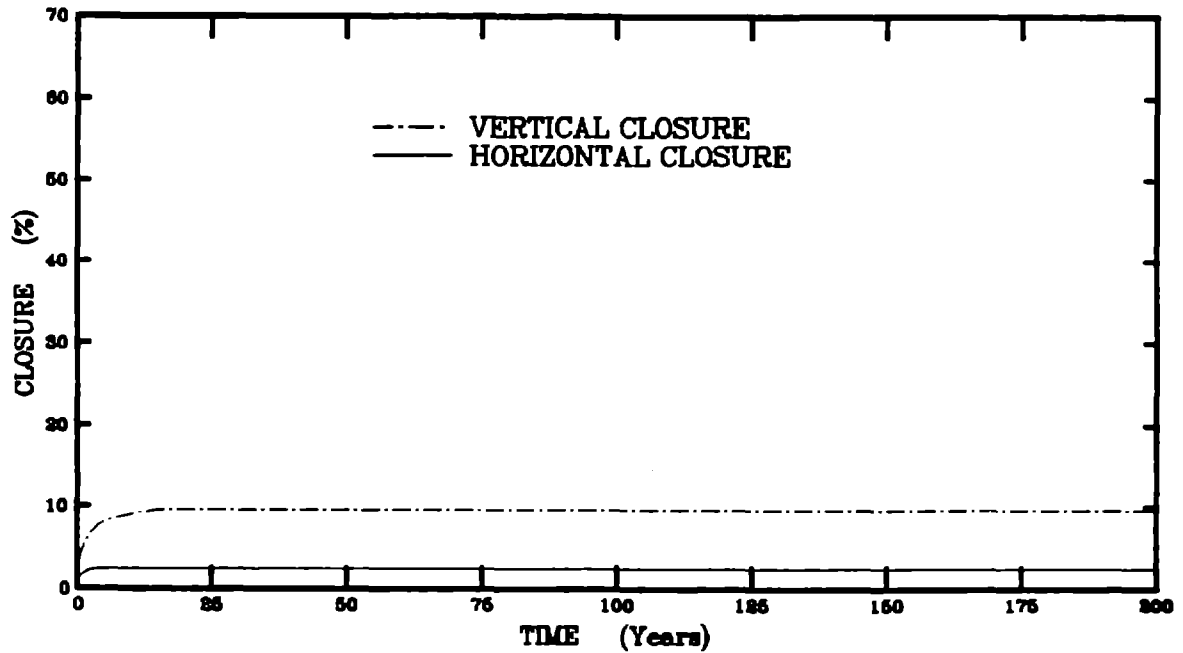


Figure 4-9. Room Closure History of a Disposal Room Filled With Vitrified Waste and Crushed Salt.

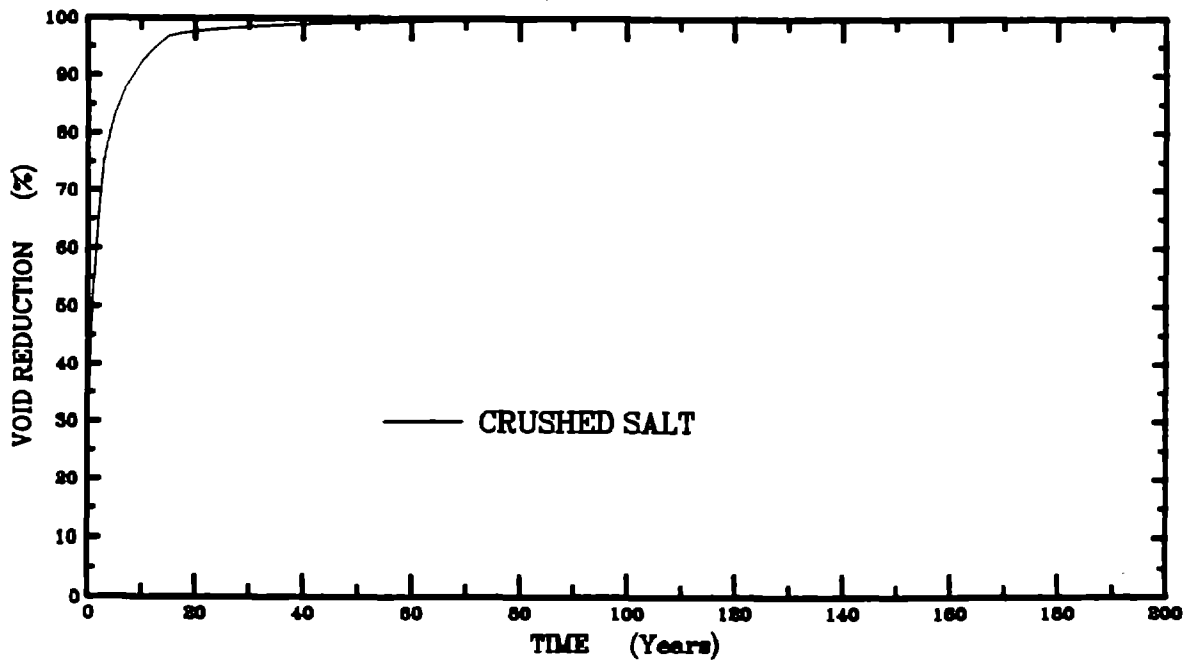


Figure 4-10. Void Reduction in the Disposal Room Filled With Vitrified Waste and Crushed Salt as a Function of Time.

The horizontal and vertical closures of the disposal room backfilled with shredded metal/crushed salt and crushed salt are shown in Figure 4-11. The maximum horizontal and vertical closures obtained are 9.6 percent and 24.2 percent, respectively. Comparison of these room closure results with those for crushed salt (Figure 4-1) shows identical behavior during the initial period with the final closures being less for the shredded metal/crushed salt mixture. Combining the shredded metal waste with the crushed salt includes two items that effect the room closure: (1) the initial porosity of the shredded metal/crushed salt mixture is less than that of the pure crushed salt and (2) the shredded metal/crushed salt mixture becomes a stiffer structural member than the pure crushed salt upon compaction. These two items result in less room closure and faster consolidation of the crushed salt backfill covering the shredded metal/crushed salt mixture.

The void reduction in the waste region, backfill region, and for the entire disposal room expressed as a percentage of the total initial void volume of the respective regions are shown in Figure 4-12 as a function of time. The percent void reduction for each region was computed using Equation 4-1. Approximately 16 years were required to reduce the void volume to 95 percent of the initial void volume for the crushed salt, while 11 years were required for the shredded metal/crushed salt mixture. As shown in Figure 4-12, the combined contents of the room required 12 years to reduce the void volume by 95 percent of the initial void volume. As illustrated in Appendix C, the average void fraction in the backfill region, waste region, and in the room reach 5 percent after approximately 11 years.

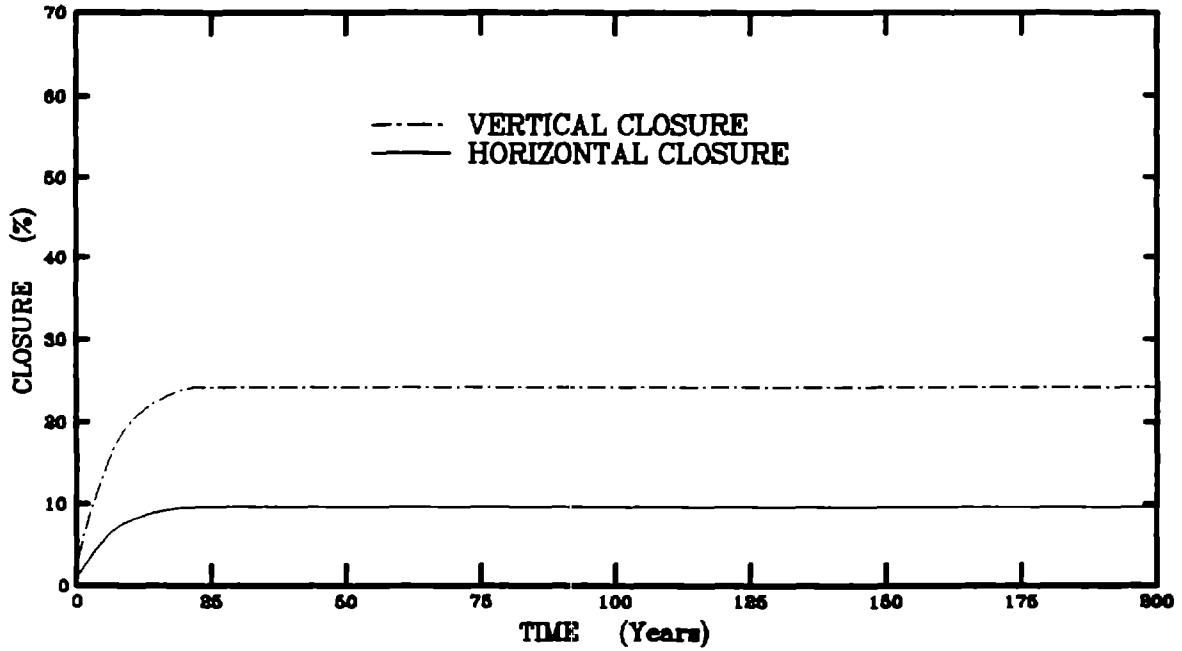


Figure 4-11. Room Closure History of a Disposal Room Filled With Crushed Salt and a Shredded Metal/Crushed Salt Mixture.

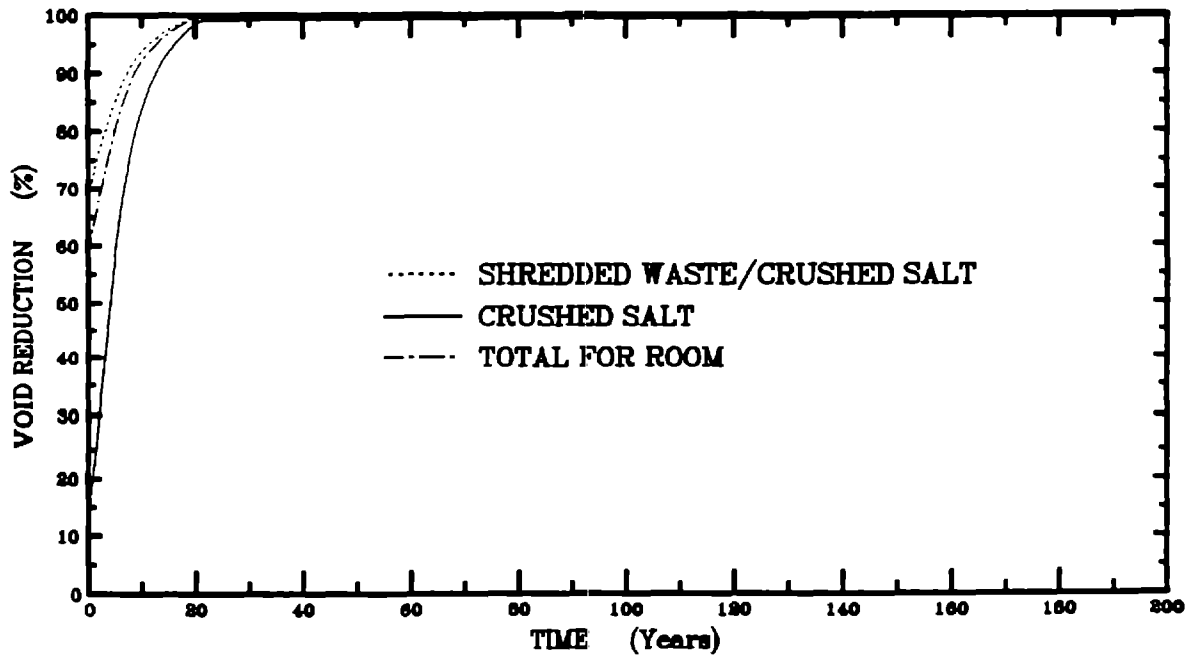


Figure 4-12. Void Reduction in the Disposal Room Filled With Crushed Salt and a Shredded Metal/Crushed Salt Mixture as a Function of Time.

5.0 SUMMARY AND CONCLUSIONS

Constitutive relations were developed and modified to simulate the backfill and host rock formation for disposal room configuration at WIPP including viscoplastic (creep), nonlinear elastic, creep consolidation, and nonlinear elastic and consolidation mixture models. These constitutive models were incorporated into the finite element computer code SPECTROM-32. The TRU waste model contains major uncertainties and assumptions that could significantly affect the results obtained. Weaknesses exist for the crushed salt constitutive model particularly with respect to its deviatoric response. The volumetric behavior of the backfill is based on hydrostatic laboratory tests, but the deviatoric response included is hypothetical. Further testing and analysis of crushed salt is required to guide the development of its constitutive model. The completed development effort provides a calculational support tool to investigate operational and performance questions relevant to the WIPP disposal room waste isolation strategies.

Different WIPP disposal room backfill configurations were examined for a simulation period of 200 years. Room contents investigated include crushed salt, a crushed salt/bentonite mixture, crushed salt covering TRU waste, crushed salt/bentonite covering TRU waste, crushed salt covering a mixture of crushed salt and shredded metallic waste, and crushed salt covering a vitrified waste. The results show that disposal room contents do not significantly affect room closure during the initial 5-year period. This is illustrated in Figures 5-1 and 5-2, which include plots of the vertical and horizontal room closure histories, respectively, for each of the cases analyzed. The one exception is the stiff, nonporous vitrified waste, which provides resistance to room deformation very early in time.

In most cases, the average void fractions became less than 5 percent within 200 years although the time required to obtain these reduced void fraction values varies significantly for the different backfill configurations. In this case, the void fraction values are computed using the initial void volume of the region as given by Equation 4-2. The one case that did not attain an average void fraction less than 5 percent is the crushed salt/bentonite mixture covering TRU waste, which reached a value of 5.09 percent after 200 years. Table 5-1 gives the time required for the average void fractions in the room, TRU waste, and surrounding backfill material to reach a value of 5 percent, and the time required for the average void fraction in the room (i.e., room refers to and includes all room contents) to reach a value of 0.5 percent. At an average void fraction of 0.5 percent, the room contents, including waste and backfill, are essentially fully compacted.

The results given in Table 5-1 are consistent with the room contents. When a stiff material is covered with crushed salt as in the case of the vitrified waste, the crushed salt compacts rapidly since the vitrified waste deforms little and the room deformation is absorbed almost entirely by the crushed salt backfill. Conversely, the TRU waste packages have initial void ratios much higher than the crushed salt and

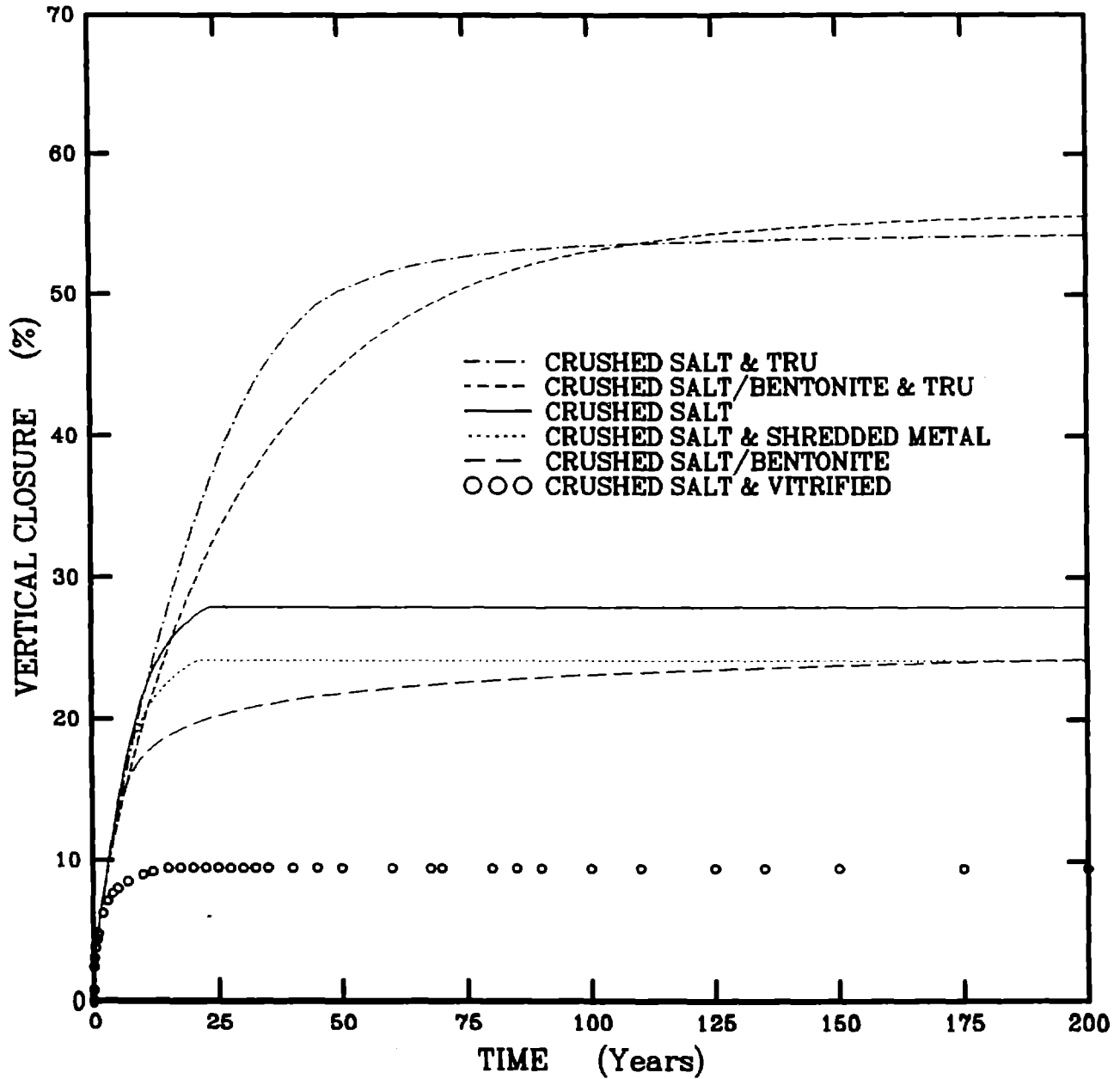


Figure 5-1. Comparisons of Vertical Closure Histories for Different Room Emplacement Scenarios.

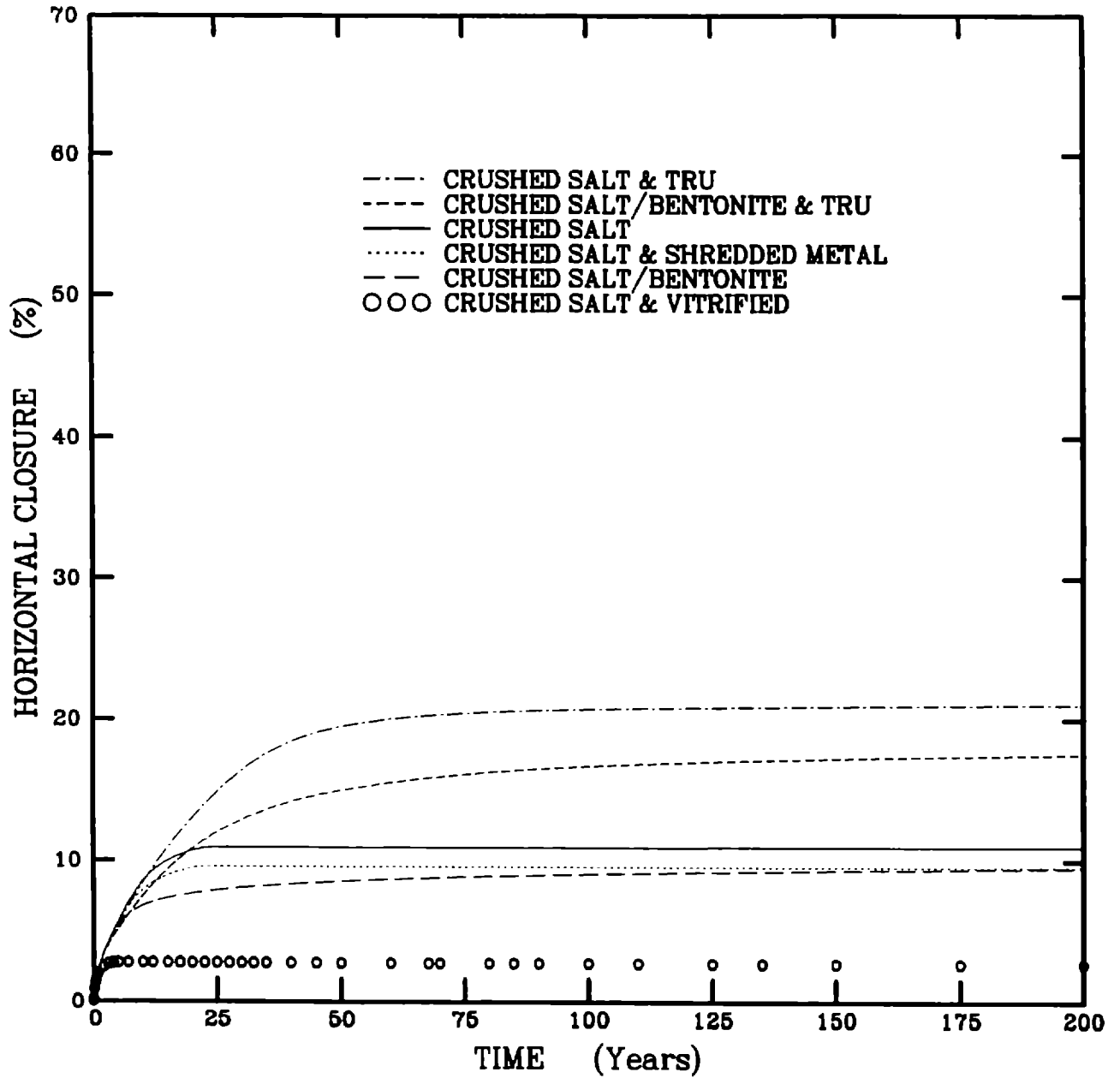


Figure 5-2. Comparisons of Horizontal Closure Histories for Different Room Emplacement Scenarios.

are significantly softer until the TRU waste is compacted significantly. Therefore, when TRU waste is included in the room, most of the room deformation is absorbed by the soft TRU waste resulting in longer times to attain reduced void fractions. When crushed salt/bentonite mixtures are assumed to be the backfill material, the consolidation rate is reduced and the times shown in Table 5-1 are significantly greater. However, as discussed in Chapter 2, the creep consolidation parameter values for crushed salt/bentonite mixtures are based on only three tests. Further testing on crushed salt/bentonite mixtures may provide information that will have a significant impact on these results.

Table 5-1. Average Void Fraction Comparisons for the Analyses

Analysis	Time to Reach Void Fraction Value (Yr)			
	5 Percent			0.5 Percent
	Room	Waste	Backfill	Room
Crushed Salt	12.7	NA ^(a)	12.7	22.8
Crushed Salt/Bentonite	191.2	NA	191.2	>200
Crushed Salt and TRU Waste	59.7	49.7	14.8	166.3
Crushed Salt/Bentonite and TRU Waste	200 ^(b)	— ^(c)	146.8	>200
Crushed Salt and Crushed Salt/Shredded Metal Mixture	10.2	9.9	10.6	19.4
Crushed Salt/Vitrified Waste	1.3	NA	6.0	13.5

(a) Not applicable.

(b) Actual value was 5.09 percent at 200 years.

(c) Value was 5.4 percent at 200 years.

Results from SPECTROM-32 and SANCHO are compared for backfilled disposal room problems with crushed salt and crushed salt-bentonite (Appendix B). The calculated deformations and stresses from the two analyses agree reasonably well despite differences in methodology such as the consolidation model, intact salt creep model, finite strain, and material properties.

6.0 NOMENCLATURE

A	=	creep consolidation material parameter [m^3/kg]
A_1	=	Munson-Dawson material parameter [s^{-1}]
A_2	=	Munson-Dawson material parameter [s^{-1}]
B_0	=	creep consolidation material parameter [$\frac{kg}{m^3 \cdot s}$]
B_1	=	creep consolidation material parameter [MPa^{-1}]
\hat{B}_1	=	Munson-Dawson material parameter [s^{-1}]
B_2	=	Munson-Dawson material parameter [s^{-1}]
c	=	Munson-Dawson material parameter [K^{-1}]
C_{ijkl}	=	compliance tensor [MPa^{-1}]
E	=	Young's modulus [MPa]
$\{f\}$	=	load vector [MN]
F	=	Munson-Dawson transient function
G	=	shear modulus [MPa]
G^f	=	fully compacted mixture shear modulus [MPa]
G_f	=	solid (intact) shear modulus [MPa]
G_m	=	inert material shear modulus [MPa]
G_s	=	crushed salt shear modulus [MPa]
G_0	=	nonlinear elastic shear modulus material constant [MPa]
G_1	=	nonlinear elastic shear modulus material constant [m^3/kg]
$H(\cdot)$	=	Heaviside step function
J_2	=	second invariant of deviator stress [MPa^2]
J_3	=	third invariant of deviator stress [MPa^3]
K	=	bulk modulus [MPa]
K^f	=	fully compacted mixture bulk modulus [MPa]
K_f	=	solid (intact) bulk modulus [MPa]
K_m	=	inert material bulk modulus [MPa]
K_0	=	Munson-Dawson material parameter

K_s = crushed salt bulk modulus [MPa]
 $[K_t]$ = tangent stiffness matrix [MPa]
 K_0 = nonlinear elastic bulk modulus material constant [MPa]
 K_1 = nonlinear elastic bulk modulus material constant [m^3/kg]
 m = Munson-Dawson material parameter
 m_s = mass fraction of salt
 m_m = mass fraction of inert material
 M = total mass [kg]
 M_m = inert material mass [kg]
 M_s = crushed salt mass [kg]
 n_1 = Munson-Dawson material parameter
 n_2 = Munson-Dawson material parameter
 q = Munson-Dawson activation volume
 Q_1 = Munson-Dawson activation energy [cal/mol]
 Q_2 = Munson-Dawson activation energy [cal/mol]
 R = universal gas constant [$\frac{cal}{mol-K}$]
 S_{ij} = deviatoric stress tensor [MPa]
 t_{ij} = square of the deviator of the reduced stress [MPa²]
 u = displacement [m]
 T = temperature [K]
 v = void reduction
 v^f = fully compacted volume fraction of a mixture
 v_f = void fraction based on current volume
 v_f^o = void fraction based on initial volume
 v_f^c = void fraction for backfill region based on current volume
 $v_f^{c^o}$ = void fraction for backfill region based on initial volume
 v_f^t = void fraction for waste region based on current volume
 $v_f^{t^o}$ = void fraction for waste region based on initial volume
 v_f^r = void fraction for room region based on current volume
 v_{is} = volume fraction of solid salt in crushed salt

- v_{is}^f = fully compacted volume fraction of solid salt in crushed salt
 v_m = volume fraction of inert material
 v_m^f = fully compacted volume fraction of inert material
 v_s = volume fraction of crushed salt
 v_0^s = initial volume fraction of crushed salt
 V = total volume [m^3]
 V^o = initial volume [m^3]
 V_{is} = solid salt volume within crushed salt [m^3]
 V_m = inert material volume [m^3]
 V_s = crushed salt volume [m^3]
 V^c = volume of backfill region [m^3]
 V^{c^o} = initial volume of backfill region [m^3]
 $V_v^{c^o}$ = initial void volume of backfill region [m^3]
 V^f = fully compacted mixture volume [m^3]
 V_s^f = fully compacted crushed salt volume [m^3]
 V^t = volume of waste region [m^3]
 V^{t^o} = initial volume of waste region [m^3]
 $V_v^{t^o}$ = initial void volume of waste region [m^3]
 V_v = void volume [m^3]
 V_v^o = initial void volume [m^3]
 α = Munson-Dawson material parameter
 β = Munson-Dawson material parameter
 δ = Munson-Dawson recovery parameter
 δ_{ij} = Kronecker delta
 Δ = Munson-Dawson workhardening parameter
 Δf = incremental load [MPa]
 Δu = incremental displacement [m]
 ΔV = volume change [m^3]
 ΔV^c = volume change in backfill region [m^3]
 ΔV^t = volume change in waste region [m^3]

ϵ_s = steady-state strain
 ϵ_v = total volumetric strain
 $\epsilon_{v,s}$ = total volumetric strain of crushed salt in a mixture
 $\epsilon_{s,1}$ = steady-state strain for dislocation climb
 $\epsilon_{s,2}$ = steady-state strain from an undefined mechanism
 $\epsilon_{s,3}$ = steady-state strain for glide
 ϵ_e^c = invariant creep strain measure
 ϵ_t^f = Munson-Dawson transient strain limit
 ϵ_v^c = inelastic volumetric strain
 $\epsilon_{v,s}^c$ = inelastic volumetric strain of crushed salt in a mixture
 ϵ_{ij} = total strain tensor
 ϵ_{ij}^c = creep strain tensor
 ϵ_{ij}^e = elastic strain tensor
 $\epsilon_{eq,1}^c$ = equivalent inelastic shear strain measure
 $\epsilon_{eq,2}^c$ = equivalent inelastic shear strain measure
 ζ = Munson-Dawson internal variable
 η = empirical constant for creep consolidation model
 Θ = generic property of a mixture
 θ = frictional material parameter in creep flow potential
 (dimensionless for pressure-dependent, degrees for frictional)
 θ_i = generic property of i^{th} material in a mixture
 κ = material constant in nonlinear TRU waste model [MPa⁻¹]
 λ = material constant in nonlinear TRU waste model [MPa⁻¹]
 μ = Munson-Dawson material parameter [MPa]
 ν = Poisson's Ratio
 ρ = density [kg/m³]
 ρ^f = fully compacted mixture density [kg/m³]
 ρ_f = final or intact material density [kg/m³]
 ρ_m = inert material density [kg/m³]
 ρ_{is} = solid salt density within crushed salt [kg/m³]

- ρ_s = crushed salt density [kg/m^3]
 ρ_0 = initial material density [kg/m^3]
 ρ_0^s = initial crushed salt density [kg/m^3]
 σ_a = axial stress [MPa]
 σ_e = invariant stress measure [MPa]
 σ_m = mean stress [MPa]
 σ_0 = Munson-Dawson cut-off stress [MPa]
 σ_e^f = invariant stress measure [MPa]
 $\sigma_{eq_1}^f$ = invariant stress measure [MPa]
 $\sigma_{eq_2}^f$ = invariant stress measure [MPa]
 σ_{ij} = stress tensor [MPa]
 τ = flow dilatancy material parameter in creep flow potential
 (dimensionless for pressure-dependent, degrees for frictional)
 ϕ = porosity
 ϕ_s = crushed salt porosity
 ϕ_0 = initial porosity
 ϕ_0^c = initial porosity of backfill region
 ϕ_0^t = initial porosity of waste region
 ψ = Lode angle [degrees]
 $\dot{\chi}$ = time rate of change of variable χ [s^{-1}]
 σ_{kk} = repeated indices imply summation ($\sigma_{kk} = \sigma_{11} + \sigma_{22} + \sigma_{33}$)

7.0 REFERENCES

Butcher, B. M., 1990. *Preliminary Evaluation of Potential Engineering Modifications for the Waste Isolation Pilot Plant*, SAND89-3095, Sandia National Laboratories, Albuquerque, NM.

Butcher, B. M., 1989. *Waste Isolation Pilot Plant Simulated Waste Compositions and Mechanical Properties*, SAND89-0372, Sandia National Laboratories, Albuquerque, NM.

Butcher, B. M., R. G. VanBuskirk, N. C. Pattie, and T. W. Thompson, 1991. *Mechanical Compaction of WIPP Simulated Waste*, SAND90-1206, in preparation, Sandia National Laboratories, Albuquerque, NM.

Callahan, G. D., 1990. *Crushed Salt Consolidation Model Adopted for SPECTROM-92*, RE/SPEC Inc., Rapid City, SD, RSI-0358, for Sandia National Laboratories, Albuquerque, NM, September.

Callahan, G. D., 1982. *A Plasticity Approach for Rock Containing Planes of Weakness*, Ph.D. Thesis, University of Minnesota, Minneapolis, MN.

Callahan, G. D. A. F. Fossum, and D. K. Svalstad, 1990. *Documentation of SPECTROM-92: A Finite Element Thermomechanical Stress Analysis Program*, DOE/CH/10378-2, prepared by RE/SPEC Inc., Rapid City, SD, RSI-0269, for U.S. Department of Energy, Chicago Operations Office, Vol. 1 and 2, February.

Corson, P. B., 1974. *Correlation Functions for Predicting Properties of Heterogeneous Materials. III Effective Elastic Moduli of Two-Phase Solids*, Journal of Applied Physics, Vol. 45, No. 7, July.

Fossum, A. F., G. D. Callahan, L. L. Van Sambeek, and P. E. Senseny, 1988. "How Should One-Dimensional Laboratory Equations be Cast Into Three-Dimensional Form?" *Proceedings, 29th U.S. Symposium on Rock Mechanics*, University of Minnesota, Minneapolis, MN.

Hashin, Z. and S. Shtrikman, 1962. *A Variational Approach to the Theory of the Effective Magnetic Permeability of Multiphase Materials*, Journal of Applied Physics, Vol. 33.

Holcomb, D. J. and D. H. Zeuch, 1988. *Consolidation of Crushed Rock Salt, Part I: Experimental Results for Dry Salt Analyzed Using a Hot-Pressing Model*, SAND88-1469, printed October 1988.

Holcomb, D. J. and M. F. Shields, 1987. *Hydrostatic Consolidation of Crushed Salt with Added Water*, SAND87-1990, Sandia National Laboratories, Albuquerque, NM.

Holcomb, D. J. and D. W. Hannum, 1982. *Consolidation of Crushed Salt Backfill Under Conditions Appropriate to the WIPP Facility*, SAND82-0630, Sandia National Laboratories, Albuquerque, NM.

Lynch, C. T., 1974. *CRC Handbook of Materials Science, Volume I General Properties*, CRC Press, Inc., Boca Raton, FL.

McClintock, F. A. and A. S. Argon, 1966. *Mechanical Behavior of Materials*, Addison-Wesley Publishing Company, Inc., Reading, MA.

Milton, G. W., 1982. *Bounds on the Elastic and Transport Properties of Two-Component Composites*, Journal of the Mechanics and Physics of Solids, Vol. 30, No. 3, pp. 177-191.

Munson, D. E., 1989. *Proposed New Structural Reference Stratigraphy, Law, and Properties*, Sandia National Laboratories Internal Memorandum, Albuquerque, NM.

Munson, D. E. A. F. Fossum, and P. E. Senseny, 1989. *Advances in Resolution of Discrepancies Between Predicted and Measured In Situ WIPP Room Closures*, SAND88-2948, prepared by RE/SPEC Inc. for Sandia National Laboratories, Albuquerque, NM, March.

Parrot, J. E. and A. D. Stuckes, 1975. *Thermal Conductivity of Solids*, Pion Limited, London, England.

Pfeifle, T. W., 1990. *Consolidation, Permeability, and Strength of Crushed Salt/Bentonite With Application to the WIPP*, SAND90-7009, prepared by RE/SPEC Inc., Rapid City, SD, for Sandia National Laboratories, Albuquerque, NM.

Pfeifle, T. W., and P. E. Senseny, 1985. *Permeability and Consolidation of Crushed Salt From the WIPP Site*, prepared by RE/SPEC Inc., Rapid City, SD, RSI-0278, for Sandia National Laboratories, Albuquerque, NM.

Pusch, R., 1980. *Swelling Pressure of Highly Compacted Bentonite*, 80-13, Division of Soil Mechanics, University of Luleå, Luleå.

Sjaardema, G. D. and R. D. Krieg, 1987. *A Constitutive Model for the Consolidation of Crushed Salt and Its Use in Analyses of Backfilled Shaft and Drift Configurations*, SAND87-1977, prepared by Sandia National Laboratories, Albuquerque, NM.

Stroup, D. E. and P. E. Senseny, 1987. *Influence of Bentonite Content on Consolidation and Permeability of Crushed Salt From the WIPP*, prepared by RE/SPEC Inc., Rapid City, SD, RSI-0309, for Sandia National Laboratories, Albuquerque, NM.

Timoshenko, S. P. and J. N. Goodier, 1970. *Theory of Elasticity*, Third Edition, McGraw-Hill Book Company, New York, NY.

Weatherby, J. R. and W. T. Brown, 1990. *Closure of a Disposal Room Backfilled With a Salt/Bentonite Mix*, Sandia National Laboratories Internal Memorandum to B. M. Butcher, Division 6332, Albuquerque, NM.

Weatherby, J. R., 1989. *Finite Element Analysis of TRU Storage Rooms Filled With Waste and Crushed Salt*, Sandia National Laboratories Internal Memorandum to B. M. Butcher, Division 6332, Albuquerque, NM.

Zeuch, D. H., 1989. *Isostatic Hot-Pressing Mechanism Maps for Pure and Natural Sodium Chloride: Applications to Nuclear Waste Isolation In Bedded and Domal Salt Formations*, SAND88-2207, printed March 1989.

APPENDIX A

**SIMULATED TRU WASTE STRESS
POROSITY DATA**

**APPENDIX A
CONTENTS**

A.1 SUMMARY	79
A.2 REFERENCES	79

APPENDIX A SIMULATED TRU WASTE STRESS — POROSITY DATA

A.1 SUMMARY

Appendix A includes axial stress-porosity data pairs supplied by Sandia National Laboratories. The data are representative of experiments conducted on simulated TRU waste by Butcher et al. [1991].

A.2 REFERENCES

Butcher, B. M., R. G. VanBuskirk, N. C. Pattie, and T. W. Thompson, 1991. *Mechanical Compaction of WIPP Simulated Waste*, SAND90-1206, in preparation, Sandia National Laboratories, Albuquerque, NM.

Compressive Stress MPa	Metallic Waste Porosity	Combustible Waste Porosity	Sludge Waste Porosity	Average Repository Porosity
0.4	0.805	0.830	0.549	0.765
0.6	0.783	0.801	0.410	0.722
0.8	0.768	0.776	0.394	0.696
1.0	0.755	0.752	0.377	0.672
1.2	0.741	0.729	0.363	0.649
1.4	0.729	0.706	0.350	0.628
1.6	0.717	0.683	0.338	0.607
1.8	0.706	0.661	0.328	0.588
2.0	0.696	0.640	0.318	0.570
2.2	0.687	0.620	0.310	0.553
2.4	0.678	0.602	0.302	0.538
2.6	0.670	0.584	0.296	0.525
2.8	0.662	0.567	0.289	0.512
3.0	0.655	0.552	0.284	0.499
3.2	0.649	0.536	0.278	0.488
3.4	0.642	0.522	0.273	0.477
3.6	0.636	0.508	0.268	0.467
3.8	0.630	0.494	0.263	0.457
4.0	0.624	0.482	0.258	0.447
4.2	0.618	0.469	0.253	0.438
4.4	0.612	0.457	0.247	0.429
4.6	0.607	0.446	0.243	0.421
4.8	0.602	0.435	0.237	0.412
5.0	0.596	0.424	0.231	0.404
5.2	0.591	0.414	0.228	0.397
5.4	0.586	0.404	0.224	0.390
5.6	0.581	0.394	0.221	0.383
5.8	0.576	0.385	0.217	0.376
6.0	0.572	0.376	0.214	0.370
6.2	0.567	0.367	0.211	0.363
6.4	0.562	0.358	0.208	0.357
6.6	0.558	0.350	0.204	0.351
6.8	0.553	0.342	0.201	0.345
7.0	0.549	0.334	0.198	0.339
7.2	0.544	0.326	0.195	0.334
7.4	0.540	0.319	0.192	0.328
7.6	0.535	0.312	0.190	0.323

Compressive Stress MPa	Metallic Waste Porosity	Combustible Waste Porosity	Sludge Waste Porosity	Average Repository Porosity
7.8	0.531	0.305	0.187	0.318
8.0	0.527	0.298	0.184	0.313
8.2	0.523	0.291	0.181	0.308
8.4	0.518	0.285	0.179	0.303
8.6	0.514	0.278	0.176	0.298
8.8	0.510	0.272	0.174	0.293
9.0	0.506	0.266	0.171	0.289
9.2	0.502	0.260	0.169	0.284
9.4	0.498	0.254	0.167	0.280
9.6	0.494	0.249	0.164	0.276
9.8	0.490	0.243	0.162	0.272
10.0	0.486	0.238	0.160	0.267
10.2	0.482	0.232	0.157	0.263
10.4	0.478	0.227	0.155	0.259
10.6	0.475	0.222	0.153	0.255
10.8	0.471	0.217	0.151	0.252
11.0	0.467	0.212	0.149	0.248
11.2	0.463	0.208	0.147	0.244
11.4	0.459	0.203	0.145	0.241
11.6	0.456	0.198	0.143	0.237
11.8	0.452	0.194	0.141	0.233
12.0	0.448	0.190	0.139	0.230
12.2	0.445	0.185	0.137	0.226
12.4	0.441	0.181	0.135	0.223
12.6	0.438	0.177	0.133	0.220
12.8	0.434	0.173	0.131	0.216
13.0	0.430	0.169	0.129	0.213
13.2	0.427	0.165	0.128	0.210
13.4	0.423	0.162	0.126	0.207
13.6	0.420	0.158	0.124	0.204
13.8	0.417	0.154	0.122	0.201
14.0	0.413	0.151	0.120	0.198
14.2	0.410	0.147	0.118	0.195
14.4	0.406	0.144	0.117	0.192
14.6	0.403	0.140	0.115	0.189
14.8	0.399	0.137	0.113	0.186

APPENDIX B

**COMPARISON OF SPECTROM-32
AND
SANCHO RESULTS**

**APPENDIX B
CONTENTS**

B.1 INTRODUCTION	91
B.2 DIFFERENCES BETWEEN ANALYSES	91
B.2.1 Basic Problem Parameters	91
B.2.2 Crushed Salt Model and Material Constants	91
B.2.3 Intact Salt Model	93
B.2.4 TRU Waste Model	93
B.3 COMPARISON OF RESULTS	93
B.4 REFERENCES	97

**APPENDIX B
TABLES**

B-1 Nonlinear Elastic Model and Material Parameters for Crushed Salt . 92

**APPENDIX B
FIGURES**

B-1	Comparison of Room Closures for a Room Filled With Crushed Salt	94
B-2	Comparison of the Average Void Fractions in a Room Filled With Crushed Salt (Current Volume)	95
B-3	Comparison of Room Closures for a Room Filled With Crushed Salt/Bentonite	95
B-4	Comparison of Room Closures for a Room Filled With Crushed Salt/Bentonite (Current Volume)	96
B-5	Comparison of Room Closures for a Room Containing TRU Waste and Crushed Salt	96
B-6	Comparison of the Average Void Fractions in a Room Containing TRU Waste and Crushed Salt (Current Volume)	97

APPENDIX B COMPARISON OF SPECTROM-32 AND SANCHO RESULTS

B.1 INTRODUCTION

The purpose of Appendix B is to compare results obtained using SPECTROM-32 and presented in this report to those obtained using SANCHO [Weatherby, 1989 and Weatherby and Brown, 1990] for those types of problems common between the different analyses. Fundamental differences between the analyses are discussed in the next section before these results are presented.

B.2 DIFFERENCES BETWEEN ANALYSES

Several differences exist between the methods used to analyze the backfilled disposal rooms. The two most significant differences relate to the constitutive relations used for the various materials and the finite-strain formulation in SANCHO versus the small-strain formulation in SPECTROM-32. The following sections elaborate on the differences between the analyses.

B.2.1 Basic Problem Parameters

The basic problem parameters consist of the room and pillar geometry, depth of the room, mesh refinement of the modeled region, temperature, and boundary conditions. The same basic problem parameters were used for all SPECTROM-32 analyses, and except for a variation in the mesh refinement, the basic problem parameters in the SPECTROM-32 analyses are identical to the crushed-salt backfill and crushed-salt/TRU waste SANCHO analyses presented by Weatherby [1989]. However, the crushed salt/bentonite backfill analysis presented by Weatherby and Brown [1990] differs from the other analyses in two ways: (1) the total mesh height was 54 m rather than 27 m and (2) the overburden pressure was 14.8 MPa rather than 14.3 MPa as shown in Figure 3-1. The mesh refinement used for the SPECTROM-32 analyses is shown in Figure 3-1 and does not vary significantly from that used by SANCHO for the crushed-salt backfill and crushed-salt/TRU waste analyses.

B.2.2 Crushed Salt Model and Material Constants

The crushed-salt consolidation volumetric response model used in both analyses was developed by Sjaardema and Krieg [1987]. Although the nonlinear elastic component of the crushed salt consolidation model was the same in the SPECTROM-32 and SANCHO analyses, corresponding elastic material constants for crushed salt used in the SANCHO analyses were reduced by a factor of 12.5 [Weatherby, 1989]. This reduction in elastic properties stems from a recommendation by Morgan [1987]

that is based on the usage of the early version of the reference constitutive relation for salt creep (i.e., WIPP secondary creep law) that produced good agreement between calculated and measured deformations of WIPP field experiments. Table B-1 gives the nonlinear elastic model for crushed salt along with the respective parameters values used in the two analyses. Note that volumetric compaction is taken to be negative.

Table B-1. Nonlinear Elastic Model and Material Parameters for Crushed Salt

Parameter	Units	Value (SPECTROM-32 Analyses)	Value (SANCHO Analyses)
K_0	MPa	0.01760	0.00141
K_1	m ³ /kg	0.00653	0.00653
G_0	MPa	0.01060	0.000864
G_1	m ³ /kg	0.00653	0.00653
K_f	MPa	20,626	1,653
G_f	MPa	12,423	1,013
ρ_0	kg/m ³	1,400	1,400
ρ_f	kg/m ³	2,140	2,140

$$K = K_0 e^{\frac{K_1 \epsilon_v}{1 + \epsilon_v}}$$

$$G = G_0 e^{\frac{G_1 \epsilon_v}{1 + \epsilon_v}}$$

where ϵ_v = total volumetric strain
 $\rho_0 = \rho (1 + \epsilon_v)$

Note: If $K > K_f$, then $K = K_f$ and $G = G_f$
 If $G > G_f$, then $G = G_f$ and $K = K_f$

The volumetric creep consolidation component of the crushed salt model is essentially the same for the SANCHO and SPECTROM-32 analyses. The crushed salt consolidation model developed by Sjaardema and Krieg [1987] given in Chapter 2 was implemented into SANCHO [Weatherby, 1989] and SPECTROM-32 [Callahan, 1990]. The volumetric creep consolidation model parameters values used in the two analyses were identical and are given in Table 2-3 for crushed salt and Table 2-5 for the crushed salt/bentonite mixture.

A deviatoric component was added to the creep consolidation model used in SPECTROM-32. Volumetric-only models are deficient because they produce unrealistic results. For example, a cylinder subjected to uniaxial compression will

also compact laterally since the cylinder has a mean stress component. As discussed in Chapter 2, a deviatoric component was arbitrarily developed to offset the lateral strain components generated under uniaxial loading. A more complex deviatoric component is difficult to justify since, until recently, laboratory data for creep consolidation were limited to tests conducted under hydrostatic loading. SANCHO used a form of the WIPP secondary creep law for intact salt as modified by Sjaardema and Krieg [1987] for the deviatoric response of the crushed salt.

B.2.3 Intact Salt Model

Recently, a new WIPP reference constitutive relation for intact salt creep was proposed [Munson, 1989]. The original baseline WIPP constitutive relation (secondary creep law) along with a Mises-type flow potential was used in the SANCHO analyses. The Munson-Dawson constitutive relation (see Chapter 2) along with a Tresca flow potential was used in the SPECTROM-32 analyses to describe the intact salt behavior. This combination was recommended by Munson [1989] because of favorable results from a previous study [Munson et al., 1989].

Similar to the crushed salt, the elastic properties of intact salt recommended by Munson [1989] were reduced by a factor of 12.5 for the SANCHO analyses. The SPECTROM-32 analyses did not use reduced elastic constants. Note that in both sets of analyses, the crushed salt elastic constants approach the intact salt elastic constants as the crushed salt becomes fully consolidated; however, the properties in the SANCHO analyses were modified by the 12.5 reduction factor.

B.2.4 TRU Waste Model

The SPECTROM-32 analyses used the nonlinear elastic material model developed in Section 2.4 for the TRU waste; whereas, SANCHO used a volumetric plasticity model.

B.3 COMPARISON OF RESULTS

Three common analyses performed using SPECTROM-32 and SANCHO exist for comparison:

1. Room completely backfilled with crushed salt.
2. Room completely backfilled with crushed salt/bentonite.
3. Room containing TRU waste covered with crushed salt.

The SANCHO results for each of these analyses were obtained by digitizing the graphical information presented in Weatherby [1989] and Weatherby and Brown [1990]. Figures B-1 through B-6 compare the room closure and average void fraction results obtained for the room simulations using SANCHO and SPECTROM-32.

Figure B-1 compares the room closure results and Figure B-2 compares the average void fraction for the two analyses of the room backfilled completely with crushed salt. The SPECTROM-32 results show faster room closure than SANCHO and consequently a shorter time to fully consolidate the backfill. Figures B-3 and B-4 show the same results for the crushed salt/bentonite backfill analysis. Despite the differences between the SPECTROM-32 and SANCHO analyses, the crushed salt/bentonite backfill analyses results compare extremely well. Figures B-5 and B-6 illustrate the comparison of the room closures and average void fractions obtained for the TRU waste covered with crushed salt.

RSI-163-90-065

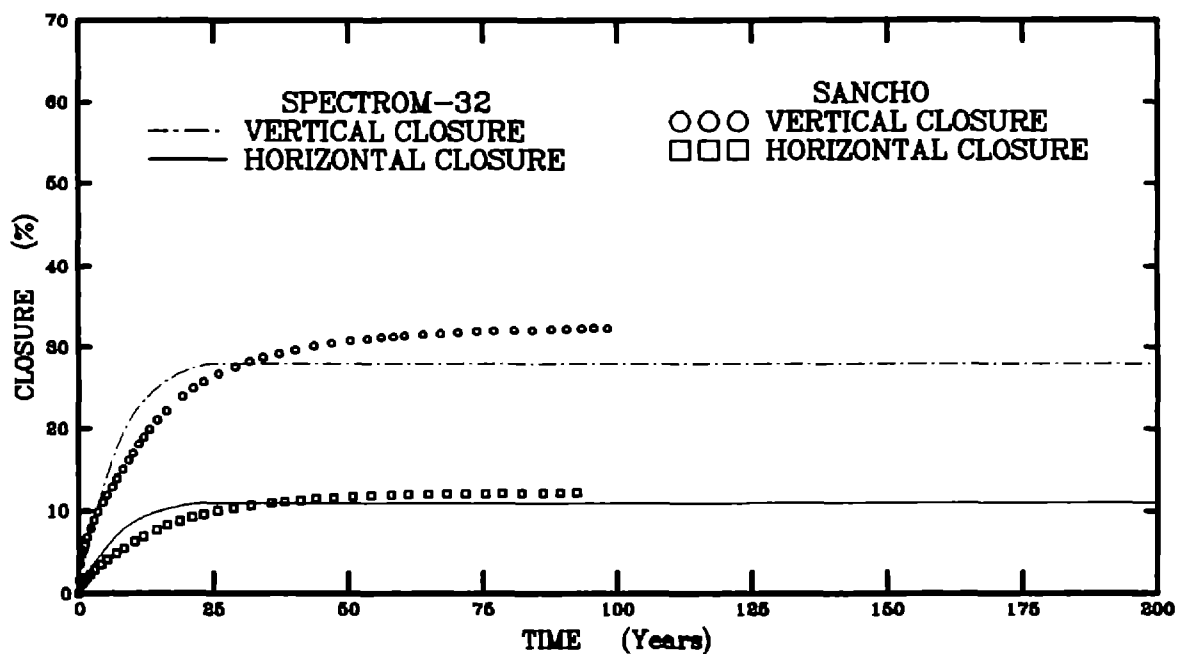


Figure B-1. Comparison of Room Closures for a Room Filled With Crushed Salt.

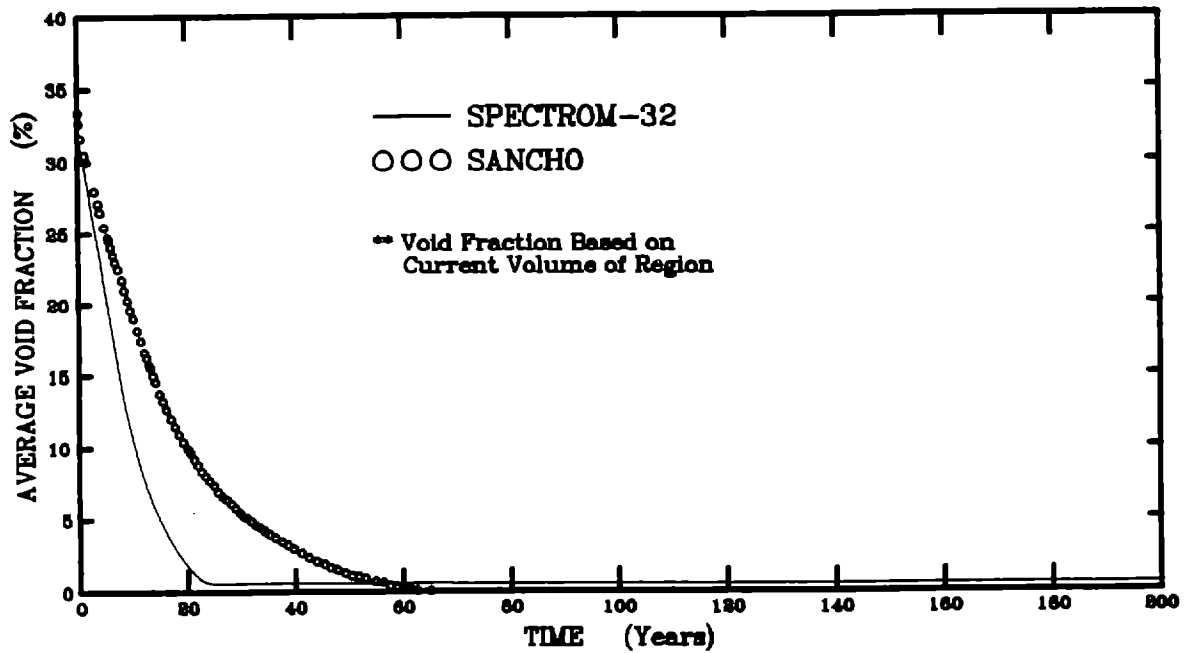


Figure B-2. Comparison of the Average Void Fractions in a Room Filled With Crushed Salt (Current Volume).

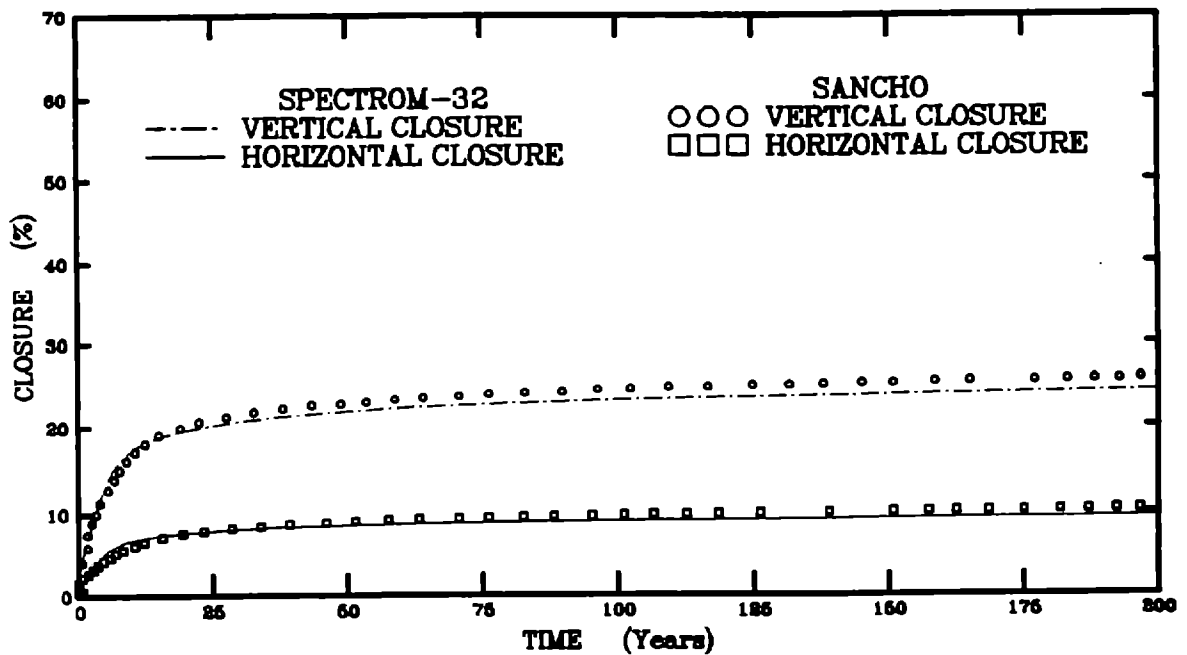


Figure B-3. Comparison of Room Closures for a Room Filled With Crushed Salt/Bentonite.

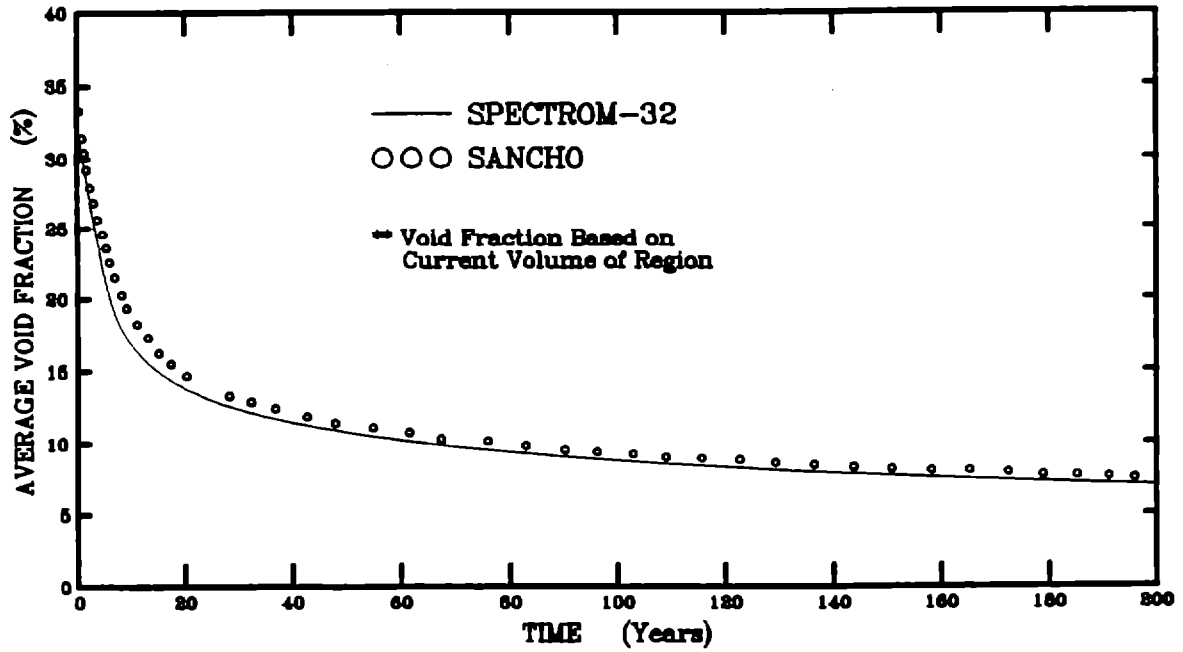


Figure B-4. Comparison of Room Closures for a Room Filled With Crushed Salt/Bentonite (Current Volume).

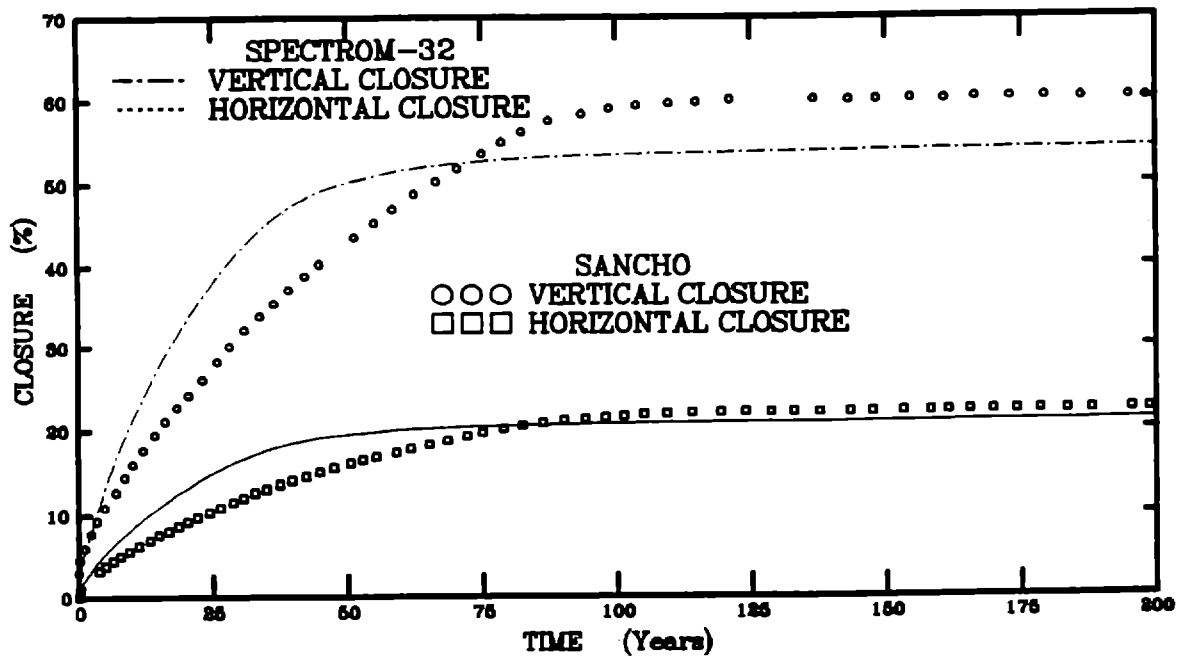


Figure B-5. Comparison of Room Closures for a Room Containing TRU Waste and Crushed Salt.

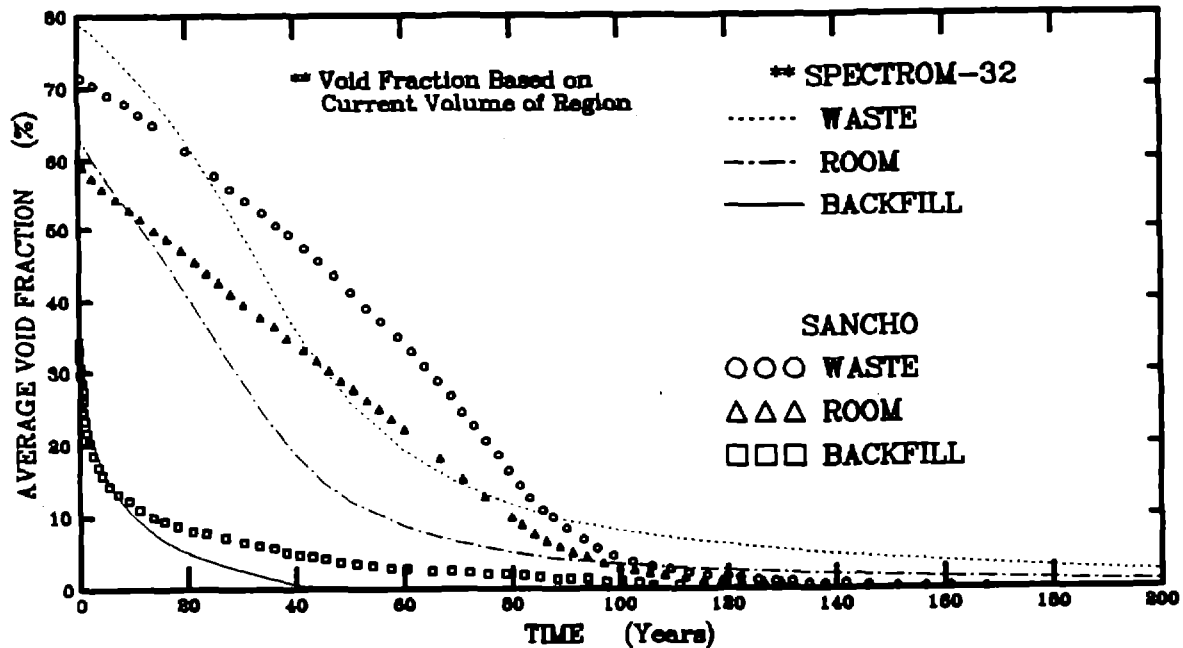


Figure B-6. Comparison of the Average Void Fractions in a Room Containing TRU Waste and Crushed Salt (Current Volume).

The results obtained from the TRU waste problem (Figures B-5 and B-6) are somewhat similar but do not compare as well as the two previously discussed analyses. An important component in this analysis is the TRU waste, and the constitutive models used in SPECTROM-32 and SANCHO for TRU waste are considerably different. Thus, the difference in the TRU waste model is thought to be the primary reason for the larger discrepancies between the two solutions.

B.4 REFERENCES

Callahan, G. D., 1990. *Crushed Salt Consolidation Model Adopted for SPECTROM-32*, RE/SPEC Inc., Rapid City, SD, RSI-0358, for Sandia National Laboratories, Albuquerque, NM, September.

Morgan, H. S., 1987. *Estimate of the Time Needed for TRU Storage Rooms to Close*, Memorandum to D. E. Munson, Sandia National Laboratories, Division 6332, Albuquerque, NM, June.

Munson, D. E., 1989. *Proposed New Structural Reference Stratigraphy, Law, and Properties*, Sandia National Laboratories Internal Memorandum, Albuquerque, NM.

Munson, D. E. A. F. Fossum, and P. E. Senseny, 1989. *Advances in Resolution of Discrepancies Between Predicted and Measured In Situ WIPP Room Closures*, SAND88-2948, prepared by RE/SPEC Inc. for Sandia National Laboratories, Albuquerque, NM, March.

Sjaardema, G. D. and R. D. Krieg, 1987. *A Constitutive Model for the Consolidation of Crushed Salt and Its Use in Analyses of Backfilled Shaft and Drift Configurations*, SAND87-1977, prepared by Sandia National Laboratories, Albuquerque, NM.

Weatherby, J. R., 1989. *Finite Element Analysis of TRU Storage Rooms Filled With Waste and Crushed Salt*, Sandia National Laboratories Internal Memorandum to B. M. Butcher, Division 6332, Albuquerque, NM.

Weatherby, J. R. and W. T. Brown, 1990. *Closure of a Disposal Room Backfilled With a Salt/Bentonite Mix*, Sandia National Laboratories Internal Memorandum to B. M. Butcher, Division 6332, Albuquerque, NM.

APPENDIX C

**AVERAGE VOID FRACTION
AND
MEAN STRESS RESULTS**

**APPENDIX C
CONTENTS**

C.1 SUMMARY 105

**APPENDIX C
FIGURES**

C-1	Average Void Fraction in a Disposal Room Filled With Crushed Salt.	106
C-2	Average Void Fraction in a Disposal Room Filled With Crushed Salt/Bentonite.	106
C-3	Average Void Fraction in a Disposal Room Filled With TRU Waste and Surrounded by Crushed Salt.	107
C-4	Average Void Fraction in a Disposal Room Filled With TRU Waste and Surrounded by Crushed Salt/Bentonite.	107
C-5	Average Void Fraction in a Disposal Room Filled With Vitrified Waste and Surrounded by Crushed Salt.	108
C-6	Average Void Fraction in a Disposal Room Filled With a Mixture of Shredded Metallic Waste and Surrounded by Crushed Salt.	108
C-7	Mean Stress History in a Disposal Room Filled With Crushed Salt. .	109
C-8	Mean Stress History in a Disposal Room Filled With Crushed Salt/Bentonite.	109
C-9	Mean Stress History in a Disposal Room Filled TRU Waste and Surrounded by Crushed Salt.	110
C-10	Mean Stress History in a Disposal Room Filled With TRU Waste and Surrounded by Crushed Salt/Bentonite.	110
C-11	Mean Stress History in a Disposal Room Filled With Vitrified Waste and Surrounded by Crushed Salt.	111
C-12	Mean Stress History in a Disposal Room Filled With a Mixture of Shredded Metallic Waste and Surrounded by Crushed Salt.	111

APPENDIX C AVERAGE VOID FRACTION AND MEAN STRESS RESULTS

C.1 SUMMARY

Appendix C includes average void fraction and mean stress results for the six cases investigated in Figures C-1 through C-6 and Figures C-7 through C-12, respectively. The average void fractions shown are computed using Equation 4-2, which is based on the initial volume of the region considered. When more than one component is included in a storage room, the average void fractions for each of the components are shown. For example, the case involving crushed salt and TRU waste room contents, with results shown in Figure C-3, includes three curves — one curve each for the TRU waste, crushed salt, and room. Each of these curves was computed using Equation 4-2 with the void volume and initial volume representing the specific region of interest. The curve labeled *Room* represents the average void fraction of the combined waste and backfill in the room (i.e., total room contents). The average void fraction for the room is computed by weighting the average void fractions in the waste and the backfill according to their respective volumes and dividing by the initial volume of the room.

Figures C-7 through C-12 illustrate the mean stress at three distinct locations in the room. These three locations are labeled *Center*, *Roof*, and *Rib*. *Center* refers to the center of the room with mean stress results taken from the element nearest the center of the room. *Roof* refers to the center of the room near the roof with mean stress results taken from the backfill element nearest the center of the room at the intact salt/backfill interface along the roof. *Rib* refers to the midheight of the room near the rib with mean stress results taken from the backfill element nearest the midheight of the room at the intact salt/backfill interface along the rib.

RSI-163-90-074

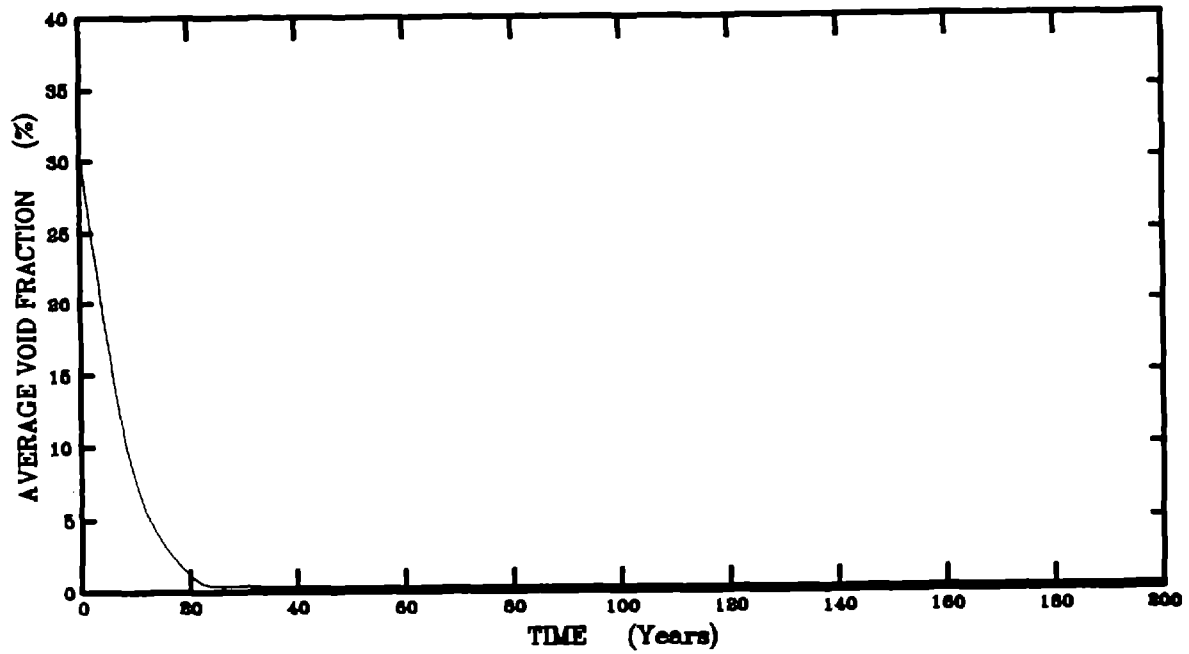


Figure C-1. Average Void Fraction in a Disposal Room Filled With Crushed Salt.

RSI-163-90-075

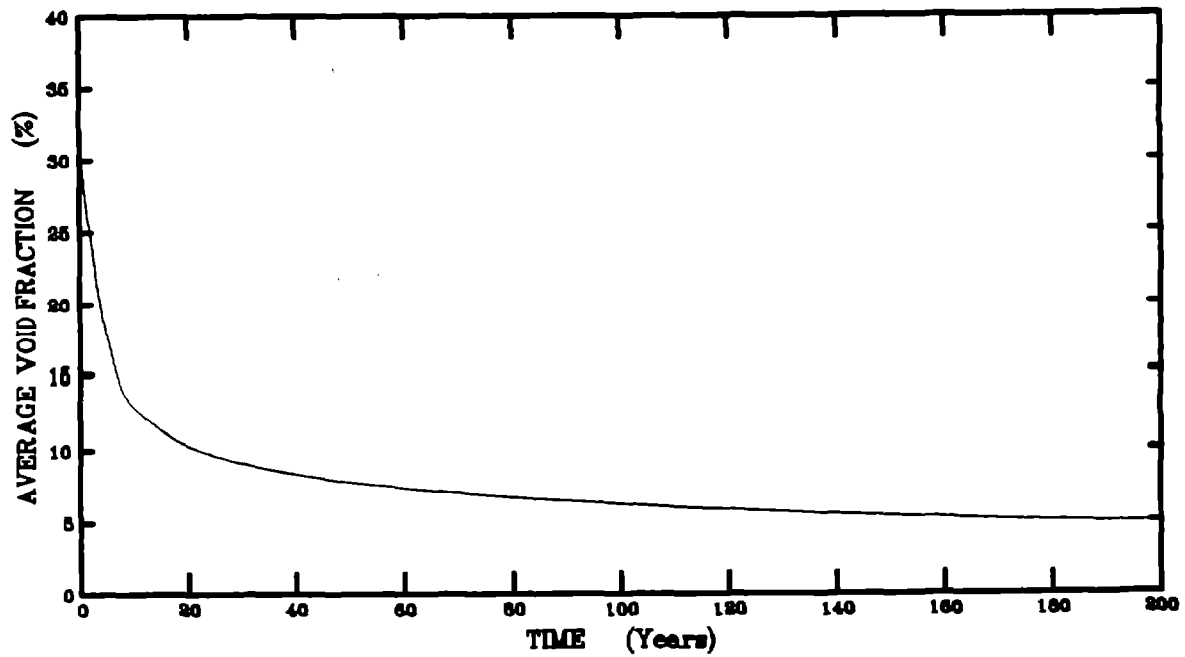


Figure C-2. Average Void Fraction in a Disposal Room Filled With Crushed Salt/Bentonite.

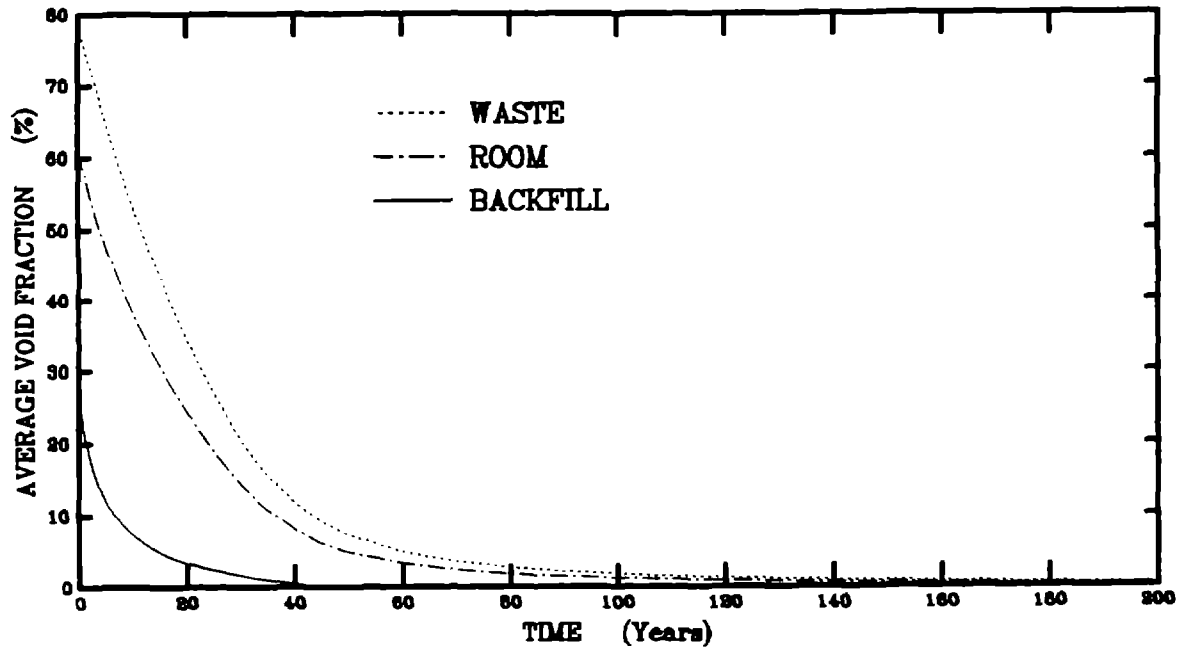


Figure C-3. Average Void Fraction in a Disposal Room Filled With TRU Waste and Surrounded by Crushed Salt.

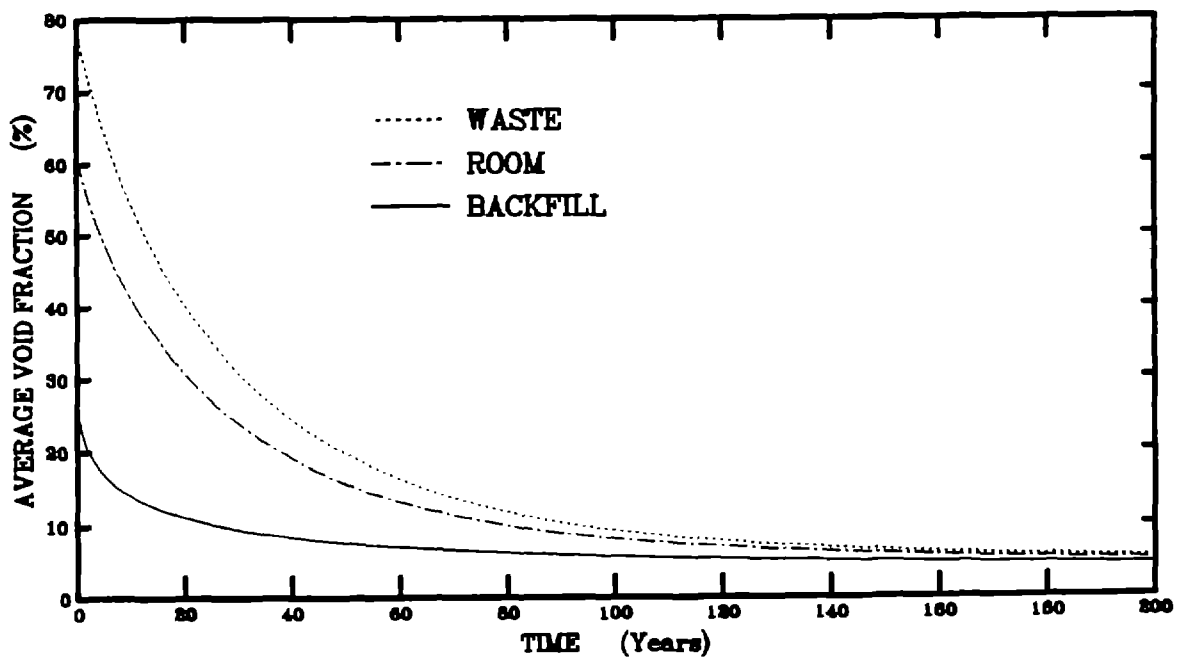


Figure C-4. Average Void Fraction in a Disposal Room Filled With TRU Waste and Surrounded by Crushed Salt/Bentonite.

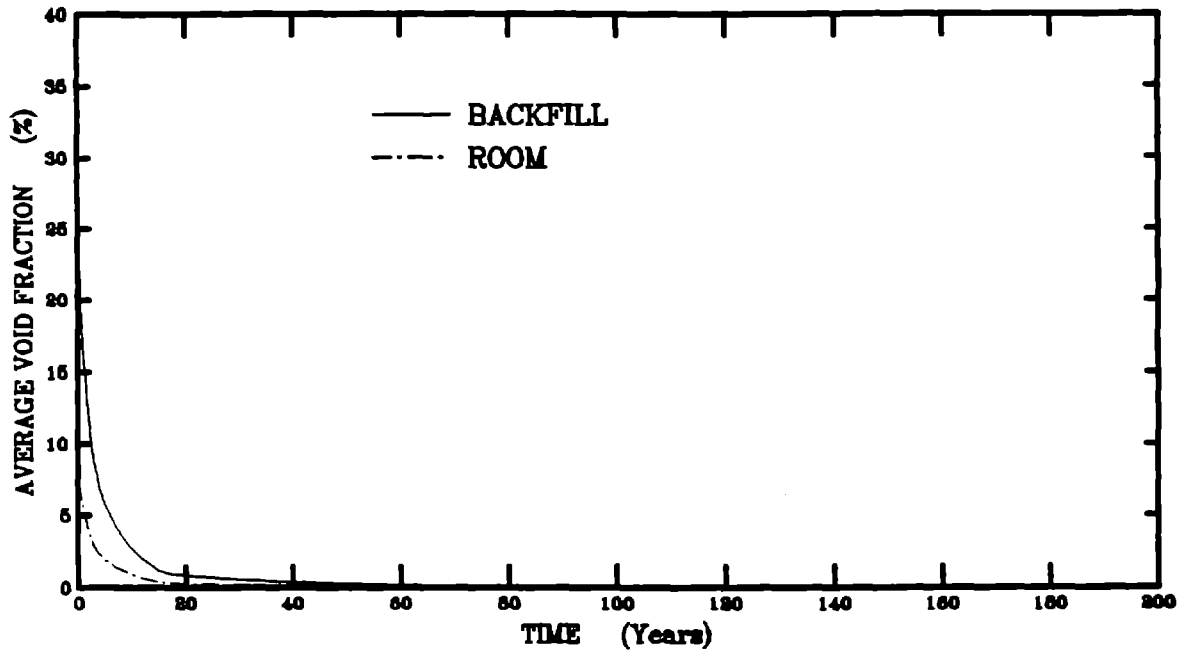


Figure C-5. Average Void Fraction in a Disposal Room Filled With Vitrified Waste and Surrounded by Crushed Salt.

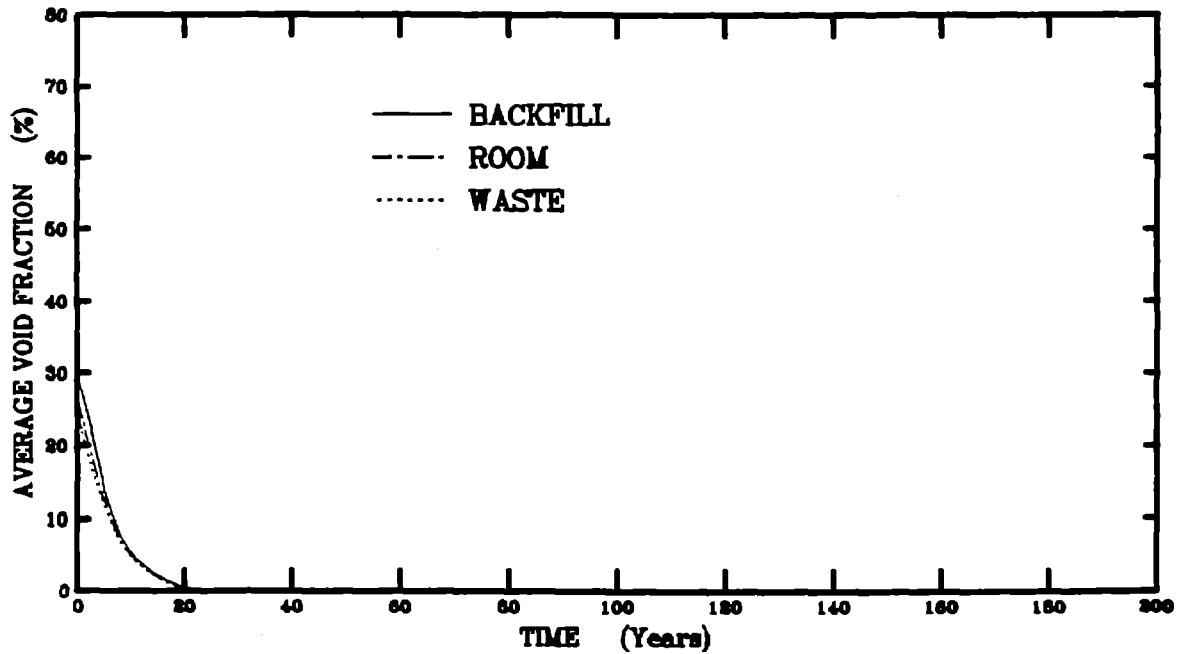


Figure C-6. Average Void Fraction in a Disposal Room Filled With a Mixture of Shredded Metallic Waste and Surrounded by Crushed Salt.

RSI-163-90-080

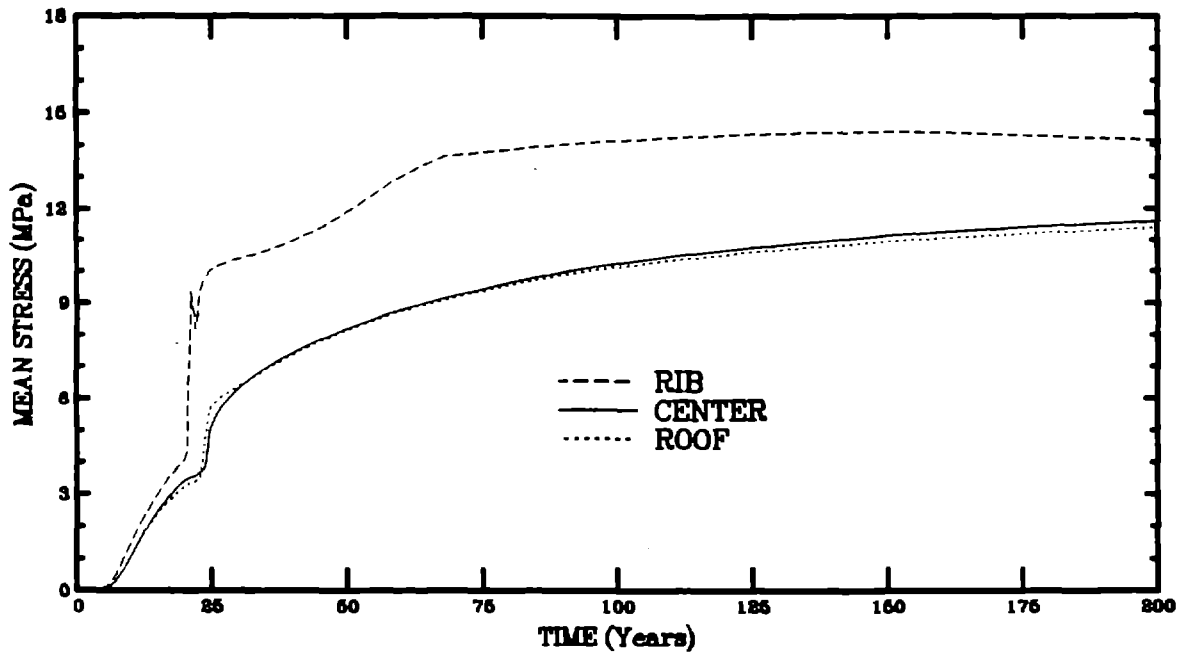


Figure C-7. Mean Stress History in a Disposal Room Filled With Crushed Salt.

RSI-163-90-081

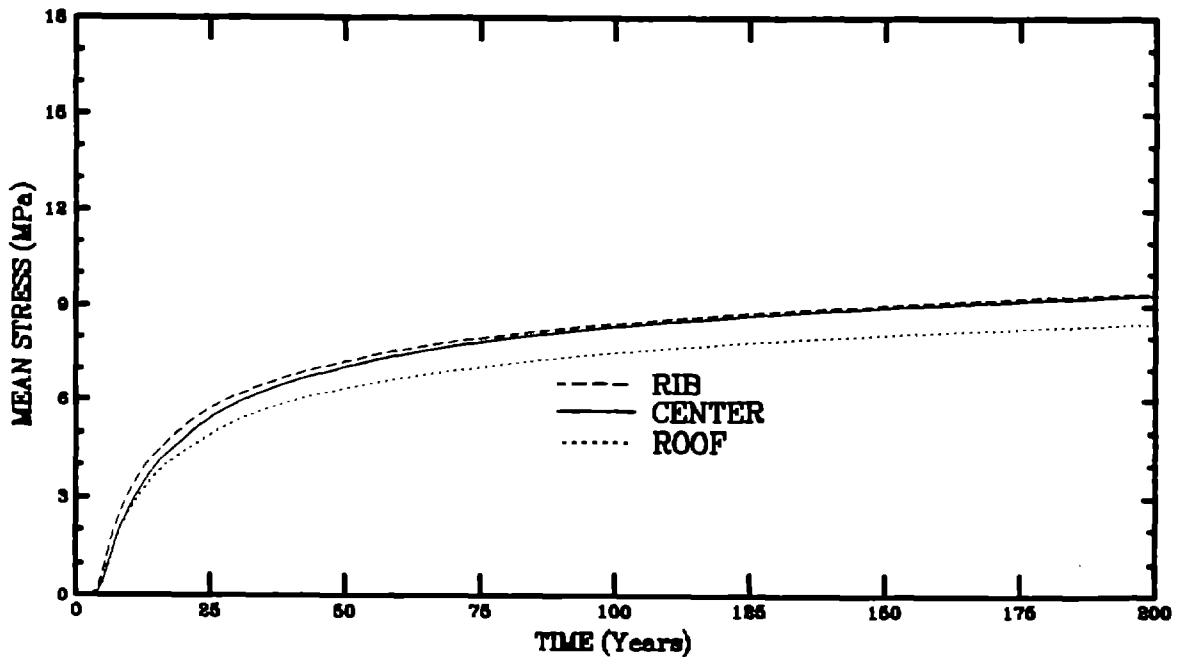


Figure C-8. Mean Stress History in a Disposal Room Filled With Crushed Salt/Bentonite.

RSI-163-90-082

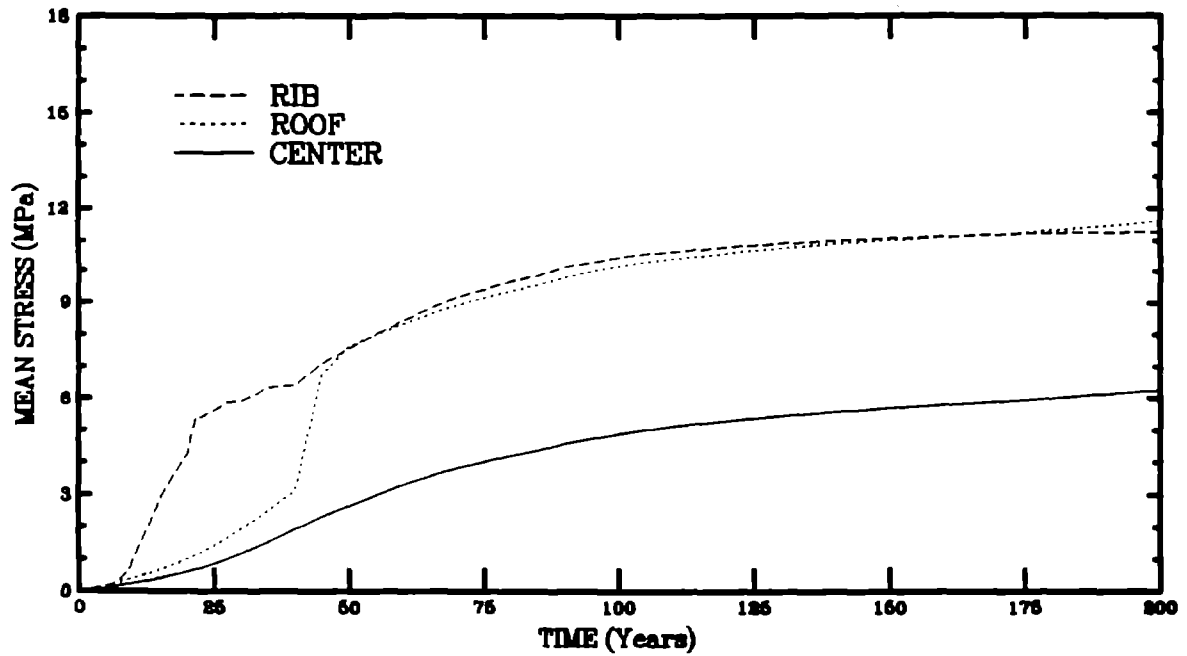


Figure C-9. Mean Stress History in a Disposal Room Filled TRU Waste and Surrounded by Crushed Salt.

RSI-163-90-083

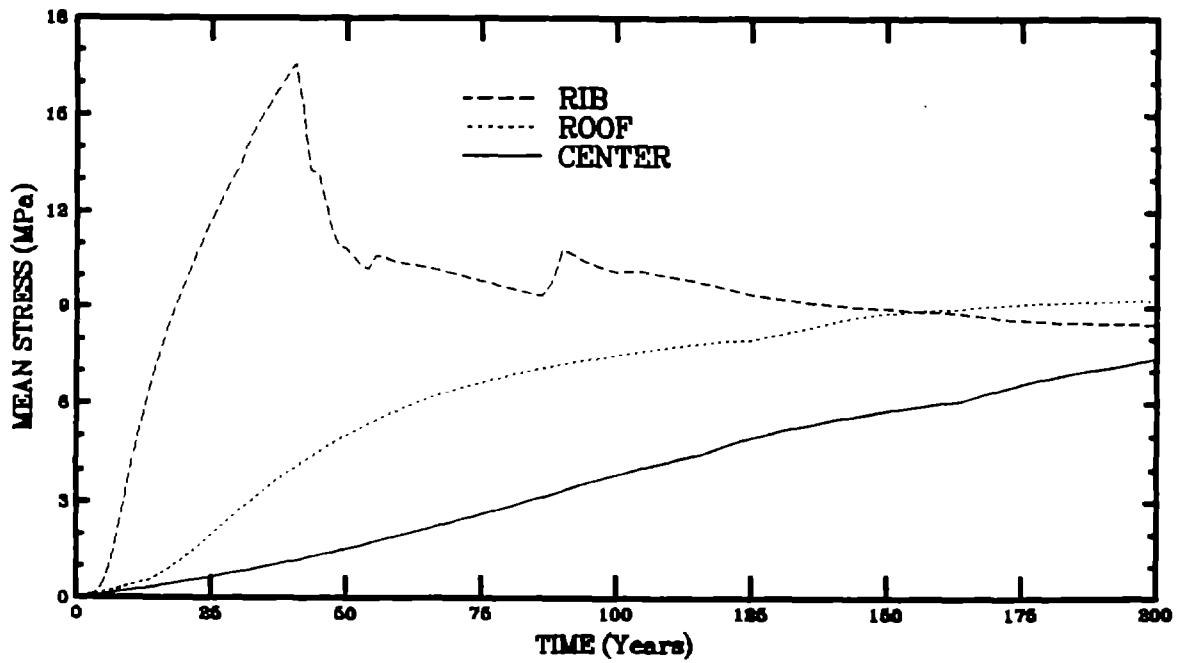


Figure C-10. Mean Stress History in a Disposal Room Filled With TRU Waste and Surrounded by Crushed Salt/Bentonite.

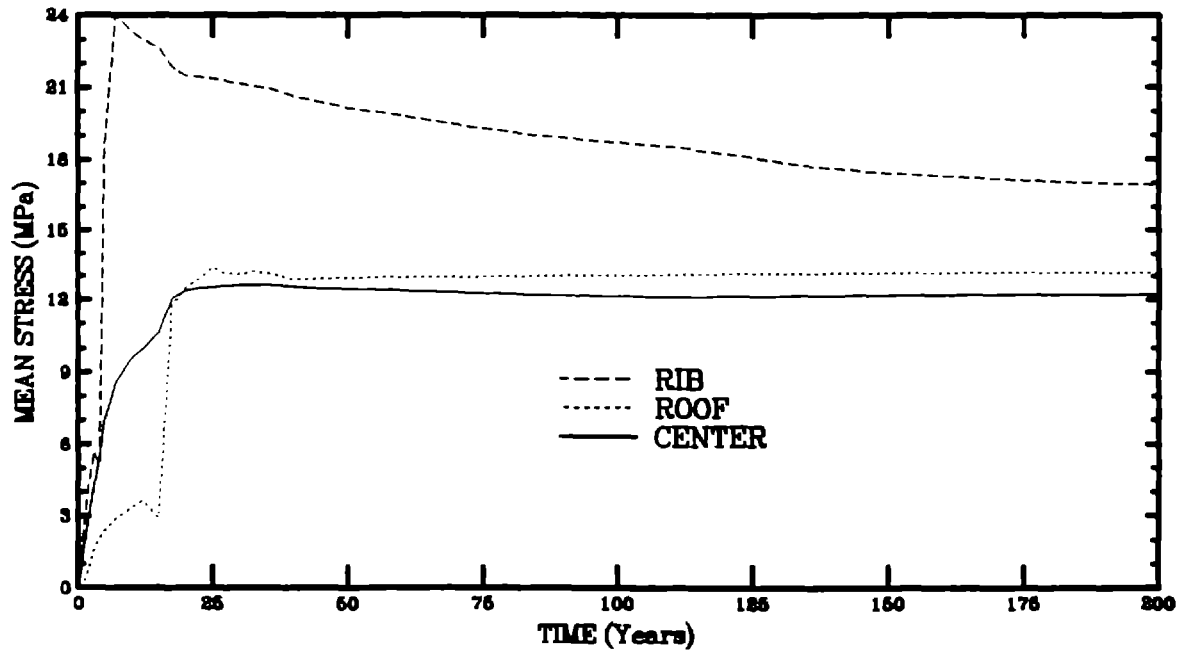


Figure C-11. Mean Stress History in a Disposal Room Filled With Vitrified Waste and Surrounded by Crushed Salt.

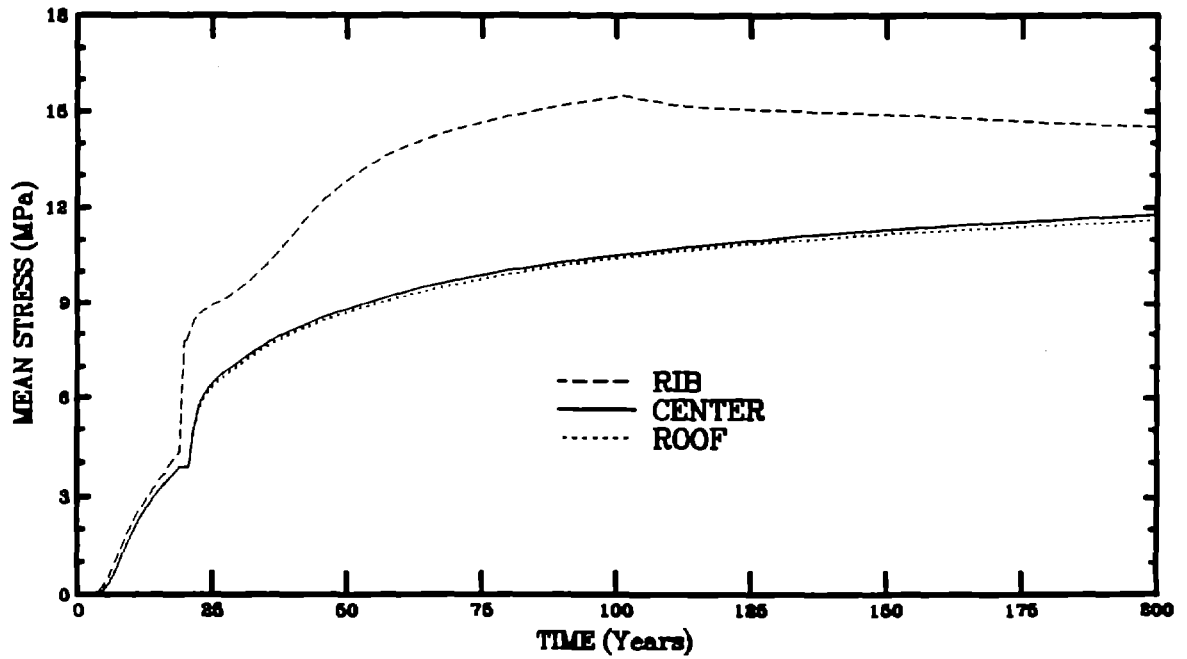


Figure C-12. Mean Stress History in a Disposal Room Filled With a Mixture of Shredded Metallic Waste and Surrounded by Crushed Salt.

DISTRIBUTION

FEDERAL AGENCIES

U. S. Department of Energy, (5)
Office of Civilian Radioactive Waste
Management

Attn: Deputy Director, RW-2
Associate Director, RW-10
Office of Program
Administration and
Resources Management
Associate Director, RW-20
Office of Facilities
Siting and Development
Associate Director, RW-30
Office of Systems
Integration and
Regulations
Associate Director, RW-40
Office of External
Relations and Policy

Forrestal Building
Washington, DC 20585

U. S. Department of Energy (3)
Albuquerque Operations Office
Attn: J. E. Bickel
R. Marquez, Director
Public Affairs Division

P.O. Box 5400
Albuquerque, NM 87185

U. S. Department of Energy
Attn: National Atomic Museum Library
Albuquerque Operations Office
P. O. Box 5400
Albuquerque, NM 87185

U. S. Department of Energy (5)
WIPP Project Office (Carlsbad)
Attn: Vernon Daub
J. A. Mewhinney
D. C. Blackstone

P.O. Box 3090
Carlsbad, NM 88221

U. S. Department of Energy
Research & Waste Management Division
Attn: Director
P. O. Box E
Oak Ridge, TN 37831

U.S. Department of Energy
Waste Management Division
Attn: R. F. Guercia
P. O. Box 550
Richland, WA 99352

U. S. Department of Energy (1)
Attn: Edward Young
Room E-178
GAO/RCED/GTN
Washington, DC 20545

U. S. Department of Energy (6)
Office of Environmental Restoration
and Waste Management
Attn: Jill Lytle, EM30
Mark Frei, EM-34 (3)
Mark Duff, EM-34
Clyde Frank, EM-50
Washington, DC 20585

U. S. Department of Energy (3)
Office of Environment, Safety
and Health
Attn: Ray Pelletier, EH-231
Kathleen Taimi, EH-232
Carol Borgstrom, EH-25
Washington, DC 20585

U. S. Department of Energy (2)
Idaho Operations Office
Fuel Processing and Waste
Management Division
785 DOE Place
Idaho Falls, ID 83402

U.S. Department of Energy
Savannah River Operations Office
Defense Waste Processing
Facility Project Office
Attn: W. D. Pearson
P.O. Box A
Aiken, SC 29802

U.S. Environmental Protection Agency
(2)
Attn: Ray Clark
Office of Radiation Programs
(ANR-460)
Washington, DC 20460

U.S. Geological Survey
Branch of Regional Geology
Attn: R. Snyder
MS913, Box 25046
Denver Federal Center
Denver, CO 80225

U.S. Geological Survey
Conservation Division
Attn: W. Melton
P.O. Box 1857
Roswell, NM 88201

U.S. Geological Survey (2)
Water Resources Division
Attn: Kathy Peter
Suite 200
4501 Indian School, NE
Albuquerque, NM 87110

U.S. Nuclear Regulatory Commission
(4)
Attn: Joseph Bunting, HLEN 4H3 OWFN
Ron Ballard, HLGP 4H3 OWFN
Jacob Philip
NRC Library
Mail Stop 623SS
Washington, DC 20555

BOARDS

Defense Nuclear Facilities Safety
Board
Attn: Dermot Winters
Suite 700
625 Indiana Ave., NW
Washington, DC 20004

U. S. Department of Energy
Advisory Committee on Nuclear
Facility Safety
Attn: Merritt E. Langston, AC21
Washington, DC 20585

Nuclear Waste Technical
Review Board (2)
Attn: Dr. Don A. Deere
Dr. Sidney J. S. Parry
Suite 910
1100 Wilson Blvd.
Arlington, VA 22209-2297

Richard Major
Advisory Committee
on Nuclear Waste
Nuclear Regulatory Commission
7920 Norfolk Avenue
Bethesda, MD 20814

STATE AGENCIES

Environmental Evaluation Group (3)
Attn: Library
Suite F-2
7007 Wyoming Blvd., N.E.
Albuquerque, NM 87109

New Mexico Bureau of Mines
and Mineral Resources (2)
Attn: F. E. Kottolowski, Director
J. Hawley
Socorro, NM 87801

NM Department of Energy & Minerals
Attn: Librarian
2040 S. Pacheco
Santa Fe, NM 87505

NM Environmental Improvement Division
Attn: Deputy Director
1190 St. Francis Drive
Santa Fe, NM 87503

LABORATORIES/CORPORATIONS

Battelle Pacific Northwest
Laboratories (5)
Attn: D. J. Bradley, K6-24
J. Relyea, H4-54
R. E. Westerman, P8-37
H. C. Burkholder, P7-41
L. Pederson, K6-47
Battelle Boulevard
Richland, WA 99352

Savannah River Laboratory (6)
Attn: N. Bibler
E. L. Albenisius
M. J. Plodinec
G. G. Wicks
C. Jantzen
J. A. Stone
Aiken, SC 29801

George Dymmel
SAIC
101 Convention Center Dr.
Las Vegas, NV 89109

INTERA Technologies, Inc. (4)
Attn: G. E. Grisak
J. F. Pickens
A. Haug
A. M. LeVenue
Suite #300
6850 Austin Center Blvd.
Austin, TX 78731

INTERA Technologies, Inc.
Attn: Wayne Stensrud
P.O. Box 2123
Carlsbad, NM 88221

IT Corporation (3)
Attn: R. F. McKinney
J. Myers
M. Abashian
Regional Office - Suite 700
5301 Central Avenue, NE
Albuquerque, NM 87108

IT Corporation (2)
Attn: D. E. Deal
P.O. Box 2078
Carlsbad, NM 88221

Los Alamos Scientific Laboratory
Attn: B. Erdal, CNC-11
Los Alamos, NM 87545

RE/SPEC, Inc.
Attn: W. Coons
P. F. Gnirk
Suite 300
4775 Indian School Rd., NE
Albuquerque NM 87110-3927

RE/SPEC, Inc. (8)
Attn: L. L. Van Sambeek
G. Callahan
T. Pfeifle
J. L. Ratigan
N. Brodsky
P. O. Box 725
Rapid City, SD 57709

Center for Nuclear Waste
Regulatory Analysis (4)
Attn: P. K. Nair
Southwest Research Institute
6220 Culebra Road
San Antonio, TX 78228-0510

Science Applications
International Corporation
Attn: Howard R. Pratt,
Senior Vice President
10260 Campus Point Drive
San Diego, CA 92121

Science Applications
International Corporation
Attn: Michael B. Gross
Ass't. Vice President
Suite 1250
160 Spear Street
San Francisco, CA 94105

Science Applications
International Corporation
Attn: T. W. Thompson
Suite 255
14062 Denver West Parkway
Golden, CO 80401

Systems, Science, and Software (2)
Attn: E. Peterson
Box 1620
La Jolla, CA 92038

Westinghouse Electric Corporation (7)
Attn: Library
Lamar Trego
W. P. Poirer
W. R. Chiquelin
V. F. Likar
D. J. Moak
R. F. Kehrman
P. O. Box 2078
Carlsbad, NM 88221

Weston Corporation (1)
Attn: David Lechel
Suite 1000
5301 Central Avenue, NE
Albuquerque, NM 87108

UNIVERSITIES

University of Arizona
Attn: J. G. McCray
Department of Nuclear Engineering
Tucson, AZ 85721

University of New Mexico (2)
Geology Department
Attn: D. G. Brookins
Library
Albuquerque, NM 87131

Pennsylvania State University
Materials Research Laboratory
Attn: Della Roy
University Park, PA 16802

Texas A&M University
Center of Tectonophysics
College Station, TX 77840

G. Ross Heath
College of Ocean
and Fishery Sciences
University of Washington
Seattle, WA 98195

Dr. Howard Adler
Oak Ridge Associated Universities
Medical Science Division
P. O. Box 117
Oak Ridge, TN 37831-0117

INDIVIDUALS

Dennis W. Powers
Star Route Box 87
Anthony, TX 79821

LIBRARIES

Thomas Brannigan Library
Attn: Don Dresp, Head Librarian
106 W. Hadley St.
Las Cruces, NM 88001

Hobbs Public Library
Attn: Ms. Marcia Lewis, Librarian
509 N. Ship Street
Hobbs, NM 88248

New Mexico State Library
Attn: Ms. Ingrid Vollenhofer
P.O. Box 1629
Santa Fe, NM 87503

New Mexico Tech
Martin Speere Memorial Library
Campus Street
Socorro, NM 87810

Pannell Library
Attn: Ms. Ruth Hill
New Mexico Junior College
Lovington Highway
Hobbs, NM 88240

WIPP Public Reading Room
Attn: Director
Carlsbad Public Library
101 S. Halagueno St.
Carlsbad, NM 88220

Government Publications Department
General Library
University of New Mexico
Albuquerque, NM 87131

THE SECRETARY'S BLUE RIBBON
PANEL ON WIPP

Dr. Thomas Bahr
New Mexico Water Resources Institute
New Mexico State University
Box 3167
Las Cruces, NM 88003-3167

Mr. Leonard Slosky
Slosky and Associates
Suite 1400
Bank Western Tower
1675 Tower
Denver, Colorado 80202

Mr. Newal Squyres
Holland & Hart
P. O. Box 2527
Boise, Idaho 83701

Dr. Arthur Kubo
Vice President
BDM International, Inc.
7915 Jones Branch Drive
McLean, VA 22102

Mr. Robert Bishop
Nuclear Management Resources Council
Suite 300
1776 I Street, NW
Washington, DC 20006-2496

NATIONAL ACADEMY OF SCIENCES,
WIPP PANEL

Dr. Charles Fairhurst, Chairman
Department of Civil and
Mineral Engineering
University of Minnesota
500 Pillsbury Dr. SE
Minneapolis, MN 55455-0220

Dr. John O. Blomeke
Route 3
Sandy Shore Drive
Lenoir City, TN 37771

Dr. John D. Bredehoeft
Western Region Hydrologist
Water Resources Division
U.S. Geological Survey (M/S 439)
345 Middlefield Road
Menlo Park, CA 94025

Dr. Karl P. Cohen
928 N. California Avenue
Palo Alto, CA 94303

Dr. Fred M. Ernsberger
250 Old Mill Road
Pittsburgh, PA 15238

Dr. Rodney C. Ewing
Department of Geology
University of New Mexico
200 Yale, NE
Albuquerque, NM 87131

B. John Garrick
Pickard, Lowe & Garrick, Inc.
2260 University Drive
Newport Beach, CA 92660

Leonard F. Konikow
U.S. Geological Survey
431 National Center
Reston, VA 22092

Jeremiah O'Driscoll
505 Valley Hill Drive
Atlanta, GA 30350

Dr. Christopher G. Whipple
Clement International
Suite 1380
160 Spear Street
San Francisco, CA 94105

Dr. Peter B. Myers, Staff
Director
National Academy of Sciences
Committee on Radioactive
Waste Management
2101 Constitution Avenue
Washington, DC 20418

Dr. Geraldine Grube
Board on Radioactive
Waste Management
GF456
2101 Constitution Avenue
Washington, DC 20418

FOREIGN ADDRESSES

Studiecentrum Voor Kernenergie
Centre D'Energie Nucleaire
Attn: Mr. A. Bonne
SCK/CEN
Boeretang 200
B-2400 Mol
BELGIUM

Atomic Energy of Canada, Ltd. (2)
Whiteshell Research Estab.
Attn: Peter Haywood
John Tait
Pinewa, Manitoba, CANADA
ROE 1L0

Dr. D. K. Mukerjee
Ontario Hydro Research Lab
800 Kipling Avenue
Toronto, Ontario, CANADA
M8Z 5S4

Mr. Francois Chenevier, Director (2)
ANDRA
Route du Panorama Robert Schumann
B.P.38
92266 Fontenay-aux-Roses Cedex
FRANCE

Mr. Jean-Pierre Olivier
OECD Nuclear Energy Agency
Division of Radiation Protection
and Waste Management
38, Boulevard Suchet
75016 Paris, FRANCE

Claude Sombret
Centre D'Etudes Nucleaires
De La Vallee Rhone
CEN/VALRHO
S.D.H.A. BP 171
30205 Bagnols-Sur-Ceze
FRANCE

Bundesministerium fur Forschung und
Technologie
Postfach 200 706
5300 Bonn 2
FEDERAL REPUBLIC OF GERMANY

Bundesanstalt fur Geowissenschaften
und Rohstoffe
Attn: Michael Langer
Postfach 510 153
3000 Hannover 51
FEDERAL REPUBLIC OF GERMANY

Hahn-Meitner-Institut fur
Kernforschung
Attn: Werner Lutze
Glienicker Strasse 100
100 Berlin 39
FEDERAL REPUBLIC OF GERMANY

Institut fur Tieflagerung (4)
Attn: K. Kuhn
Theodor-Heuss-Strasse 4
D-3300 Braunschweig
FEDERAL REPUBLIC OF GERMANY

Kernforschung Karlsruhe
Attn: K. D. Closs
Postfach 3640
7500 Karlsruhe
FEDERAL REPUBLIC OF GERMANY

Physikalisch-Technische Bundesanstalt
Attn: Peter Brenneke
Postfach 33 45
D-3300 Braunschweig
FEDERAL REPUBLIC OF GERMANY

D. R. Knowles
British Nuclear Fuels, plc
Risley, Warrington, Cheshire WA3 6AS
1002607 GREAT BRITAIN

Shingo Tashiro
Japan Atomic Energy Research
Institute
Tokai-Mura, Ibaraki-Ken
319-11 JAPAN

Netherlands Energy Research
Foundation ECN (2)
Attn: Tuen Deboer, Mgr.
L. H. Vons
3 Westerduinweg
P.O. Box 1
1755 ZG Petten, THE NETHERLANDS

Svensk Karnbransleforsorjning AB
Attn: Fred Karlsson
Project KBS
Karnbranslesakerhet
Box 5864
10248 Stockholm, SWEDEN

SANDIA INTERNAL

400 L. D. Tyler
1510 J. C. Cummings
1514 H. S. Morgan
1514 J. R. Weatherby
1514 J. G. Arguello
1514 C. M. Stone
3141 S. A. Landenberger (5)
3151 G. C. Glaycomb (3)
3145 Document Control (8)
for DOE/OSTI
6000 D. L. Hartley
6232 W. R. Wawersik
6232 D. H. Zeuch
6232 W. A. Olsson
6233 J. C. Eichelberger
6233 J. L. Krumhansl
6300 T. O Hunter
6310 T. E. Blejwas, Acting
6313 L. E. Shephard
6315 M. D. Siegel
6340 W. D. Weart
6340 S. Y. Pickering
6341 R. C. Lincoln
6341 Staff (9)
6341 Sandia WIPP Central Files
DRM (10)
6342 D. R. Anderson
6342 Staff (11)
6343 T. M. Schultheis
6343 Staff (2)
6344 E. Gorham
6344 Staff (10)
6345 B. M. Butcher, Acting (10)
6345 Staff (9)
6346 J. R. Tillerson
6346 Staff (7)
8523 R. C. Christman (SNLL Library)
9300 J. E. Powell
9310 J. D. Plimpton
9320 M. J. Navratil
9325 L. J. Keck (2)
9330 J. D. Kennedy
9333 O. Burchett
9333 J. W. Mercer
9334 P. D. Seward